Summer 8-8-2020

Differential Expression of RNA in the Rat Peripheral Nervous System Following Nerve Injury and Treatment with Pain-Relieving Celecoxib-Loaded Nanomedicine

Andrea Stevens
Duquesne University

DIFFERENTIAL EXPRESSION OF RNA IN THE RAT PERIPHERAL NERVOUS SYSTEM FOLLOWING NERVE INJURY AND TREATMENT WITH PAIN-RELIEVING CELECOXIB-LOADED NANOMEDICINE

A Dissertation

Submitted to the Bayer School of Natural and Environmental Sciences

Duquesne University

In partial fulfillment of the requirements for

the degree of Doctor of Philosophy

By

Andrea Marie Jacobs Stevens

August 2020

DIFFERENTIAL EXPRESSION OF RNA IN THE RAT PERIPHERAL NERVOUS SYSTEM FOLLOWING NERVE INJURY AND TREATMENT WITH PAIN-RELIEVING CELECOXIB-LOADED NANOMEDICINE

By

Andrea Marie Jacobs Stevens

Approved June 12, 2020

Dr. John Archie Pollock Professor of Biological Sciences (Committee Chair)	Dr. Jelena M. Janjic Associate Professor of Pharmaceutical Sciences (Committee Member)
Dr. Benedict J. Kolber Associate Professor of Biological Sciences (Committee Member)	Dr. Sarah Woodley Associate Professor of Biological Sciences (Committee Member)
Dr. Philip Paul Reeder Dean and Professor, Bayer School of Natural and Environmental Sciences	Dr. Joseph R. McCormick Chair, Biological Sciences Professor of Biological Sciences

ABSTRACT

DIFFERENTIAL EXPRESSION OF RNA IN THE RAT PERIPHERAL NERVOUS SYSTEM FOLLOWING NERVE INJURY AND TREATMENT WITH PAIN-RELIEVING CELECOXIB-LOADED NANOMEDICINE

By

Andrea Marie Jacobs Stevens

August 2020

Dissertation supervised by Dr. John A. Pollock

Adapted from:

A. Stevens, L. Liu, D. Bertovich, J.M. Janjic, J.A. Pollock. Differential expression of neuroinflammatory mRNAs in the rat sciatic nerve following chronic constriction injury and pain-relieving nanoemulsion NSAID delivery to infiltrating macrophages. *International Journal of Molecular Sciences* 2019; 20(21): 5269. Doi.org/10.3390/ijms20215269.

A. Stevens, M. Saleem, B. Deal, J.M. Janjic, J.A. Pollock. Targeted COX-2 inhibiting nanomedicine results in pain-relief and differential expression of RNA in the dorsal root ganglia of injured male rats. *Molecular Pain In Press* 2020.

M. Saleem*, **A. Stevens*,** B. Deal, L. Liu, J. M. Janjic, J. A. Pollock. A new best practice for validating tail vein injections in rat with near infrared labeled agents. *Journal of Visualized Experiments* 2019; e59295. *Co-authors contributed equally.

J. M. Janjic, K. Vasudeva, M. Saleem, **A. Stevens**, L. Liu, S. Patel, J. A. Pollock. Low-dose NSAIDs reduce pain via macrophage targeted nanoemulsion delivery to neuroinflammation of the sciatic nerve in rat. *Journal of Neuroimmunology* 2018; 318: 72-79.

The neuroinflammatory response to peripheral nerve injury is associated with chronic pain and significant changes in the expression profiles of RNAs in neurons, glia and infiltrating immune cells: a neuro-immune triad. Chronic constriction injury (CCI) of the rat sciatic nerve provides an opportunity to mimic neuropathic injury and quantitatively assess behavior and differential gene expression in individual animals. Macrophages that phagocytose intravenously injected nanoemulsion carrying the non-steroidal anti-inflammatory, NSAID, Celecoxib, naturally accumulate at the site of injury resulting in relief of CCI behavioral hyper-sensitivity. It is not known beyond the inhibition of cyclooxygenase-2 (COX-2) activity and the reduction in prostaglandin E2 (PGE2), what gene expression may be altered by this treatment. Previously, we showed that a single intravenous injection of nanoemulsion containing celecoxib (0.24 mg/kg) reduced inflammation of the sciatic nerve and relieved pain-like behavior for up to 6 days. To elucidate aspects of the molecular mechanisms underlying CCI pain as well as pain relief, I assessed an NSAID-loaded nanoemulsion macrophage-targeted therapy to explore changes in RNA expression in both pain and pain-relieved states. Sciatic nerve and dorsal root ganglia (DRG) tissue from CCI animals was used to evaluate the expression profiles utilizing quantitative polymerase chain reactions (qPCR) and RNA sequencing, respectively. In the injured sciatic nerve treated with drug-loaded nanoemulsion, I observed mRNA changes consistent with the reduced recruitment of macrophages evident by a reduction in chemokine and cytokine mRNA expression.

Furthermore, genes associated with selective adhesion of macrophages, as well as changes in the neuronal and glial associated mRNAs were observed. Moreover, several neuroactive genes were found to respond to the celecoxib loaded nanoemulsion in animals receiving pain relief as compared to animals that received drug-free vehicle including: Monoamine oxidase B (MAOB), NMDA-Receptor 2b (Grin2b), Calcium channel TRPV3, Interleukin IL-6, Voltage-dependent Calcium channel subunit alpha 1B (Cacna1b/$C2_v2.2$), Integrin alpha M (Itgam/Cd11b), Sodium channel $Na_v1.7$ (Scn9a), and Preprotachykinin-1 (Tac1), which produces neurokinin A and substance P.

The transcriptome of the ipsilateral DRGs was assessed using high throughput RNA sequencing to provide insight into the molecular mechanisms involved in the underlying neuroimmune response. Comparing the DRG transcriptome of CCI animals treated with celecoxib-loaded nanoemulsion (CXB-NE) as well as drug-free (vehicle) nanoemulsion (DF-NE) to naïve, unoperated rats revealed significant differential RNA expression of 115 genes. Differential expression of particular transcripts was validated by quantitative PCR in the DRG and the bioinformatics tool PANTHER (protein annotation through evolutionary relationship) revealed that the differentially expressed genes involved in the neuroinflammatory response are associated with several key signaling mechanisms. This study showed that by directly inhibiting COX-2 activity in infiltrating macrophages at the site of injury on the sciatic nerve, there was a subsequent change in RNA expression in cell bodies of the DRG. While it is not surprising that peripheral nerve injury is associated with extensive changes in the expression profile of RNAs in the associated DRG, it is clear that attenuating the activity of COX-2 and the corresponding reduction in PGE2 at the site of injury results in changes in the

transcriptome of the associated DRG reflecting pain relief as well as the partial reversal of the gene expression profiles in the injured sciatic nerve associated with chronic pain. Overall, it can be concluded that by solely targeting COX-2 production in macrophages in the CCI model, there is a direct effect of gene expression changes related to cells associated with the neuroimmune triad, the axon regeneration process, and the chronic pain response.

DEDICATION

I would like to dedicate this to both of my parents, Sandi and Mike Jacobs. My dad always encouraged me to explore nature and science and has remained an inspiration to me since I was a little girl. He always told me to be anything I wanted to be and never to limit myself. I also would like to dedicate this to my husband, Dejan, and children, Daryn, Zara, and Baby Boy, who have remained ever-supporting in my doctoral endeavors and always continue to inspire me. To my children, know that you can do anything you want as long as you strive to work hard.

ACKNOWLEDGEMENT

I would like to firstly thank my Ph.D. adviser, Dr. John Pollock. Thank you for your support in and out of the lab. Your encouraging words always mean the most to me. My committee members, Dr. Janjic, Dr. Kolber and Dr. Woodley for their continued support and essential feedback that allowed me to shape my dissertation. A special thanks to Dr. J. for her extra special support both in science and personally. The Bayer School and Department of Biology have been pivotal in allowing me to pursue my research work and become a well-shaped scientist. I would also like to acknowledge my labmates Dr. Kiran Vasudeva, Dr. Muz Saleem, Brooke Deal, Young Lee, and Dylan Bertovich.

TABLE OF CONTENTS

Page

LIST OF TABLES

Page

LIST OF FIGURES

Page

LIST OF ABBREVIATIONS

CCI; chronic constriction injury

DRG; dorsal root ganglia

CXB; Celecoxib

COX-2; cyclooxygenase-2

CXB-NE; Celecoxib-loaded nanoemulsion

NSAID; non-steroidal anti-inflammatory drugs

DF-NE; drug-free nanoemulsion

NIRF; near infrared fluorescence

IV; intravenous

Chapter 1: Introduction

1.1 Chronic neuropathic pain

Pain is an important sensation. Acute pain serves to notify the body of an event that may be dangerous or damaging. However, when pain lasts longer than normal healing or occurs in the absence of a noxious stimuli and persists, it is known as chronic[1]. Chronic pain can be a debilitating disease to those who suffer from it. It is documented that chronic pain affects 1 in 3 Americans over a lifetime and cost up to 600 billion dollars annually in lost wages, hospital and treatment costs, and related expenses[2]. This research focuses on peripheral neuropathic pain – a type of chronic pain that occurs as a result of damage or injury to the peripheral nervous system. Symptoms of chronic pain are characterized variously as being spontaneous, occurring randomly in time and dispersed without patterns throughout the body. Chronic pain can also present as an exaggerated sensitivity to noxious stimuli, called hyperalgesia, or as a painful response to an innocuous stimuli, known as allodynia. Pain is often associated with inflammation, which signals the peripheral nervous system in various ways. The peripheral nerve signals are then transmitted to the central nervous system where they are ultimately interpreted as pain. Treating chronic pain has been elusive as most current treatments fail to target the underlying mechanisms, instead focusing on the symptoms associated with inflammation in the periphery or aspects of the interpretation of nociceptive signals by the central nervous system.

Non-steroidal anti-inflammatory drugs (NSAIDs) are a class of drugs that targets the underlying inflammatory response by inhibiting cyclooxygenase 1 and 2 (COX-1 and COX-2). Although, still used to supplement the treatment of chronic pain, NSAIDs are no

longer used as a primary treatment due to the high incidence of adverse events such as cardiac-related deaths[3]. For this and other reasons, epidemiological studies report that many patients with neuropathic pain (peripheral neuropathy) do not receive appropriate treatment that provides relief [4]. One reason is that treatments fail to target the underlying cellular and molecular mechanisms of neuropathy. For instance, opioid agonists are commonly used, however, they merely treat the symptom of pain and tend to exacerbate the neuroimmune interactions associated with the loss of opioid efficacy [5-8]. Additionally, the adverse effects of long-term opioid use including addiction, may outweigh the benefits of its moderate effectiveness to relieve neuropathic pain symptoms[4].

Peripheral neuropathy is characterized by a dynamic molecular and cellular response, consisting of two phases that can each contribute to hypersensitivity and pain. First, neuropathy is associated with a change in the immune cell microenvironment surrounding the damaged neurons leading to localized neuroinflammation [5, 9]. Second, injured axons degenerate distally followed by axon regeneration [10-12]. In combination, chronic pain results from altered neuronal activity that emerges from the interplay between the injured neurons with neighboring glial cells and the infiltrating immune system leading to long term changes in gene expression that may affect the pain phenotype. This research utilizes a chronic pain model in rats [chronic constriction injury; CCI] to study the changes that occur in RNA expression at the site of injury and in the associated dorsal root ganglia (DRG), and furthermore this research focuses on studying the altered expression of RNAs in response to a macrophage-targeted NSAID nanomedicine.

I hypothesized that RNA expression changes would occur after CCI both at the site of injury and at its corresponding cell bodies within the dorsal root ganglia. Furthermore, that these RNA expression changes will not be confined to changes within a single cell type, but multiple cell types associated with the neuroimmune triad. In addition, when macrophage-targeted nanomedicine is given to animals in the pain state, differences in RNA expression would be noted beyond the NSAID-loaded macrophages with alterations in RNA expression evident in neurons, glial cells, and other immune cells. We expect that after nerve injury, as well as after treatment with NSAID-loaded nanomedicine, differences will be seen in the underlying biological pathways, including axon regeneration, the immune response, and in signaling.

1.2 Chronic constriction injury (CCI) and the rat as a model of hypersensitivity

Small animal models enable scientists to study the molecular and cellular biology of neuropathic pain in a manipulatable setting. Chronic constriction injury (CCI) as a model of peripheral mononeuropathy was first described for the rat in 1988 by Bennett and Xie[13] (**Figure 1A, B**). CCI causes intraneural edema at and around the common sciatic nerve. In this model, four chromic gut sutures are loosely ligated around the sciatic nerve, leading to inflammation and pain. In sham control animals, the common nerve is exposed and isolated, but no sutures are used. Naïve controls receive no surgical intervention. The pain-like behavioral signs associated with CCI include mild to moderate autotomy, guarding, excessive licking, limping of the ipsilateral hindpaw, and avoidance of placing weight on the injured side [14]. Hypersensitive, pain-like behaviors

for CCI develop within a week and include thermal hyperalgesia, mechanical allodynia, chemical hyper-reactivity, and cold allodynia.

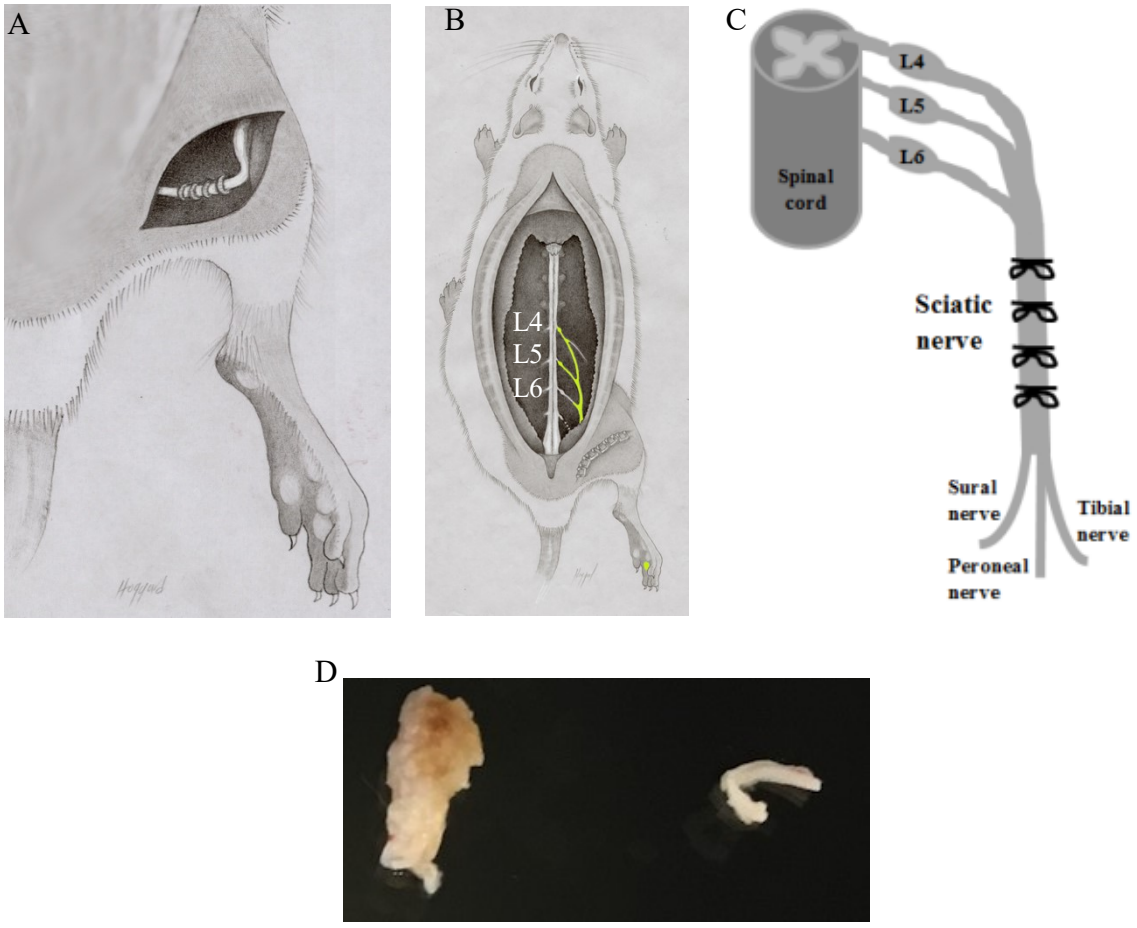

Figure 1. Chronic constriction injury in rats. Chronic constriction injury (CCI) can be used to mimic chronic pain symptoms as seen in humans, including mechanical allodynia and hyperalgesia. (A) The sciatic nerve of the rat is exposed in the rat hindleg under anesthetic and aseptic conditions, where 4 loose ligatures are tied around the common sciatic nerve to induce neuroinflammation. (B) The common sciatic nerve stems from the corresponding from lumbar (L4-L6) dorsal root ganglia sensory neurons and (C) splits distally into the sural, tibial, and peroneal nerves, which innervate the lower limb. (D) On the left, ipsilateral CCI nerve on day 12 demonstrating diffuse inflammation of the entire common sciatic nerve. On the left, contralateral common sciatic nerve (no CCI surgery performed). Illustrations in (A,B) by Robert Hoggard.

CCI is a reliable and reproducible model that mimics the peripheral neuropathic pain states in human such as complex regional pain syndrome[13]. CCI has also been extensively reported on in the literature to describe aspects of the molecular mechanisms associated with spontaneous pain and abnormal sensation[14]. Furthermore, the procedure has the advantage that the sciatic nerve itself can be easily identified and removed post-CCI due to its large size and accessibility. CCI has been documented to last for up to 3 months[13], possibly because the dissolution of chromic gut sutures over time[249].

Twelve days after CCI surgery, the dissected ipsilateral sciatic nerve is neuroanatomically different than its contralateral counterpart (**Figure 1D**). Like other peripheral nerves, the sciatic nerve has an epineural sheath surrounding myelinated and unmyelinated axons as well as a perineurial layer containing vasculature, Schwann cells, immune cells and fibroblasts. In the injured nerve, one significant difference is inflammation, which is present in the fasciculated nerve fibers, evident in histological examination of the dissected nerve (**Figure 1D**).

The CCI injury caused by nerve constriction persists for at least seven weeks[13] and can last months[18]; however, distinct from the acute surgical pain, 'chronic' pain-like behavior begins as early as day 3 post-surgery. Prior to day 3, animals experience transient acute post-operational pain, a well-studied phenomenon in both humans and animals[17]. Although CCI shows many of the symptoms consistent with neuropathy in humans, it also elicits thermal hyperalgesia, which is not a symptom of clinical neuropathic pain in humans[17].

1.3 Role of Neuroinflammation in Pain

Neuroinflammation is accompanied by the infiltration of leukocytes and increased production of inflammatory mediators within the peripheral nervous system (PNS) or central nervous system[19]. Neuroinflammation in the PNS results in a complex and persistent feedback loop that is established to cause more inflammatory signaling within the injured axons, immune cells, and Schwann cells [20,21]. Innate immunity is an integral part of neuroinflammation, whereby the release of danger-associated molecular patterns (DAMPs) in response to injury stimulate pattern recognition receptors that induce inflammasome formation[234, 235, 236]. Although a multitude of inflammatory molecules contribute to neuroinflammation, IL-18 has been shown to be a central mediator in CCI, contributing to an increase in other central cytokines such as IL-1β[20]. Each of these are unique in that they are involved in activating the inflammasome machinery, which in turns leads to an increased pain response in CCI animals. The inflammasome is a multimeric protein complex responsible for cleaving the inactive precursor pro-IL-1β and pro-IL into their proteolytically active forms[234, 239] in macrophages, T cells, mast cells, and neutrophils [237]. Activation and increased expression of IL-1β and IL-18 leads to the production of different cell surface receptors within the site of injury that can ultimately affect signaling and expression changes in the cell bodies of the dorsal root ganglia and in the dorsal horn of the spinal cord[20,22-24].

1.3.1 Involvement of nociceptive neurons in neuroinflammation and pain

Distinguishing between pain and nociception is an important concept in biology. Pain is an unpleasant sensory and emotional experience associated with actual or

potential tissue damage[1] and is always subjective. On the other hand, nociception, first described by Sir Charles Sherrington as the biological detection of a noxious event, which may include psychological and other responses to it[25]. When there is increased pain due to normally noxious stimuli, it is referred to as hyperalgesia. Whereas when nociceptors respond to a stimulus that is normally innocuous, it is referred to as allodynia. Primary sensory neurons are the main conveyors of painful stimuli and act as nociceptors. Their cell bodies are located within dorsal root ganglia or trigeminal ganglia, with peripheral terminals innervating the skin and muscle and central terminals in the dorsal horn of the spinal cord or trigeminal nucleus of the brain. The sciatic nerve is composed of a mixed population of motor and sensory axons with innervation stemming from predominantly L4 and L5 DRGs (approximately 95%), and with some innervation from the cell bodies in L6 DRG (approximately 5%).

Nociceptors are considered the first-responders to tissue injury, given their wide somatosensory distribution and their ability to quickly propagate many sensory signals[26]. Nociceptors have receptive endings that have a relatively high stimulus threshold, allowing for detection of possible damaging stimuli. Nociceptors can be encapsulated (or free) and are commonly associated with slowly conducting unmyelinated C fibers, lightly myelinated Aδ fibers, and heavily myelinated Aβ fibers of small- and large-diameter[15-17]. Additionally, subpopulations of nociceptors can be classified based on the cell content and receptor expression. Pain sensitization is defined as an increased responsiveness of nociceptor neurons to their normal or subthreshold afferent input [1]. During inflammation, nociceptor's thresholds are reduced, leading to an increase in action potentials and neuronal activity.

Peripheral sensitization, a major mechanism underlying the pain response, can be defined as the increased responsiveness and reduced threshold of nociceptive neurons in the periphery to the stimulation of their receptive fields, such as that developing upon inflammation[27]. A review by Watkins and Grace (2014)[9] outlines the RNA and protein expression changes in IL-1β, TrpV ion channels, voltage-gated sodium channels, Toll-like receptors (TLRs), and cell adhesion molecules. These are all accompanied with peripheral sensitization leading to the development of central sensitization (spontaneous discharge within the spinal cord primary nociceptive neurons), as well as an altered glial environment, changes in peripheral cell signaling, and molecular changes to the nociceptors themselves – each of which contribute to the underlying neuroimmune response.

1.3.2 Involvement of Immune Cells and Glia in neuroinflammation and pain

Extravasation of blood-borne (hematogenous) immune cells such as macrophages, T cells and neutrophils into damaged tissue along with the resident immune cells (macrophages, mast cells, endothelial cells), activation of glial cells, such as Schwann cells and satellite cells all contribute to the inflammatory state in CCI (**Figure 2**). After the in-concert production of both pro- and anti-inflammatory mediators, nociceptor neurons which express the molecules for pain signaling (Ras/MAP, NF-κB, JAK/STAT, Phosphoinositol 3/IP3) become activated. This, in turn results in the activation of their respective second messengers such as calcium or cAMP, followed by the influence of signaling cascades such as kinases including PKA, CAMK, PI3K, MAPKs, ERK, and JNK[89]. Among other things, the activation of these signaling kinases leads to a

hyperexcitable state of cells involved in the neuroimmune triad, contributing to the activation of the pain state, by leading to long-term changes in gene expression within each of the involved cell types.

The activation of immune- and immune-like glial cells exhibit distinct temporal profiles to the peripheral nerve, DRG, spinal cord and brain. Initially, neutrophils are the first leukocyte to become activated and infiltrate the site of injury. This response peaks within hours and lasts up to three days. In the peripheral nerve, it is accompanied by complement activation[28], mast cell degranulation[29], and dedifferentiation of resident Schwann cells into phagocytic (or ensheathing) Schwann cells[30]. It is followed by the extravasation of circulating monocytes within three days of injury. Research in male rats has shown that circulating monocytes differentiate into tissue macrophages where they peak as the prominent infiltrating immune cell type present at the injured sciatic nerve between day 3 and beyond[23]. Within days to weeks after macrophage activation and infiltration, T cells are recruited[19, 23, 31, 32]. In the DRG cell bodies, resident satellite cells and macrophages become activated within 24 hours of injury and continue to be expressed for at least three weeks after the initial injury[30].

Schwann cell activation begins at the site of injury signified by an unknown axon death alert signal[33]. Activated Schwann cells are referred to as ensheathing Schwann cells, and no longer myelinate the axon, but instead aide in the repair process. These ensheathing cells contribute to the neuroimmune response in a multitude of ways. They promote the survival of injured neurons via the secretion and production of neurotrophic growth factors (including GDNF, BDNF, NGF, and VEGF)[33]. They serve to recruit more immune cells, specifically macrophages, to the distal stump, via the secretion of

cytokines (such as TNF-α, IL-1α, IL-1β, IL-6, and MCP-1)[33]. These dedifferentiated Schwann cells contribute to the breakdown of injured myelinated axons at the distal stump with autophagic mechanisms, acting more like phagocytic cells, and less like myelin-producing Schwann cells[33]. The clearing of myelin at the site of injury and guidance via the formation of Bungner bands, which occur after Schwann cells become deinnervated and the remaining basement membrane forms endoneurial tubes that contribute to axonal regeneration[33,34].

In neuropathic pain, T cells experience a shift in T-cell subset responses and T-cell related cytokine expression profiles that change later in the neuroimmune response compared to other immune cells[35]. Several subtypes of T cells exist in neuropathic pain including helper T cells including Th1, Th2, Th17 and regulatory T cells, although the role of each still remains elusive. Helper T cells can be identified as being CD4-positive. TH1 cells produce predominantly pro-inflammatory cytokines such as IFN-γ and TNF-α and TH2 cells release anti-inflammatory cytokines IL-4 and IL-10[35]. Regulatory T cells and Th17 are both involved in the adaptive immune response and produce IL-17, whose role in neuropathic pain has become better understood[36, 37]. IL-17 is solely produced by these subsets of T cells and plays an active role in modulating immune responses by enhancing the production of TNF-α, IL-1β, and granulocyte colony stimulating factor (G-CSF), which is a neutrophil-mobilizing factor[36] . Additionally, T cell release of IL-17 is regulated by IL-23 and IL-15 after CCI[36, 38, 39]. Stoll and colleagues have analyzed the temporal expression pattern of IL-17 in the sciatic nerve of mice after CCI. They found that IL-17 expression peaked on day 7 and its' regulators, IL-23 and IL-15, peaked earlier. Additionally, they found IL-17-positive T cells in the endoneurium (the layer

surrounding an individual nerve) of the injured nerve one-week post injury, during peak pain behavior, suggesting T cell's role in the chronic immune response underlying CCI-induced nerve injury.

Neutrophil accumulation at the site of injury peaks 24 hours after injury, accumulating in the endoneurium and are found to persist up to 7 days after injury [40]. Neutrophils are attracted by an increase in the release of nerve growth factor (NGF), chemokine (C-X-C motif) ligand 1 (CXCL1) and leukotriene B4 [26]. Aside from the initial release of inflammatory mediators from the injured nerve tissue, neutrophil degranulation also contributes to the milieu of mediators, adding to inflammatory signals[41]. Seven days after CCI, neutrophil count increased three-fold in the ipsilateral DRG compared to sham[41]. This was accompanied by neutrophil degranulation characterized by an increased expression of the macrophage-recruiting MCP-1 mRNA in the ipsilateral DRG[41]. Neutrophil degranulation results in the release of chemotactic factors specific to monocytes[40], cytokines (TNF-α, IFN-γ, IL-8), chemokines, monocyte adhesion molecules (integrins such as MAC-1, CD11b/CD18 complex; and selectins), prostaglandins and leukotrienes, as well as pre-formed receptors[42]. Neutrophil activation and proliferation serve in the initial recruitment of macrophages and other immune cells[26, 42] as well as leading to further sensitization of nociceptive neurons[40].

Like neutrophils, mast cells can degranulate, leading to subsequent changes in the neuroimmune cross-talk at the site of injury. Upon degranulation, mast cells release pain-producing substances that activate or sensitize nociceptors[43]. Resident mast cells surrounding peripheral nerves facilitate recruitment of neutrophils, T cells and macrophages to the site of inflammation by their production and release of nerve growth

factor (NGF) and other inflammatory mediators[41,43,44]. NGF binds nerve growth factor receptors (trkA) on nociceptive neurons and other peripheral cell types leading to activation of signaling mechanisms that further the recruitment of additional inflammatory cells[43,45]. The dynamic milieu of inflammatory mediators present can induce activity in axons in ways that can influence retrograde transport of signaling molecules to the cell body of the DRG neurons, thereby affecting gene expression of those cells[43]. It has been recently found by our lab that degranulating mast cells are involved in the CCI response following the pain-relieving administration of non-steroidal anti-inflammatory (NSAID) drug-loaded nanoemulsion (CXB-NE) that selectively targets cyclooxygenase-2 production in circulating monocytes and activated macrophages. Saleem et. al. (2019)[46] found a reduction of mast cell numbers in CCI animals given CXB-NE compared to those given drug-free (vehicle) nanoemeulsion (DF-NE) in the ipsilateral sciatic nerve, with no detectable difference at the ipsilateral DRG[46].

Overall, immune and immune-like glial cells release inflammatory mediators that modulate nociceptor neuron activity and pain sensitivity, which in turn cause nociceptors to release neuropeptides and neurotransmitters that act on immune and immune-glial cells to modulate their function by leading to gene expression changes[26]. The inflammatory mediators include neurotransmitters, growth factors, neurotrophins, cytokines, chemokines, and various small molecules such as Substance P, calcitonin gene-related peptide (CGRP), bradykinin, ATP, growth factors, and prostaglandins. These molecules, along with the cells that secrete and produce them, act in concert to influence the development and maintenance of neuropathic pain and the further recruitment of immune

and immune-like glial cells, contributing to this cascade of neuroinflammation that leads to chronic pain.

1.3.3 Macrophages play a major role in neuroinflammation and pain

Monocyte-derived macrophages are known to play a role in peripheral nerve injury at the site of injury in the sciatic nerve and later at the level of the neuronal cell bodies in the dorsal root ganglia (DRG)[46, 50-53]. Recent studies have shown the importance of macrophages at the DRG in the induction and maintenance of pain[250]. Hematogenous macrophages accumulate preferentially around injured axons[36] guided by molecular cues such as monocyte chemoattractant protein-1 (MCP-1)[54] , the lesser studied monocyte chemoattractant protein-5 (MCP-5), and the leukocyte adhesion complex of MAC1, which is formed by the integrins, ITGAM/CD11b and ITGB2/CD18 [55]. Monocyte entry is mediated, in part, by the release of MCP-1. MCP-1 is produced in injured nerve and other immune cells and functions by binding to chemokine receptor CCR2 on the monocyte-derived macrophage[56]. The role of MCP-5 is not known in the pathogenesis of neuropathic pain. Macrophages [and other leukocytes] functions are modulated by the highly abundant α_M and β_2 integrins ITGAM/CD11b and ITGB2/CD18, respectively, which form a heterodimer known as MAC1 or CR3[55]. MAC-1 is normally present in an inactive confirmation in circulating monocytes, but is rapidly activated to mediate leukocyte adhesion, migration, and accumulation at the sites of inflammation[55]. Blocking this complex and its ligands and ablation of genes encoding CD11b or CD18 decrease the severity of inflammation in many animal models[55].

Macrophages exert their influence in multiple ways (**Figure 2**) including the production and secretion of cytokines/chemokines or through a gap-junction like connection, which pass small molecules with neurons[52]. Resident and hematogenous macrophages produce the pro-inflammatory cytokine IL-6 and increase expression of cyclooxygenase 2 (COX-2), which produces prostaglandin E_2 (PGE_2), all of which contribute to the inflammatory response[32, 51] (**Figure 2**). In the sciatic nerve after injury, it has been previously shown that several molecules were specifically associated with CD68-positive, CD11b-positive and MAC1-positive macrophages including; TNF-α, IL-6, IL-18, MIF (macrophage migration inhibitory factor), CCL3 (macrophage inflammatory protein 1-α/chemokine (C-C motif) ligand 3), and CCL4 (macrophage inflammatory protein 1-β/chemokine (C-C motif) ligand 4) [20,52, 57, 58].

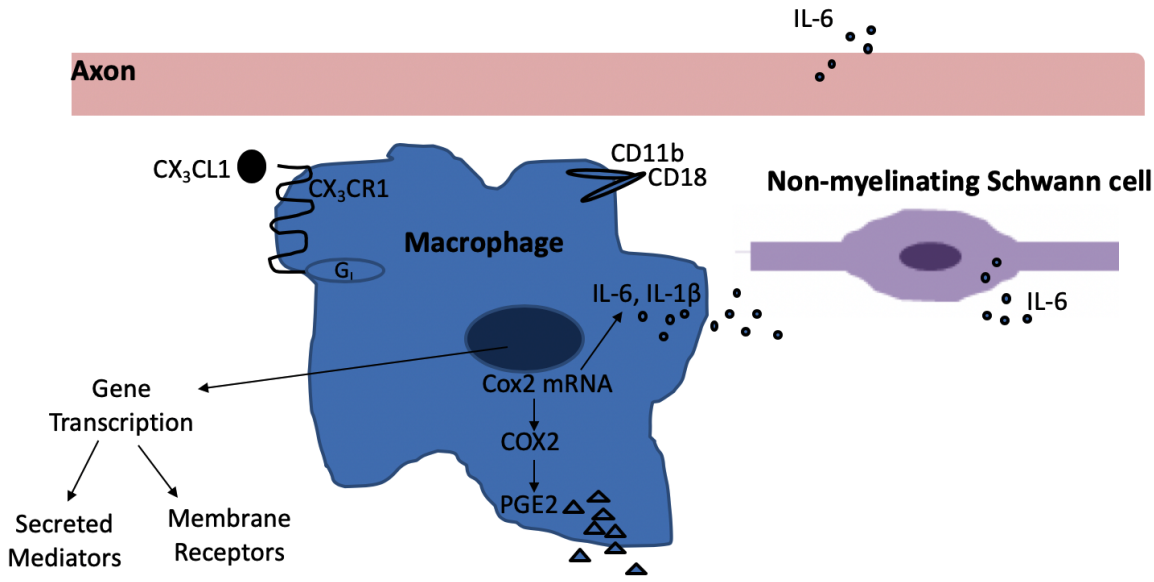

Figure 2. Macrophages play a key role in regulating neuropathic pain. Macrophages exert their overall effect by interacting with other neuroimmune cells and changing expression in key genes and proteins involved in neuroinflammation, leading to overall changes in the gene transcriptome of the neuroinflammatory cells involved.

1.4 Mechanism of Celecoxib

Non-steroidal anti-inflammatory drugs (NSAIDs) were once utilized to treat neuropathic pain, however, due to the lack of efficacy and adverse events associated with some NSAIDs, they are no longer mentioned in current neuropathic pain treatment guidelines[1]. This can be attributed to the detrimental adverse events associated with the 'coxib' class of NSAIDs in clinical trials[3]. 'Coxibs' are selective cyclooxygenase-2 (COX-2) inhibitors and include drugs such as celecoxib. When given orally, COX-2 inhibitors have been associated with a high risk of acute myocardial infarction (MI). Studies examining the risk of myocardial infarction (MI) in patients taking NSAIDs such as CXB have presented conflicting results[3].

NSAIDs such as Celecoxib, posses an active COX-2 binding site, in which the enzyme cyclooxygenase-2 will bind upon induction. Celecoxib acts to attenunate production of prostaglandins from arachidonic acid by blocking cyclooxygenases[59]. Prostaglandins have been shown to produce hyperalgesia and lead to nociceptor sensitization via a direct action on the sensory neurons[60]. In addition, PGE_2 has the ability to modulate voltage-gated sodium channels in sensory neurons via enhancing the excitability and leading to PGE_2-induced hyperalgesia[60, 61]. COX-2 expression is enhanced in multiple cell types, including macrophages. Inflammasome induction in macrophages leads to secretion of IL-18 and IL-1β, both of which are cleaved proteolytically from their precursors via the activation of caspase-1. Both of these cytokines can induce COX and subsequent PGE_2 production[62-64]. PGE_2 in turn stimulates the production of other inflammatory mediators such as the calcitonin gene-related peptide, CGRP, contributing to the positive feedback loop created by the dynamic neuronal-immune cell-and glial interactions[65]. Following peripheral nerve injury, there is a marked upregulation of many inflammatory mediators in the endoneurium of the injured nerve, including COX-2[66]. Many inflammatory mediators such as growth factors, cytokines (IL-1β, IL-6, and TNF-α), and intracellular calcium increases have been shown to induce COX-2 expression via downstream signaling activation of NF-κB and MAPK pathways[67]. Membrane lipids are broken down by phospholipase A2 resulting in an increase arachidonic acid (AA) in the lipid bilayer. AA is a precursor in the production of prostaglandins, where the COX reaction via PGH_2 is the rate limiting step in the production of PGE_2 (**Figure 3**). PGE_2 is a key mediator in peripheral sensitization[68]. It increases neuronal activity[69] and hyperalgesia[70] when administered spinally.

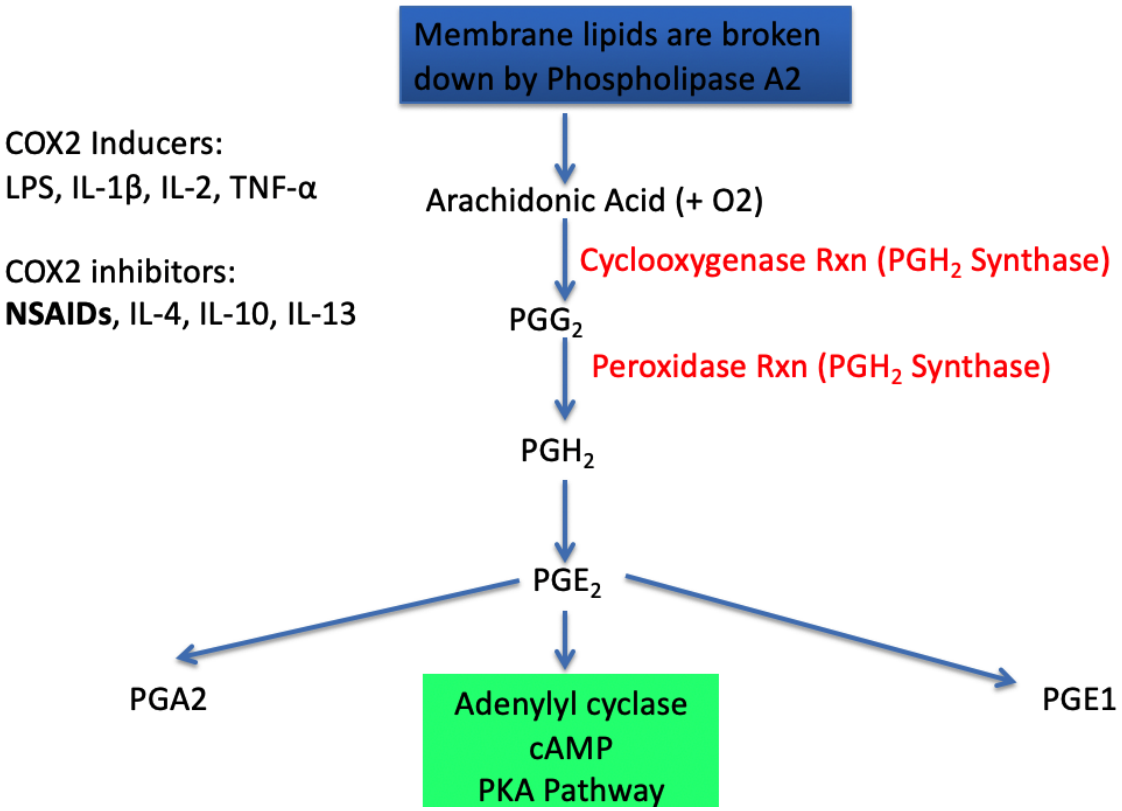

Figure 3. COX-2 induction leads to the production of PGE_2, a potent inflammatory mediator. COX is the rate limiting step in the production of prostaglandins (PGs). After nerve injury, arachidonic acid is released from cell membranes, ultimately leading to the induction of COX-2 and subsequent PGE2 production.

1.5 Celecoxib-loaded nanomedicine

Dr. Jelena Janjic (Duquesne University Graduate School of Pharmaceutical Sciences) has developed theranostic nanoemulsions that can treat neuropathic pain[71-73]. Theranostic nanoemulsions have a drug-loading capability (and thus act as a therapeutic) and can also carry a near infrared fluorescent dye (NIRF) as a diagnostic to see where the packaged particle is delivered to after intravenous tail vein administration[46, 48, 49, 71, 73]. CXB is a selective COX-2 inhibitor (**Figure 4**) that attenuates COX-2 activity leading to a reduction in PGE2 production[46, 48, 71]. When CXB is packaged in a nanoemulsion (~140 µm in size) and delivered intravenously, the droplets are directly phagocytosed by

circulating monocytes, which then accumulate as macrophages at the site of injury. The effect on CCI pain relief for the CXB nanoemulsion represents a 2000-fold reduction in CXB dosage[46, 48] as compared to oral CXB studies[57].

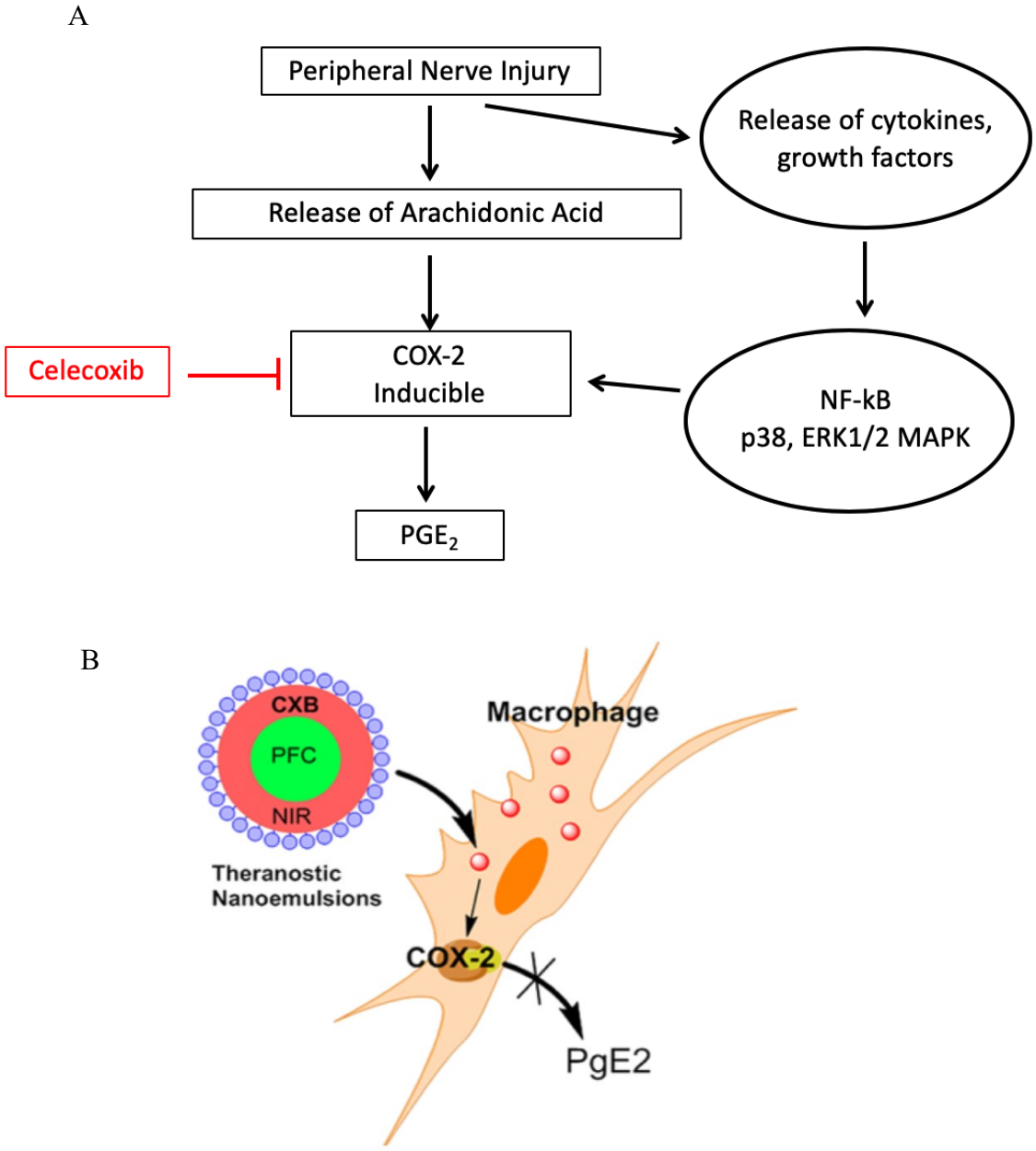

Figure 4. The mechanism of Celecoxib-loaded nanoemulsion. Celecoxib (CXB) inhibits COX-2 production. (A) COX-2 is induced during neuroinflammation and can be selectively inhibited by Celecoxib, preventing PGE_2 production. (B) The Janjic group has designed and developed a perfluorocarbon (PFC) theranostic nanoparticle, which can be loaded with a therapeutic agent (in this case Celecoxib) and a near infrared red (NIR) dye that is phagocytosed by circulating monocytes. Image courtesy of Jelena Janjic.

Janjic and co-workers demonstrated feasibility of targeting cyclooxygenase-2 (COX-2) enzyme in macrophages both in vitro and in vivo [48, 71, 73]. A single dose of CXB-NE (0.24 mg/kg of celecoxib) provided pain relief for up to 6 days in the CCI rat [46, 48]. The same nanoemulsions have been loaded with NIRF dye allowing for the visualization of inflammation at the site of injury in vivo[46, 74]. Previous work (in conjunction with my work) has observed that at the site of injury there is a reduction in inflammation as visualized in live animals by near infrared fluorescence (NIRF)[46-48] and a significant reversal in pain-like behavior[46, 49,71]. With immunohistochemical studies, the Pollock laboratory noted a nearly 50% reduction in the density of infiltrating macrophages at the site of injury when CXB-NE is given compared to CCI DF-NE animals[46, 47]. Within the DRG, a macrophage reduction was also seen on day 12, however, macrophage density was 40% less compared to the injured sciatic nerve, with the most dramatic reduction seen in macrophage density on day 18 within the DRG[47]. Furthermore, for the macrophages that remain in the injured sciatic nerve even while treated with celecoxib-loaded nanoemulsion (CXB-NE), there was a reduction in PGE_2 production[46, 48] and a shift in M1 to M2 polarity[46]. A reduction in mast cell numbers as well as a reduction in mast cell degranulation[46] when CXB-NE is present has also been shown.

1.6 Gene expression changes as a driver of chronic pain

Ultimately, nerve damage leads to changes in expression of genes involved in nociception. Furthermore, the interplay between the gene expression changes within damaged neurons, resident and hematogenous immune cells, and the immune-like glial

cells is known to exacerbate the heightened nociceptive response. These dynamic neuroimmune interactions appear to be responsible for neuropathic pain[9, 40, 75].

The three-way communication and mutual activation of the neurons, glia and immune cells drives subsequent changes in intracellular signaling pathways[26] and additional changes in gene expression[76]. Gene expression changes are not restricted to the site of injury on the sciatic nerve but are also evident proximally in the cells of the DRG[47, 49]. For example, Vasudeva et al. (2014)[47] has previously shown GAP43, NPY and TRPV1 mRNA expression changes in the DRG and furthermore, that TRPV1 protein expression changes in specific CCI DRG cell bodies of neurons that innervate the affected foot (identified by DiD retrograde labeling)[47]. In other studies, qPCR of mRNA expression in the injured sciatic nerve for 84 neuroinflammatory genes revealed several distinct differences between naïve, CCI and CCI treated with pain-relieving therapy[49]. Changes in the expression of mRNAs for cytokines and chemokines is consistent with the inflammation and corresponding infiltration of macrophages at the site of injury (MCP-1, IL-18, IL-1β)[20, 46].

1.7 Specific Aims

To investigate the molecular cell biology of chronic pain from chronic constriction injury and the effects of the targeted celecoxib therapy, I have assessed RNA changes in the injured sciatic nerve and the DRG. I hypothesized that injured CCI animals given CXB-NE will exhibit changes in RNA expression 12 days post-injury compared to CCI given DF-NE as well as sham and naïve negative controls that are involved in the production of inflammatory mediators, and neuroinflammatory and pain

response. Furthermore, I also hypothesized that attenuation of this cross-talk would result when COX-2 inhibition is targeted to a single cell type – the macrophage. COX-2 inhibition in macrophages using CXB-NE would influence cells within and near the site of injury would lead to the alleviation of pain behavior noted in injured animals.

Each of the specific aims follows the same schedule of experiments as noted in **Figure 5**. CCI and sham surgeries are performed on day zero, mechanical allodynia behavioral testing (described in Section 2.3) is performed consecutively 1 day after surgery until euthanasia and tissue collection on day 12. In addition, nanoemulsion injection (described in brief in Section 2.4 and in detail in Section A.2) is conducted one-week post-surgery and LiCOR live animal imaging is performed on days 8 and 11 (described in Section 2.5).

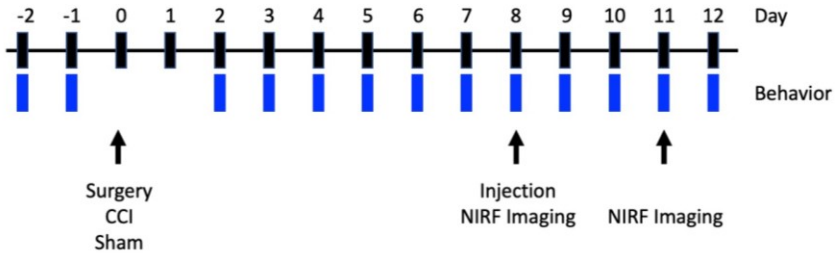

Figure 5. Sequence of experimental events. CCI/sham surgeries are performed on day zero, behavioral testing on days 1-12, tail-vein injection of nanomedicine on day 8, and live animal imaging on day 11.

Specific Aim 1: Evaluate differences in mRNA expression in the sciatic nerve in response to peripheral nerve injury and celecoxib-loaded nanoemulsion (CXB-NE) therapy at day 12 post chronic constriction injury using a quantitative PCR gene array.

First, I assessed mRNA expression in the injured sciatic nerve through quantitative PCR of a collection of 84 genes associated with neuroinflammation. In this

study, I evaluated the molecular expression changes at the site of injury on day 12 post-CCI surgery, a time of significant pain-like hypersensitivity for untreated animals or maximum pain relief for treated animals. Comparison of the expression profiles of mRNAs in the injured nerve to mRNA from comparable sciatic nerve were acquired from sham surgical animals as well as CCI animals treated with nanoemulsion containing celecoxib (CXB-NE) or vehicle nanoemulsion that is drug free (DF-NE). Here I hypothesized that by inhibiting COX-2 and by attenuating the production of PGE_2 in circulating monocytes and tissue macrophages, there would be a subsequent change in macrophage signaling, including integrins, cytokines, and the involvement of other cell types that participate in releasing inflammatory mediators at the site of injury that leads to decreased pain behaviors when administered at a chronic pain state in rats. In addition, I believed signaling involved in neuro-immuno-glial cross-talk would be dampened at the site of injury indicated by a decrease in expression of the genes involved in these pathways. To further understand changes in key macrophage-related genes, immunohistochemistry of the macrophage marker CD11b was assessed within the site of injury using confocal microscopy.

I was able to demonstrate significant changes in the neuroinflammatory mRNAs present within the injured sciatic nerve including genes associated with macrophages as well as neurons and Schwann cells among other cell types in this study. This research illustrates the need to better understand the molecular mechanisms involved in this neuroinflammatory-mediated multi-cellular response, and how by inhibiting only COX-2, we are able to alter the expression of several genes at the site of injury while changing the pain-like behavior state.

Specific Aim 2: Assess the transcriptome of RNA expression changes in the dorsal root ganglia (DRG) under the same conditions of Aim 1 using RNA Sequencing.

Within the corresponding DRG are the cell bodies for the injured axons found within the sciatic nerve, as well as infiltrating immune cells and glial cells. Thus, gene expression profiling of RNAs differentially expressed here may shed light on the molecular phenomena occurring at the site of injury on the one hand as well as the basis of the neurophysiological signaling associated with hypersensitivity, which is sent on to the central nervous system. RNA sequencing of L4-L5 DRGs allow for the exploration of the molecular and biological mechanisms of neuropathic pain through the analyses of whole transcriptome changes after nerve injury. RNA sequencing of L4-L5 DRGs allow for the exploration of the molecular and biological mechanisms of neuropathic pain through the analyses of whole transcriptome changes after nerve injury. Using RNA sequencing, several studies have previously examined pain-associated changes in expressed RNA in the DRG[24, 77-79]. Here I hypothesized that ultimately, the inflammatory milieu and tissue response at the site of injury would be communicated to the DRG where changes in expression profiles are of particular importance given that these cells are a component of primary sensory neurons, acting as the bridge between the peripheral and central nervous system. I have reported differential expression of the RNA transcriptome in the cells of the DRG when the animal is experiencing significant pain as compared to a naïve normal and also CCI animals under the influence of an anti-inflammatory pain-relieving celecoxib nanoemulsion. The pain-relieving therapy relies on reducing prostaglandin E_2 (PGE_2). By utilizing high throughput RNA sequencing, we reveal transcriptome changes in the DRG associated with the celecoxib-nanoemulsion pain-

relief in males. I find differential expression of RNAs associated with neurons, activated glial cells, multiple immune cells, as well as inflammatory mediators. Additionally, while I confirm a subset of genes previously reported in literature that are known to respond to drug therapy[80, 81], I go on to reveal genes differentially expressed that have not been previously identified as 'pain' genes. RNAs described in this study are inclusive of both protein-coding and non-protein-coding, including annotated long non-coding RNAs (lncRNAs) and microRNAs (miRNAs).

Chapter 2: Methods

As adapted from:

A. Stevens, L. Liu, D. Bertovich, J.M. Janjic, J.A. Pollock. Differential expression of neuroinflammatory mRNAs in the rat sciatic nerve following chronic constriction injury and pain-relieving nanoemulsion NSAID delivery to infiltrating macrophages. *International Journal of Molecular Sciences* 2019; 20(21): 5269. Doi.org/10.3390/ijms20215269.

A. Stevens, M. Saleem, B. Deal, J.M. Janjic, J.A. Pollock. Targeted COX-2 inhibiting nanomedicine results in pain-relief and differential expression of RNA in the dorsal root ganglia of injured male rats. *Molecular Pain In Press* 2020.

M. Saleem*, **A. Stevens*,** B. Deal, L. Liu, J. M. Janjic, J. A. Pollock. A new best practice for validating tail vein injections in rat with near infrared labeled agents. *Journal of Visualized Experiments* 2019; e59295. *Co-authors contributed equally.

Further contributions:

The University of Pittsburgh Genomics Research Core (Dr. Janette Lamb and colleagues) performed RNA sequencing of L4-L5 DRG RNA for the three conditions tested.

The University of Pittsburgh Genomics Analysis Core (Dr. Uma Chandran and colleagues) performed differential expression of data obtained from RNA sequencing.

2.1 Animals and Ethics Statement

Adult male Sprague-Dawley rats (Hilltop Animals, Springdale, PA) weighing 225-250 g at the time of surgery were used in all protocols that were performed in accordance with the guidelines outlined in the Guide for the Care and Use of Laboratory Animals of the National Institutes of Health and the regulations of the Institutional Animal Care and Use Committee (IACUC) at Duquesne University and the approved protocol #1501-01. Animals were acclimated to standard living conditions and kept on a 12-hour light, 12-hour dark cycle and given food and water ad libitum. Animals were socially housed, kept on paper bedding, and given special diet (Research Diets, Inc, New Brunswick, NJ; catalog #AIN-93G) to avoid autofluorescence during imaging. Efforts were made to minimize the number of animals used and the time experiencing pain. The sample size was calculated based on power analysis of our previous work and the statistical significance of the data accumulated in the various tests applied to each animal and its recovered tissues. Specific Aim 1 (corresponding Chapter 3) used 3 to 8 animals per condition and Specific Aim 2 (corresponding Chapter 4) used a sample size of 3-4 per condition.

2.2 Chronic Constriction Injury (CCI)

Chronic constriction injury (CCI) was performed[13,46-48] as it emulates peripheral neuropathic pain by causing intraneural edema at and around the common sciatic nerve. Briefly, animals were anesthetized using respiratory isoflurane. All surgical procedures were performed under aseptic conditions. The biceps femoris and gluteus superficialis muscles were exposed and separated on the hindleg, followed by exposure and isolation

of the sciatic nerve. Four chromic gut sutures were loosely ligated around the common sciatic nerve, separated by 1 mm gaps. The muscle and skin layers were then closed. In this procedure, chromic gut sutures contribute to the neuroinflammatory response. In sham control animals, the common nerve is exposed and isolated, but no sutures were used. Naïve controls received no surgical intervention.

2.3 Behavioral testing

Mechanical allodynia testing was conducted two days prior to surgery and the following days post-operatively, days 3, 4, 5, 8, 11, and 12. All behavioral testing was conducted blinded to surgery and treatment. Testing was performed in naïve, sham, CCI CXB-NE, and CCI DF-NE rats using the up-down method as described previously[46, 82, 83]. Calibrated Semmes-Weinstein von Frey monofilaments were applied to the plantar surface of the right and left hind paws in the region innervated by the common sciatic nerve. The monofilaments were applied in ascending order of gram force ranging from 0.41 to 15.13 gram force. The 50% paw withdrawal threshold was calculated using the median lethal dose (LD50), and treatment groups were analyzed by two-way ANOVA and Tukey's post-hoc test using GraphPad Prism 8.0 [46].

2.4 Intravenous tail vein injections (See Appendix A for detailed protocol)

The celecoxib loaded nanoemulsion (CXB-NE) and the drug-free nanoemulsion (DF-NE)[84, 85] were injected intravenously through the right lateral tail vein on day 8 post-surgery[74]. Rats were lightly anesthetized with isoflurane and given 0.24 mg/kg of celecoxib nanoemulsion (or drug-free vehicle) using a 27-gauge needle. By near infrared

imaging of the tail vein before and after injection, we can establish whether the injection was optimal (injected directly into the tail vein and little residual fluorescence is shown) or suboptimal (injected subcutaneously with a high degree of fluorescence in the tail)[74]. When injected into the bloodstream, the nanoparticle is phagocytosed by circulating monocytes and naturally delivered to the site of injury, which has been confirmed in previous studies, where those cells differentiate into tissue macrophages[46-48].

2.5 Near Infrared Fluorescence (NIRF) Imaging

On day 11 post-surgery, live NIRF imaging was conducted on lightly anaesthetized (1.5% Isoflurane) rats. The left and right hindlegs were imaged on the LiCOR Pearl Impulse Small Animal Imager (Lincoln, NE). Near infrared dye accumulates at the site of injury superficial to the site of incision on the hindleg as it picked up by monocyte-derived macrophages[47]. Images are acquired in the 700 nm channel and a white light channel (to reveal the animal's posture) and analyzed with LiCOR Image Studio Lite (version 5.0) as based on previous studies[47]. A hand-drawn region of interest (ROI) is drawn over the sciatic nerve region on the hindleg and relative fluorescence is calculated (total fluorescence divided by area within the ROI) and normalized to background.

2.6 Tissue Dissection and Preparation for Histology or RNA Studies

Rats were euthanized by CO_2 asphyxiation in a chamber on day 12. For Specific Aim 1 (corresponding Chapter 3), right and left sciatic nerves were dissected immediately upon euthanasia. Sciatic nerve tissues for immunohistochemistry were post-fixed in 4% paraformaldehyde (PFA), moved to 0.4% PFA after 24 hours, and within 1 week, placed

in a 30% sucrose 1X PBS solution before being mounted in OCT medium and cut longitudinally in 20 µm sections. Sciatic nerve tissue for RNA studies were not fixed, but immediately transferred to RNAlater (Life Technologies, New York) and kept at -20°C until RNA extraction was performed. For Specific Aim 2 (corresponding Chapter 4), lumbar level 4 and 5 (L4 and L5) dorsal root ganglia (DRG) were collected immediately following euthanasia, transferred to RNAlater and kept at -20°C until RNA extraction was performed.

2.7 RNA extraction and cDNA conversion

Total RNA was extracted from intact ipsilateral and contralateral sciatic nerves and DRG using the RNAeasy Plus Mini Kit (Qiagen) according to the kit's instructions. Tissue disruption and homogenization was done with a mortar and pestle and then with QiaShredder columns (Qiagen). RNA quality and concentration were assessed on the NanoDrop 1000 Spectrophotometer (Thermo Fisher Scientific, Delaware) and was determined by running a sample with RNA loading dye (Ambion, USA) on a 1% agarose gel and inspecting for distinct 18S and 28S bands, indicating lack of degradation. Quantity was determined by A260/A280 measurement. All samples had A260/A280 ratios of 1.9−2.3. Total RNA was used for complimentary DNA conversion by the RT^2 First Strand Kit (Qiagen). Three to eight animals per condition were used. For RNA sequencing tissues (Chapter 3), RNA quantification was performed using a Qubit (Thermo Fisher Scientific, USA) and integrity was measured with Tape Station (Agilent, USA). Only RNA samples with a minimum RNA integrity number (RIN) value above 6.6 were used for sequencing[248].

2.8 Quantitative PCR and Analysis

For Specific Aim 1 (Chapter 3), RT^2 RNA Quality Control PCR Array (Qiagen, PARN-999Z) was used to assess each sample prior to gene expression profiling. Gene expression profiling was analyzed by RT^2 Rat Neuropathic and Inflammatory Pain Arrays (Qiagen, PARN-162Z) on the ABI StepOnePlus cycler (Applied Biosystems, USA) with RT^2 SYBR green with ROX (Qiagen) according to manufacturer's instructions. Each array contains 84 genes related to neuropathic pain and inflammation (**Table 5**), 5 housekeeping genes, and 7 controls. Each array was performed in triplicate and normalized to Rplp1 in the sciatic nerve or Gapdh in the DRG.

Data presented in Chapter 3 [49] was initially analyzed with Qiagen's RT^2 profiler PCR Array Data Analysis software. A list of differentially expressed genes was identified using a 2-tailed Student's t-test. Changes in gene expression between the pain group and the control group were illustrated as a fold increase/decrease (shown as fold regulation) and were considered to be upregulated/downregulated, respectively. The criteria were a P value <.05 and a mean difference equal to or greater than 2-fold. Next, a subset of differentially expressed genes were further analyzed by individual RT^2 primer assays (Qiagen) following the Livak method[86]. Fold change values were calculated compared to the sham control group. A 2-tailed Student's t-test, standard deviation and error were calculated. The results were expressed as means with standard deviations. For the significance test, a one-way analysis of variance followed by post hoc testing and Tukey's multiple comparison test with GraphPad Prism (version 7.3, San Diego, CA). A P value ≤ 0.05 was considered statistically significant in all analyses.

2.9 Immunohistochemistry and Microscopy

For Specific Aim 1 (Chapter 3), sciatic nerves from naïve, CCI CXB-NE, and CCI DF-NE rats (3 per condition) were used for immunohistochemistry to explore the CD68 macrophage (Abcam, ab125212, 1:100), and CD11b (Life Technologies, MA181606, 1:100) macrophage infiltration. Tissue sections were post-fixed in 4% PFA solution in 1X PBS, permeabilized with 0.3% Triton X-100 solution, blocked with 1X PBS normal donkey serum, and stained with primary and secondary antibodies. The sections were washed and incubated overnight with secondary 1:200 Alexa Fluor antibodies (Invitrogen, Carlsbad, CA) and then washed and mounted with Prolong Gold DAPI nuclear stain (Invitrogen). All stained sections were viewed on the Nikon Eclipse Ni-U microscope and images were acquired with the Nikon NIS-Elements software.

2.10 RNA Sequencing and Analysis

For Specific Aim 2 (Chapter 4), to determine genes involved in the neuroinflammatory response perpetuated by chronic constriction injury (CCI) in receiving celecoxib-loaded nanoemulsion (CXB-NE) versus those receiving vehicle (DF-NE), total RNA from pooled L4 and L5 DRGs from an individual animal was analyzed using an Illumina sequencer 12 days after CCI surgery. Library preparation was performed according to manufacturer's instructions using the Takara SMARTer Stranded Total RNA-Seq Kit, Pico input Mammalian v1 (Mountain View, CA), with two ng total RNA input. Total RNA is converted to cDNA via reverse transcription with random hexamers and proprietary code-switching technology maintained the RNA strand information. Five cycles of PCR added barcode sequencing indexes followed by double

SPRI size selection. Ribosomal cDNA was depleted via the cleavage with Zap-R and mammalian specific R-probes. Remaining library was enriched with twelve cycles PCR followed by SPRI bead reaction clean up. Library was loaded on a NextSeq500 (Illumina, USA) at 1.8 pM with 20% Phi-X. The sequences were trimmed and reads with a minimum of 75 base pairs were used. RNA sequencing was performed by the Genomics Research Core at the University of Pittsburgh.

The resulting sequencing data were mapped to the Rattus norvegicus reference genome from ENSEMBL using HISAT whole genome and SALMON whole transcriptome mapping. Reads per kilobase per million (RPKM) mapped reads were calculated for each gene hit count to determine expression levels. Relative differential expression analysis for each transcript between the groups was calculated as the number of readings mapping to each transcript normalized by the transcript length and the total number of mapped reads using Student's t-test. Differential expression analysis was done in conjunction with the Genomics Analysis Core at the University of Pittsburgh. Heatmaps were generated using Prism 8 Version 8.4.2. Genes with expressed RNAs shared between all three conditions (Naïve, CXB-NE, and DF-NE) and 57 genes that had an FDR ≤ 0.05 and considered to be statistically significant amongst the three conditions were mapped with the Log_2 of the counts per million (CPM).

2.11 Gene Ontology and Enrichment Analysis

For Specific Aim 2 (Chapter 4), genes previously annotated based on relevant functional gene ontology descriptions were compared to our dataset using Gene Ontology (GO) database. Gene Ontology (GO) annotations and functional enrichment analysis

were applied to investigate the roles of all differentially expressed genes between CCI DF-NE and CCI CXB-NE animals. PANTHER pathway analysis based on functional classifications and GO analysis hierarchical categories according to the Biological Process, Molecular Function, and Cellular Components of the differentially expressed RNAs (http://www.pantherdb.org) of FDR ≤0.05 were used in **Figure 3**. Reactome pathway analyses were also applied (FDR ≤0.05) (http://www.reactome.org) to elucidate annotated pathways involved in the pain state when CXB-NE is administered compared to DF-NE to the pain state.). KEGG Pathway functional analysis was performed using g:Profiler (version e99_eg46_p14_f929183) with a g:SCS multiple testing correction method applying a significance threshold of 0.05 [247]. All differentially expressed genes were applied to the Gene Expression Database (http://informatics.jax.org) to further demonstrate their individual roles in the maintenance and transduction of neuropathic pain under CCI conditions when COX-2 is attenuated in circulating monocytes.

2.12 Literature search of neuroinflammatory genes

A comprehensive literature search containing the search term chronic constriction injury (CCI), celecoxib, and each term category in Chapter 5 was conducted in peer-reviewed primary literature databases (PubMed, Science Direct, PubMed Central, amongst others). In addition, the Gene Expression Database and Gene Ontology (GO) PANTHER database were both utilized for gene function.

2.13 Validation of RNA Sequencing by Quantitative Real-time PCR

For Specific Aim 2 (Chapter 4), the extracted total RNA from the DRGs was reverse transcribed into cDNA using RT^2 First Strand Kit (Qiagen, Germantown, MD, USA) according to the manufacturer's instructions. Quantitative PCR (qPCR) using pooled L4 and L5 DRG tissues from rats from the RNA sequencing study and additional rats were used. qPCR was performed using individual RT^2 primer assays (Qiagen) on the ABI StepOnePlus cycler (Applied Biosystems, USA) with RT^2 SYBR green with ROX (Qiagen) according to manufacturer's instructions. Each reaction was performed in triplicate and normalized to the housekeeping gene Gapdh. Analysis was done using the Livak method[86] where fold change values were calculated compared to the naive control group. A 2-tailed Student's t-test, standard deviation and error were calculated. A one-way analysis of variance followed by post hoc testing and Tukey's multiple comparison test with GraphPad Prism (version 8, San Diego, CA). A P value ≤ 0.05 was considered statistically significant in all analyses.

Chapter 3: Differential expression of neuroinflammatory mRNAs in the rat sciatic nerve following chronic constriction injury and pain-relieving nanoemulsion NSAID delivery to infiltrating macrophages

Andrea M. Stevens, Lu Liu, Dylan Bertovich, Jelena Janjic, and John A. Pollock.

Full citation:

A. Stevens, L. Liu, D. Bertovich, J.M. Janjic, J.A. Pollock. Differential expression of neuroinflammatory mRNAs in the rat sciatic nerve following chronic constriction injury and pain-relieving nanoemulsion NSAID delivery to infiltrating macrophages. *International Journal of Molecular Sciences* 2019; 20(21): 5269. Doi.org/10.3390/ijms20215269.

This work has been published in the Special issue *Neuroimmune Interactions* of the journal *International Journal of Molecular Sciences*. Additional supplemental data is presented in this version.

3.1 Contributions Statement

Andrea Stevens did all work in this chapter except where noted below:

Dylan Bertovich, PURE Undergraduate Research student in Dr. John A. Pollock's laboratory, contributed to Figure 7, in which he was responsible for staining tissues and assisted in creating the figure.

Lu Liu, Graduate Student in Dr. Jelena Janjic's laboratory; preparation of nanoemulsion preparation and contributed to NIRF imaging.

Jelena Janjic, Associate Professor in Graduate School of Pharmacy at Duquesne University and co-founder of Duquesne University's Chronic Pain Research Consortium, together with Dr. Pollock, jointly designed the experimental approach for evaluating nanoemulsions in the CCI rat model for effects on neuropathic pain. Dr. Janjic conceived and designed the overall macrophage-targeted drug delivery approach with nanoemulsions, the nanoemulsion composition and processes for fabrication.

John A. Pollock, Professor of Biology and Principle Investigator, jointly designed the approach to assess the differential expression of mRNAs (with Andrea Stevens); all experiments were performed by Andrea Stevens under the guidance of John A. Pollock.

Original draft preparation by Andrea Stevens, additional writing and review was by all authors.

3.2 Introduction

Peripheral nerve injury underlying neuropathic pain affects over 100 million Americans and costs roughly $600 billion annually[2]. This type of injury can be modeled in small animals with chronic constriction injury (CCI) of peripheral nerves and is known to result in spontaneous pain-like behavior including amplified responses to painful

stimuli (hyperalgesia), non-painful stimuli (allodynia) and thermal hypersensitivity[13,46,47]. Peripheral nerve injury is characterized by a complex molecular and cellular response, consisting of two main components. First, the injury is associated with a change in the immune cell microenvironment surrounding the damaged neurons leading to a local response known as neuroinflammation[5,9]. Second, healing and axon regeneration are engaged[10,11]. The initial immune response consists of infiltration of immune cells to the site of injury at the sciatic nerve, activation of immune and glial cells, and Wallerian degeneration of distal nerve fibers[87-89]. This process includes the recruitment of circulating monocytes to the site of injury, which release pro-inflammatory cytokines, chemokines, trophic and growth factors that cause neuronal hypersensitivity in the periphery[90]. The neurons themselves exhibit neuronal plasticity[91] leading to spontaneous firing, decrease in threshold, and an increase in responsiveness. Schwann cells along the injured axons dedifferentiate into an activated state where they switch from a myelinating phenotype to a phagocytic cell type, similar to macrophages. In addition, the injured neurons and Schwann cells produce and release inflammatory mediators[92] such as cytokines, chemokines, neurotrophic factors, Substance P, and prostanoids that all contribute to the neuroinflammatory milieu.

Monocyte-derived macrophages are known to play a role in peripheral nerve injury at the site of injury in the sciatic nerve and later at the level of the neuronal cell bodies in the dorsal root ganglia[40, 46, 51-53]. These hematogenous macrophages accumulate preferentially around injured axons[36] guided by molecular cues such as monocyte chemoattractant protein-1 (MCP-1)[54], the lesser studied monocyte chemoattractant protein-5 (MCP-5), and the leukocyte adhesion complex of MAC1, which is formed by

the integrins, ITGAM/CD11b and ITGB2/CD18[55]. Together with injured axons and activated Schwann cells, the infiltrating immune cells (macrophages, T cells, mast cells, and neutrophils) are crucial for normal function and recovery after nerve injury [40,93]. Each cell type appears to exhibit profiles of gene expression that contribute to the production of inflammatory mediators that further influence the neuropathic pain state[30, 31, 94, 95] . Schwann cells at the site of injury through the distal nerve dedifferentiate by altering gene expression[94]. Within two days of chronic constriction injury, the Schwann cells stop producing myelinating proteins, and in turn, increase the expression of regeneration-associated genes such as GAP-43, neurotrophic factors and their receptors like GDNF, and cytokines such as IL-6[89]. Hematogenous macrophages also produce the pro-inflammatory cytokine IL-6 and increase expression of cyclooxygenase 2 (COX-2), which produces prostaglandin E_2 (PGE_2), all of which contribute to the inflammatory response [32, 51].

Janjic and co-workers demonstrated feasibility of targeting cyclooxygenase-2 (COX-2) enzyme in macrophages using cell specific delivery with near infrared labeled nanoemulsion (NE) loaded with non-steroidal anti-inflammatory (NSAID) drug, celecoxib (CXB)[71, 73]. The celecoxib loaded nanoemulsion (CXB-NE), when administered to CCI rats leads to significant reversal in pain-like behavior [46,71]. CXB-NE selectively inhibits COX-2 enzyme leading to dramatically reduced production of PGE_2 in monocyte-derived macrophages at the site of injury[48, 71-73]. Not only does the single dose of CXB-NE (0.24 mg/kg of celecoxib) provide pain relief for about 6 days, we have observed that at the site of injury there is a reduction in inflammation as visualized in live animals by near infrared fluorescence (NIRF), as well as histologically visualized

reduction in the density of infiltrating macrophages at the site of injury[46, 48]. Furthermore, for the macrophages that remain in the injured sciatic nerve even while treated with celecoxib-loaded nanoemulsion (CXB-NE), there is a reduction in PGE_2 production[46, 48] and a shift in M1 to M2 polarity[46]. We also seen a reduction in mast cell numbers as well as a reduction in mast cell degranulation[46].

To further explore the molecular cell biology of the resultant chronic pain and the effects of the targeted celecoxib therapy, we assessed mRNA expression in the injured sciatic nerve through quantitative PCR of a collection of 84 genes associated with neuroinflammation. In this study, we evaluated the molecular expression changes at the site of injury on day 12 post-CCI surgery, a time of significant pain-like hypersensitivity for untreated animals or maximum pain relief for treated animals. We compared the expression profile of mRNAs in the injured nerve to mRNA from comparable sciatic nerve acquired from sham surgical animals as well as CCI animals treated with nanoemulsion containing celecoxib (CXB-NE) or vehicle nanoemulsion that is drug free (DF-NE). We demonstrated significant changes in the neuroinflammatory mRNAs present within the injured sciatic nerve including genes associated with macrophages as well as neurons and Schwann cells among other cell types. Relative to vehicle (DF-NE), the mRNAs expressed in the drug treated (CXB-NE) exhibit decreased expression of seven known neuroinflammatory genes found in various cell types (Grin2b/NMDAR2b, IL-6, Itgam/Cd11b, Maob, Scn9a/Na_v1.7, Tac1, TrpV3) and the increased expression of the neuronal Cacna1b/Ca_v2.2. Many of the changes evident in the sciatic nerve that result from injury and the changes in response to pain reliving therapy, may have their basis in regulated differential expression of key mRNAs. This research illustrates the need to

better understand the molecular mechanisms involved in this neuroinflammatory-mediated multi-cellular response, and how by targeting only one inflammatory mediator, we are able to alter the expression of several genes while changing the pain-like behavior state.

3.3 Materials and Methods (See Chapter 2 and Appendix A for detailed methodology)

3.4 Results

3.4.1 Relief of pain hypersensitivity in the CCI model with a drug-loaded nanoemulsion

First demonstrated by Bennett and Xie[13] chronic constriction injury (CCI) of a peripheral nerve is known to induce hypersensitivity, which is interpreted as neuropathic pain caused by the neuroinflammation. Here we reported that after baseline behavioral testing, CCI or sham surgery was performed on Day 1, followed by behavioral testing daily on days 2 through 12 post-surgery. The effects of celecoxib-loaded nanoemulsion (CXB-NE) treatment on CCI rats was determined by using the paw withdrawal threshold when probed with von Frey filaments of increasing diameter [82, 83]. All CCI animals experienced mechanical allodynia one-week post-injury, with a maximum in pain-like behavior plateauing on day 8 (**Figure 6A**), at which time celecoxib-loaded nanoemulsion (CXB-NE) or drug-free nanoemulsion (DF-NE) is administered by tail vein injection [74]. Data are expressed as the mean +/- SD (n=5 per group). Significance was determined by two-way ANOVA followed by Tukey's post-hoc test (GraphPad Prism, version 7.0; $P \leq 0.05$). No statistically significant difference is evident in the comparison of sham control to the non-surgical naïve animal ($P = 0.185$). Furthermore, no statistically significant

difference was observed between CCI DF-NE animals compared to CCI animals receiving no nanoemulsion at all ($P = 0.083$). A statistically significant difference in allodynia is evident between sham and naïve controls compared to CCI starting on day 5 post-surgery ($P < 0.0001$). One day after the nanoemulsion celecoxib drug therapy, treated animals exhibited a statistically significant reduction in hypersensitivity ultimately to return to a withdrawal latency equivalent to sham/naïve within three days of the tail vein injection. On day 12, the drug treated CCI animals exhibited a statistically significant relief in pain-like behavior as compared to both the CCI DF-NE (vehicle) and the CCI only (no nanoemulsion) animals (0.624, $P < 0.0001$).

The nanoemulsion used in this study acts as both a therapeutic (delivering celecoxib) and diagnostic (loaded with a near infrared dye)[46-48, 71, 74, 84]. Live animal near infrared fluorescent (NIRF) imaging on day 11 demonstrated increased inflammation at the site of injury (**Figure 1A** and **Figure 6A**) as compared to naïve control animals (**Figure 6B**). CCI animals given the drug-loaded nanoemulsion (CXB-NE) exhibited a decreased NIRF signal as compared to DF-NE (**Figure 6D**), indicating a reduction in macrophage infiltration. Macrophages directly influence the milieu of inflammatory mediators such as cytokines and chemokines[20]. Although macrophages and other infiltrating immune cells accumulate at the site of injury post-CCI at day 12, neuronal-centric changes also contribute to the induction and maintenance of pain.

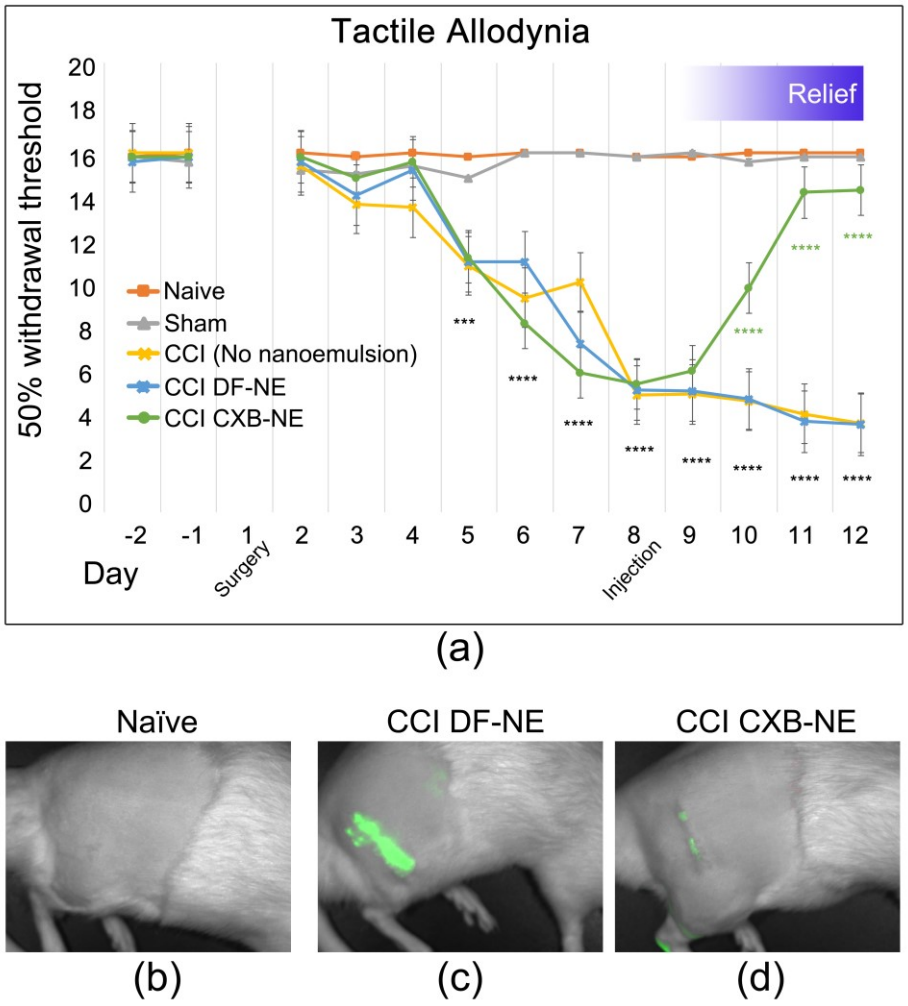

Figure 6. CXB-NE ameliorates mechanical allodynia and inflammation in CCI-induced neuropathic male rats. (a) Mechanical stimulus evokes pain-like hypersensitivity in CCI animals. Treatment with CXB-NE provides a recovery from pain-like behavior comparable to sham and naïve control rats by day 12 (displayed as ****), but not in CCI rats given DF-NE. Data are expressed as a mean +/- SD with a n = 5 per group. Significance was determined by two-way ANOVA followed by Tukey's multiple comparison test ($p < 0.0001$). No statistical significance of difference of sham control compared to naïve, whereas the statistically significant difference is evident in the CCI animals compared to sham controls on days 5 through 8. (b-d) Live animal NIRF imaging on day 11 shows decreased fluorescence in CCI animals treated with CXB-NE (b), compared to those administered DF-NE (c). (d) Non-surgical naïve animals exhibit no fluorescence.

3.4.2 Overview of mRNA expression changes for genes associated with CCI chronic pain

While attenuating COX-2 activity at the site of injury through CXB-NE therapy, we examined the mRNA expression of 84 genes previously identified as associated with

neuropathic and inflammatory pain in the rat (Qiagen, PARN162-Z; **Table 5**). The dissected segment of the injured sciatic nerve includes axon fibers as well as myelinating Schwann cells and dedifferentiated Schwann cells, endothelial cells, and infiltrating macrophages among other activated immune cells. A quantitative analysis of the qPCR C_T values for the mRNAs identified by all 84 genes was carried out using Qiagen's RT^2 Profiler Array Software and displayed as a volcano plot between all data groups (**Figure 7**). This software creates a 'volcano plot,' which displays statistical significance versus fold change, by plotting P-value against the fold regulation change with the significance of the differential expression. Here, fold regulation values greater than 1 indicate increased gene expression, whereas fold regulation values less than zero indicate reduced expression.

In order to visualize gene expression changes of the entire 84 gene set, volcano plots were generated for each pairwise comparison (CCI DF-NE versus sham, CCI CXB-NE versus sham, and CCI DF-NE versus CCI CXB-NE). Illustrated in **Figure 7**, genes displaying statistically significant increased expression are shown in blue while reduced expression is indicated with red. Those that exhibited changes in expression but that are not statistically significant are shown in black. Because the printed graphic cannot support tags that name every data point, the differential expression of all the genes are listed in **Table 1**. Comparing CCI DF-NE animals (pain state) to the sham surgical control reveals that there were 24 of the 84 genes with increased expression and 16 genes with reduced expression (**Figure 7A; Table 1A**). In sham versus CCI CXB-NE animals (pain relieved), 19 genes showed increased expression and 14 exhibited decreased expression (**Figure 7B; Table 1B**). Comparing both CCI conditions (drug free to drug

treated), there were 7 genes upregulated and 1 downregulated (**Figure 7C; Table 1C**). The mRNA expression in sciatic nerve compared between naïve animals, sham surgical animals treated with CXB-NE, and sham surgical animals treated with DF-NE (vehicle), analyzed with one-way ANOVA revealed no statistically significant difference (**Figure 14)**.

Under the influence of immune cells, glia and the neuronal cell bodies in the corresponding dorsal root ganglia, the axons that make up the sciatic nerve exhibit exaggerated responses marked by hyperexcitability as well as changes in local expression of key mRNAs encoding products involved in hyperalgesia pain-like behaviors. For example, Calcitonin Gene-Related Peptide (CGRP) mRNA encodes a calcitonin peptide involved in the maintenance of neuropathic pain[96]. CGRP is significantly reduced in the CCI pain state, but not responsive to the CXB-NE drug therapy (CCI CXB-NE exhibited a fold change of 0.13; CCI DF-NE 0.12 when compared to sham). Similarly, the Neurotrophic receptor tyrosine kinase 1 (Ntrk1) mRNA is also reduced in the CCI pain state, and not responsive to the CXB-NE drug therapy as compared to sham (CCI CXB-NE fold change of 0.17 and CCI DF-NE fold change of 0.13). However, several mRNAs encoding ion channels exhibit significant differential expression in the sham surgical control versus the CCI celecoxib-loaded- (CXB-NE) and vehicle-loaded (DF-NE) nanoemulsions. These include Scn9a (Sodium voltage-gated channel, type IX or $Na_v1.7$), TrpV3 (Transient receptor potential 3), and Cacna1b (Calcium voltage-gated channel alpha 1B or $Ca_v2.2$).

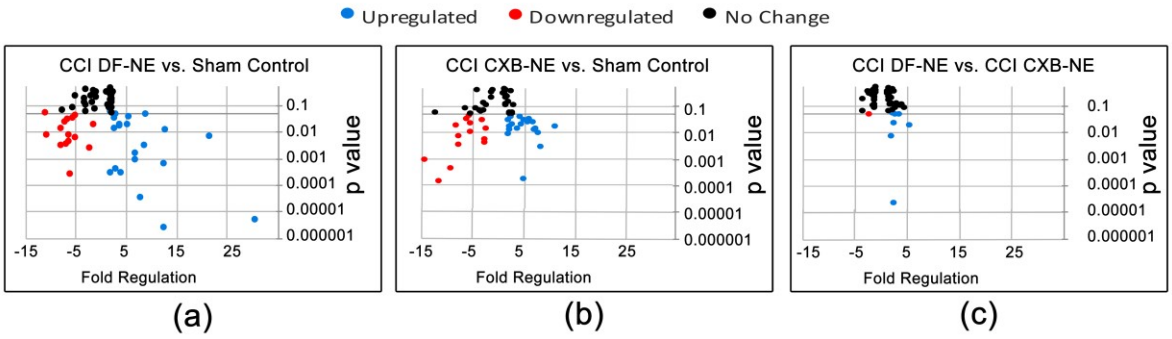

Figure 7. Neuroinflammatory gene expression changes in mRNA of sciatic nerve isolated on day 12 post-CCI injury, four days after nanoemulsion injection. In total, 84 genes associated with neuropathic and inflammatory pain were measured from Qiagen's RT^2 array (PARN-162Z). Qiagen's RT^2 profiler PCR Array Data Analysis software yielded differential expression of genes given as fold regulation in (a) CCI DF-NE compared to sham control, (b) CCI CXB-NE compared to sham, and (c) comparison of the two CCI conditions. Upregulated genes (blue), downregulated genes (red), and unchanged genes (black). P value <0.05, 2-tailed Student's t-test. The differential expression and p values for all genes are listed in Table 1.

Celecoxib selectively inhibits COX-2, blocking prostaglandin synthases [40]. Although induction of COX-2 occurs in multiple cells (Schwann cells, neurons, and macrophages), by directly targeting COX-2 and subsequent PGE_2 production in only invading macrophages, we find that there is a reduction in PGE_2 in the injured sciatic nerve[46,47]. In CCI CXB-NE, there is a marked increased expression in of Prostaglandin receptor 1 (Ptger1; fold change 2.29) and Prostaglandin E Synthase 2 (Ptges2; 2.21 fold change). However, there is no significant changes of expression for Prostaglandin receptors 3 and 4 (Ptger3 and Ptger4) when comparing the pain states with or without drug relative to sham control. Furthermore, no gene expression changes in any of the conditions were noted for other key mediators in the PGE_2 pathway, including Prostaglandin E Synthase (Ptges), Prostaglandin E Synthase 3 (Ptges3), Prostaglandin-Endoperoxide Synthase 1/2 (Ptgs1 also known as COX-1 and Ptgs2 also known as COX-2).

When comparing CCI DF-NE (pain state) to sham, genes that exhibited increases in expression ranged from 1.68 fold for Gdnf to 30.5 fold for Mcp5, whereas downregulated expression ranged from -1.62 fold for Mapk3 to -11.03 Oprk1 (**Figure 7A**). In CCI CXB-NE (pain relief) animals versus sham, 19 genes showed increased expression and 14 exhibited decreased expression, ranging from a fold regulation of 11.02 in Mcp5 to -14.23 in Scn9a ($Na_v1.7$) (**Figure 7B**). Comparing both CCI DF-NE to CCI CXB-NE conditions, there were seven genes with elevated expression in the pain state relative to the drug treated pain-relief state and one gene that exhibited reduced mRNA expression (**Figure 7C**). Gene expression between naïve, sham CXB-NE, and sham DF-NE were compared and showed no statistically significant difference between these controls (See Section 3.6 for supplemental data).

Table 1. Gene list representing volcano plots in Figure 7. Expression changes are represented as fold regulation. Positive values indicate an increased expression, whereas negative values indicate decreased expression. (a) Genes differentially expressed in CCI DF-NE versus sham, (b) genes differentially expressed in CCI CXB-NE versus sham, (c) genes differentially expressed in CCI DF-NE versus CCI CXB-NE. One-way ANOVA with Tukey's post-hoc testing with a P value ≤0.05 was performed.

1. CCI DF-NE vs. Sham

Upregulated CCI DF-NE Gene	Fold Regulation	P Value	Downregulated CCI DF-NE Gene	Fold Regulation	P Value
Actb	6.61	0.0008	Cacna1b	-6.35	0.006
B2m	1.75	0.0002	Calca	-7.91	0.002
Adrb2	4.97	0.017	Cckbr	-6.67	0.02
Ccl12/Mcp5	30.5	>0.00001	Grm1	-6.67	0.02
Ccr2	2.41	0.03	Grm5	-6.42	0.004
Cd4	8.34	0.003	Kcnj6	-7.16	0.02
Cnr2	2.68	0.045	Kcnq3	-5.76	0.03
Comt	2.73	0.0004	Maob	-6.18	0.0002
Cx3cr1	12.47	0.0006	Mapk3	-1.62	0.016
Ednra1	3.59	0.018	Ntrk1	-7.88	0.012
Gch1	3.76	0.0002	Oprd1	-5.03	0.005
Gdnf	1.68	0.059	Oprk1	-11.03	0.048
Il-18	6.57	0.001	Opr1m	-10.85	0.007
Il-1α	8.81	0.04	Penk	-5.21	0.03
Il-1β	21.52	0.006	Ptger3	-2.19	0.002
Il-6	12.5	0.01	Scn9a	-6.89	0.003
Itgam/Cd11b	12.12	>0.00001			
Itgb2/Cd18	11.49	>0.00001			
P2rx4	2.93	>0.00001			
P2rx7	3.5	0.016			
Prok2	5.42	0.03			
Ptger4	2.39	0.013			
Tlr2	12.22	>0.00001			
Tnf	7.76	>0.00001			
Actb	6.61	0.0008			

2. CCI CXB-NE vs. Sham

Upregulated CCI CXB-NE Gene	Fold Regulation	P Value	Downregulated CCI CXB-NE Gene	Fold Regulation	P Value
Actb	8.18	0.002	Cacna1b	-3.03	0.02
B2m	1.84	0.009	Calca	-7.5	0.003
					0.013
Adrb2	4.9	0.02	Edn1	-2.25	0.007
Alox5	2.38	0.03	Grm5	-7.64	0.02
Ccl12/Mcp5	11.02	0.017	Il-2	-5.22	0.04
Ccr2	2.58	0.02	Kcnq3	-5.7	0.00013
Cd4	7.35	0.01	Maob	-11.54	0.003
Comt	1.89	0.03	Mapk3	-2.47	0.003
Cx3cr1	7.78	0.009	Ntrk1	-5.98	0.03
Gdnf	4.51	0.02	Oprd1	-5.31	0.01
Il-18	4.27	0.04	Oprm1	-8.02	0.01
Il-1β	6.06	0.03	Ptger3	-2.46	0.005
Il-6	3.63	0.013	Scn9a	-14.23	0.0009
Itgam/Cd11b	5.06	0.0001	Trpv3	-9.12	0.0004
Itgb2/Cd18	6.84	0.02			
P2rx4	2.28	0.01			
Ptger1	2.29	0.01			
Tlr2	7.12	0.01			
Tnf	5.64	0.02			

(C) CCI DF-NE vs. CCI CXB-NE

Upregulated CCI DF-NE Gene	Fold Regulation	P Value	Downregulated CCI DF-NE Gene	Fold Regulation	P Value
Grin2b	2.37	0.021	Cacna1b	-2.1	0.04
Il-6	3.44	0.04			
Itgam/Cd11b	2.39	>0.00001			
Maob	1.87	0.007			
Scn9a	2.06	0.05			
Tac1	2.69	0.04			
Trpv3	5.33	0.01			
Grin2b	2.37	0.021			

3.4.3 Altered expression of key mRNAs involved in neuroinflammation

By day 12; four days after the nanoemulsion injection, the drug treated animals behave as the sham and naïve, exhibiting no hypersensitivity while the vehicle treated animals exhibit un-abated hypersensitive pain-like behavior (**Figure 6A**). Each of the neuroinflammatory genes differentially expressed in the array are listed in **Table 2,**

Table 3, and Table 4 according to their cell-specific expression based on past pain-related studies in the literature. Each of the tables illustrates known roles for the described genes based on a literature review from PubMed. The differential RNA expression fold change described is from the data contained in this report for the analysis of the Neuropathic and Inflammatory pain RT^2 array. Fold change of CCI CXB-NE rat sciatic nerve mRNAs relative to sham control and fold change of CCI DF-NE mRNAs relative to sham control were analyzed with Qiagen's RT^2 profiler PCR Array Data Analysis software, where statistically significant differentially expressed mRNAs were identified using a 2-tailed Student's t-test, with a P value <0.05, as calculated by the Qiagen software. Changes in gene expression between the pain group and the control group are illustrated as a fold increase/decrease and are considered to be upregulated/downregulated, respectively. Genes previously associated with expression in neurons, Schwann cells, circulating monocytes, macrophages, and T cells (citations noted in the **Tables 2, 3 and 4**) are found to be expressed at high levels in the pain state in the present study. Additionally, a superset of this data can be found in **Table 1. Table 2 and Table 3** list differential expression revealing that eighteen of the 84 genes that were previously reported as exhibiting neuronal expression are affected by our treatments. Additionally, 6 genes are associate with immune cell, and another 15 of the differentially expressed mRNAs are typically found in multiple cell types that include Schwann cells, endothelial cells, and neuronal cells, all exhibiting elevated expression in the pain state.

Table 2. Differential expression of mRNAs typically associated with neurons.

Gene Symbol	Gene Description	Fold change relative to sham for CCI DF-NE	Fold change relative to sham for CCI CXB-NE	GenBank	Citation
Actb[1]	Beta-actin	6.61	8.18	NM_031144	97
Cacna1b/$Ca_V2.2$	Calcium channel, voltage-dependent, N type, alpha 1B subunit	0.16	0.33	NM_147141	98
Calca/CGRP	Calcitonin-related polypetide alpha	0.12	0.13	NM_017338	99,100
Comt	Catechol-O-methyltransferase	2.73	1.89	NM_012531	101, 102
Ednra	Endothelin receptor type A	3.59	0.44	NM_012550	103
Grm1	Glutamate receptor, metabotropic 1	0.15	Not detected	NM_017011	104
Grm5	Glutamate receptor, metabotropic 5	0.16	0.13	NM_017012	105
Kcnj6	Potassium inwardly-rectifying channel, subfamily J, member 6	0.14	Not detected	NM_013192	106
Kcnq3	Potassium voltage-gated channel, KQT-like subfamily, member 3	0.17	0.18	NM_133322	105, 106
Ntrk1/TrkA	Neurotrophic tyrosine kinase receptor, type 1	0.13	0.17	NM_021589	107, 108
Oprd1	Opioid receptor, delta 1	0.2	0.19	NM_012617	109
Orpk1	Opioid receptor, kappa 1	0.09	Not detected	NM_017167	109
Oprm1	Opioid receptor, mu 1	0.09	0.12	NM_013071	109
P2rx4	Purinergic receptor P2X, ligand-gated ion channel 4	2.96	2.28	NM_031594	110
Scn9a/$Na_V1.7$	Sodium channel, voltage-gated, type IX, alpha	0.15	0.07	NM_133289	111
TrpV3	Transient receptor potential cation channel, subfamily V, member 3	Not detected	0.11	NM_001025757	112-114

[1] Denotes genes individually analyzed by qPCR.

Ten of the differentially expressed genes that are revealed by the Qiagen RT^2 Profiler Array software were re-analyzed with RNA from new animals utilizing individual qPCR assays with the same primers. In this way, the sample size was increased for each gene (n = 8-10 per condition). The genes chosen show statistically significant differential RNA expression in the Neuropathic and Inflammatory RT^2 array analysis and are known to be involved in the neuroinflammatory response. Macrophage-associated genes analyzed

included Itgam/Cd11b (**Figure 8A**), Itgb2/Cd18 (**Figure 8B**), and Mcp5/Ccl12 (**Figure 8C**). ITGAM/CD11b and ITGB2/CD18 form the integrin MAC-1 complex, which is responsible for the recruitment and adhesion of leukocytes to the site of injury[55,121]. The role of chemokine MCP-5 (monocyte chemotactic protein 5) in neuropathic pain has not been studied in the CCI model but is thought to behave like MCP-1, which is involved in the recruitment of monocytes/macrophages to injured tissue[122].

Table 3. Differential expression of mRNAs typically associated with immune cells.

Gene Symbol	Gene Description	Fold change relative to sham for CCI DF-NE	Fold change relative to sham for CCI CXB-NE	Cell Expression	GenBank	Citation
Adrb2	Adrenergic beta-2 receptor	4.97	4.9	Macrophages, Circulating monocytes	NM_012492	115
Ccr2	Chemokine (C-C) receptor 2	2.41	2.58	Macrophages	NM_021866	116, 117
Cd4[1]	CD4 cell	8.34	7.35	T Cells	NM_012705	118
Cnr2	Cannabinoid receptor 2	2.68	Not detected	Macrophages	NM_012784	119-120
Itgam/ Cd11b[1]	Integrin, alpha M	12.12	5.06	Macrophages, Circulating monocytes	NM_012711	121 121
Itgb2/ Cd18[1]	Integrin, beta 2	11.49	6.84	Macrophages, Circulating monocytes	NM_001037780	121
Mcp5/ Ccl12[1]	Chemokine (C-C motif) ligand 12	30.5	11.02	Macrophages	NM_001105822	122
Ptgs2	Prostaglandin E synthase 2	Not detected	2.21	Macrophages, Circulating monocytes	NM_001107832	123

[1] Denotes genes individually analyzed by qPCR.

Table 4. Differential expression of mRNAs typically associated with multiple cells in the periphery.

Gene Symbol	Gene Description	Fold change relative to sham for CCI DF-NE	Fold change relative to sham for CCI CXB-NE	Cell Expression	GenBank	Citation
Cx3cr1[1]	Chemokine (C-X3-C motif) receptor 1	12.47	7.78	Macrophages, Circulating monocytes, neuronal, T cells	NM_133534	68, 92
Gch1	GTP cyclohydrolase 1	3.76	Not detected	Macrophages, neuronal, T cells, Mast cells	NM_024356	124
Gdnf[1]	Glial cell derived neurotrophic factor	1.68	4.51	Neuronal, Schwann cells	NM_019139	125
IL-18[1]	Interleukin 18	6.57	4.27	Macrophages, Circulating monocytes, neuronal, Schwann cells	NM_019165	20, 126
IL-1β[1]	Interleukin 1 beta	21.52	6.06	Macrophages, Circulating monocytes, neuronal, endothelial cells	NM_031512	127-129
IL-6[1]	Interleukin 6	12.5	3.63	Macrophages, Circulating monocytes, Schwann cells	NM_012589	127, 130
Maob	Monoamine oxidase B	0.16	0.09	Neuronal, Schwann cells, endothelial cells	NM_013198	131
Mapk3	Mitogen-activated protein kinase 3	0.62	0.40	Neuronal, Schwann cells	NM_017347	96
Ptger1	Prostaglandin E receptor 1	Not detected	2.29	Macrophages, neuronal	NM_013100	132
Ptger3	Prostaglandin E receptor 3	0.46	0.41	Macrophages, neuronal	NM_012704	132
Ptger4	Prostaglandin E receptor 4	2.39	2.14	Macrophages, neuronal	NM_032076	132
Tlr2	Toll-like receptor 2	12.22	7.12	Macrophages, Circulating monocytes, Schwann cells, T cells	NM__198769	89
Tnf	Tumor necrosis factor	7.76	5.64	Macrophages, Circulating monocytes, Schwann cells, T cells	NM_012675	127

[1] Denotes genes individually analyzed by qPCR.

Other differentially expressed genes include Actb, Gdnf, Cd4, Cx3cr1, IL-1β, IL-6 and IL-18. These expression profiles are associated with multiple cell types including neurons, Schwann cells, monocytes/macrophages, and T cells (**Tables 2, 3 and 4**). β-actin and Cd4 (**Figure 9A-B**) are significantly increased in expression in the CCI condition relative to sham, but their expression level is not sensitive to the drug therapy CXB-NE treatment. Similarly, Cx3cr1/Gpr13 is increased in its mRNA expression in the CCI conditions relative to sham. While the Cx3cr1/Gpr13 in the drug treated CXB-NE condition is reduced relative to the DF-NE, the reduction is not statistically significant in this experiment (**Figure 9C**). Interestingly, Gdnf is significantly increased in its mRNA expression in the drug treated CXB-NE CCI condition (**Figure 9D**). IL-6, IL-1β and IL-18 (**Figure 10**) all exhibit significantly increased mRNA expression in the CCI (DF-NE, pain-state) as compared to sham, and that they are also each responsive to the drug therapy. No expression was seen in sham animals.

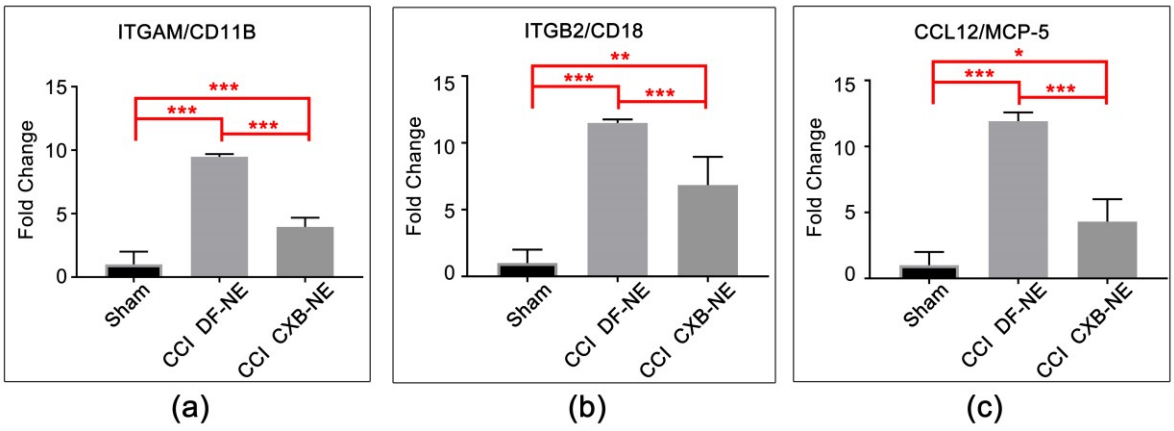

Figure 8. mRNA expression of macrophage-related genes at the site of injury. (a) Itgam/Cd11b mRNA is significantly elevated in the CCI pain-state (DF-NE) over sham, and is significantly reduced in the CXB-NE drug treated CCI condition. (b) Itgb2/Cd18 (integrin β-2) mRNA is significantly elevated in the CCI pain state (DF-NE) over sham, and is significantly reduced in the CXB-NE drug treated CCI condition. (c) Mcp-5 mRNA is significantly elevated in the CCI pain-state (DF-NE) over sham, and is significantly reduced in the CXB-NE drug treated CCI condition. One way ANOVA with Tukey post-hoc analysis is considered statistically significant if P value < 0.05. Sham = 6, CCI CXB-NE n = 8, CCI DF-NE n = 6.

3.4.4 Differential expression of mRNAs in the CCI (pain state) compared to celecoxib-treated CCI (pain relieved)

Genes that exhibited differential expression of mRNAs in the CCI conditions were compared to the mRNA expression levels in the drug treated condition (**Table 1C**). This helps to reveal genes where their expression is directly affected by CXB-NE COX-2 inhibition in monocyte-derived macrophages in the sciatic nerve. Differential expression of the mRNAs between the CCI pain state and drug-treated pain state shows that seven genes are down-regulated and one gene is upregulated in the treated animals (**Figure 11**). Maob expression is elevated in the CCI pain-state (DF-NE) and exhibits a downregulation in CCI CXB-NE. The pro-inflammatory mediator interleukin-6 (IL-6) mRNA expression is primarily produced by Schwann cells, neurons, circulating monocytes and macrophages[51] and exhibits an elevated pattern of expression that is decreased when CXB-NE is present. Itgam/Cd11b is expressed by circulating monocytes and macrophages[55] and shows a 2-fold reduction in expression when circulating monocytes are targeted with celecoxib treatment in the CCI state. Grin2b/NMDAR2b, Scn9a/Na_v1.7, Maob, Tac1 and TrpV3 are all exhibiting increased expression in the pain state, while reduced when CXB-NE provides relief and are each previously associated with neuronal expression[111, 113-115]. In contrast, the voltage-dependent calcium channel, Cacna1b, is significantly increased in CCI CXB-NE animals compared to CCI DF-NE.

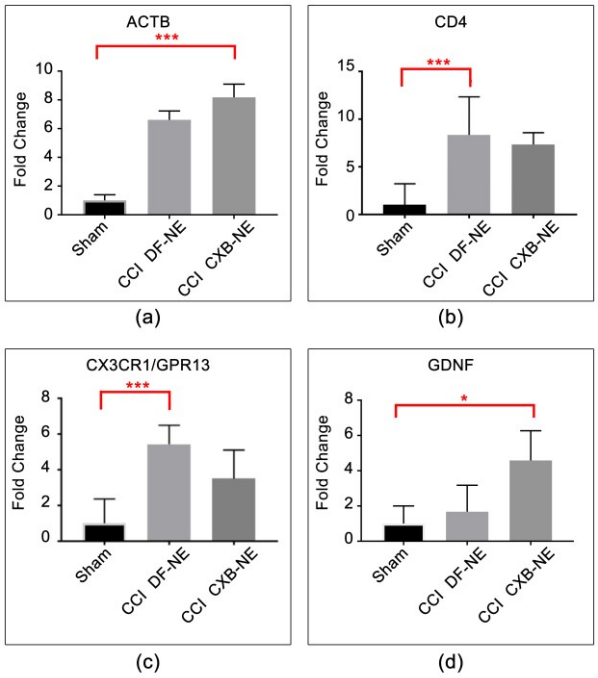

Figure 9. mRNAs responsive to CCI. (a) Actin beta (Actb) mRNA expression is elevated in response to CCI treatment and is not responsive to CXB-NE drug therapy. (b) Cd4 is typically associated with T cells and is similarly responsive to CCI treatment but is not responsive to CXB-NE therapy. (c) Cx3cr1 (Chemokine CX-3-C motif, receptor 1) is expressed widely on the cell surface of neurons, macrophages, circulating monocytes, T cells, and Schwann cells. The mRNA expression is elevated in response to CCI treatment. (d) Gdnf (glial-derived neurotrophic factor) is produced by neurons and glial cells and appears to be responsive in the CCI condition to the CXB-NE drug therapy. One way ANOVA with Tukey post-hoc analysis is considered statistically significant if P value < 0.05. Sham = 6, CCI CXB-NE n = 8, CCI DF-NE n = 6.

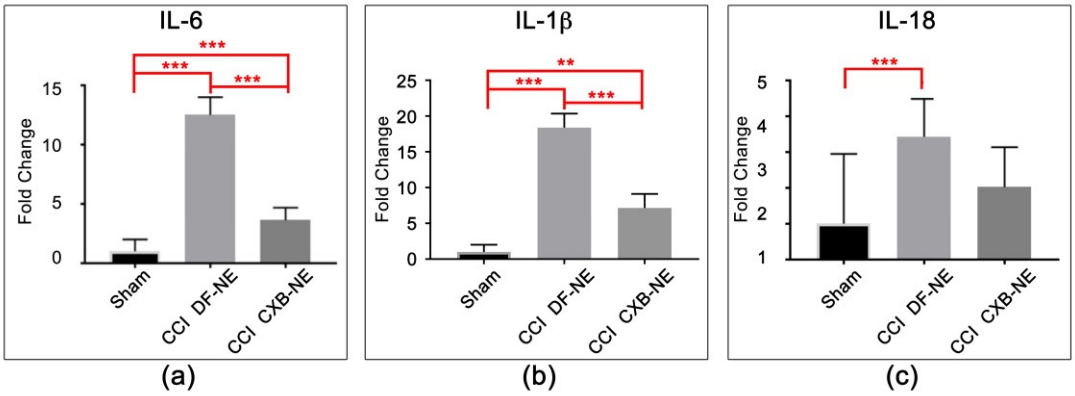

Figure 10. Cytokine mRNA expression at the site of injury. (a) cytokine IL-6 (interleukin-6) mRNA is significantly increased in response to CCI, and is significantly attenuated with CXB-NE drug therapy. (b) IL-1β (interleukin-1 beta) mRNA is significantly increased in response to CCI, and is significantly attenuated with CXB-NE drug therapy. (c) IL-18 (interleukin-18) are produced and released by multiple cell types at the site of CCI injury is significantly increased in response to CCI, and is attenuated with CXB-NE drug therapy. One WAY ANOVA with Tukey post-hoc analysis is considered statistically significant if p value < 0.05. sham = 6, CCI CXB-NE n = 8, CCI DF-NE n = 6.

3.4.5 Identification of CD68 and CD11b macrophages within the site of injury

Our previous studies show a decrease in the number of CD68 macrophages that infiltrate the injured nerve under the same conditions using CXB-NE[46, 48]. Anti-CD68 is a pan macrophage marker that has the ability to identify macrophages that are both phagocytic as well as cells that are actively producing and releasing cytokines and chemokines, whereas anti-CD11b is associated with more specific macrophages[133]. We find that the CD11b-positive cells also co-express CD68 in the pain state, but that not all CD68 positive cells are CD11b positive (**Figure 12**). CD11b-positive macrophages tend to be small and round in nature (**Figure 12 A-D**), where CD68-positive macrophages can also be large, foamy, and irregularly shaped (**Figure 12 E-H**). CD68 positive macrophages are found predominantly within the injured sciatic nerve, with low expression of CD11b positive macrophages (**Figure 12 K,L**), whereas CD11b/CD68 positive macrophages are found primarily in the epineurium surrounding the nerve fibers (**Figure 12 I,J**). These findings are consistent with previous literature of neuropathic pain models showing protein expression of both CD11b positive and CD68 positive macrophages with immunohistochemistry [52, 58, 133]. Parallel downregulation of CD11b macrophages is consistent with the reduction in expression of inflammatory mediators such as IL-6, IL-18, and IL-1β as noted by their mRNA expression.

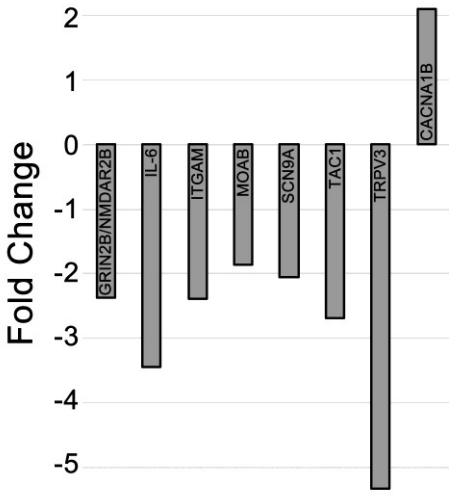

Figure 11. mRNA differential expression comparing CCI CXB-NE relative to CCI DF-NE animals. CCI animals given CXB-NE exhibit decreased expression of 7 known neuroinflammatory genes found in various cell types in the pain state and increased expression of the axonal Cacna1b gene when compared to CCI DF-NE animals. One way ANOVA with Tukey post-hoc testing. Reflects $p < 0.01$.

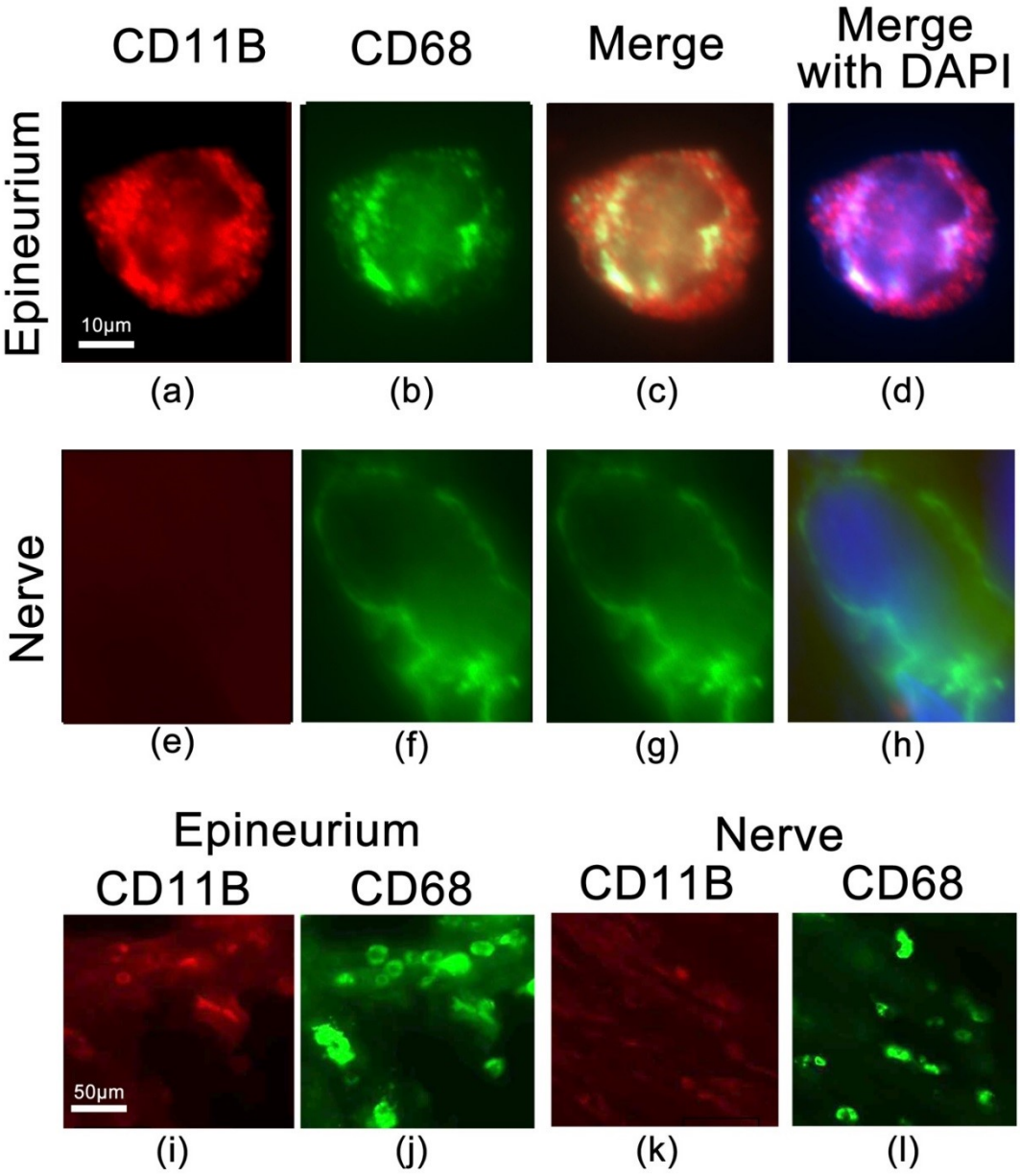

Figure 12. A subset of CD68 positive macrophages co-express the integrin ITGAM/CD11b, detected with anti-CD11b antibody. Co-expressing cells are predominantly found in the epineurium (a-d), whereas the CD68 positive macrophages in the nerve track do not co-express CD11b (e-h). (i,j) reveals the co-expressing CD11b and CD68 cells predominate in the epineurium, but only CD68 positive cells are prominent in the nerve (k-l).

3.5 Discussion

3.5.1 Peripheral nerve injury is associated with differential expression of neuroinflammatory mRNAs

This study revealed that mRNA expression changes were seen directly at the site of injury where neuroinflammation is rampant. Furthermore, that within 4 days of celecoxib-loaded nanoemulsion administration, aside from a reduction in pain-like behavior and reduction in PGE_2 production, shift in macrophage polarity and reduction in Mast Cell degranulation[46, 48], we now find that the regulated expression of several mRNAs are responsive to the drug-therapy. This drug induced-differential expression of mRNAs for key neuroinflammatory genes is a result of the nanoemulsion drug being delivered to macrophages in the pain state.

Overall, our data revealed changes in the mRNA expression of genes associated with neuroinflammation, which is consistent with phenotypic behavioral changes as demonstrated by the assessment of tactile allodynia of the affected hind leg. CCI animals demonstrate no significant allodynia during the initial Wallerian degeneration phase occurring between days 1 to 3 [30] and show an decreased pain threshold during days 4 to 5 and beyond [46, 48]. By day 8 post-surgery, we observed a plateau in hypersensitivity that persists in un-treated animals[46, 48]. However, following intravenous injection of celecoxib-loaded nanoemulsion on the eighth day post-surgery, we showed that beginning as early as a day later, there was a significant reduction in mechanical allodynia, consistent with prior observations[46, 48]. We have previously demonstrated that this single dose (0.24 mg/kg) of celecoxib provides relief from hypersensitivity that lasts about 6 days[46, 48]. This represents greater than a 2000-fold reduction in dosage that would be needed were traditional daily oral dosing utilized[134]. This change in behavioral

phenotype overlaps with the prolonged neuroimmune response occurring in and around the site of injury. This is characterized by the changes in behavioral activity and activation of resident immune and immune-like glial cells[56, 95, 135]. In vivo imaging of the ipsilateral hindleg revealed an increased near infrared signal consistent with an accumulation of nanoemulsion-labeled macrophages at the site of injury, indicative of neuroinflammation associated with infiltrating macrophages [46-48]. Immunohistochemical investigation of dissected sciatic nerves reveals that CCI CXB-NE animals on day 12 exhibit a reduced infiltration of macrophages as compared to CCI DF-NE animals[46, 48]. COX-2 as well as with PGE_2 are present in the injured rat sciatic nerves following CCI injury[46, 48] suggesting injured nerve-derived invading macrophages may influence the neuroimmune cellular environment within the sciatic nerve through possible autocrine and paracrine pathways[52]. Here we showed that the heightened and persistent neuroimmune response in the peripheral nerve injury leads to changes in mRNA expression at the site of injury, and that it involves multiple cell types, including neurons, macrophages, Schwann cells, degranulating Mast cells and T cells; all of which contribute to the production of inflammatory mediators at the site of injury.

3.5.2 Targeting COX-2 in macrophages contributes to a decrease in macrophage-related mRNAs at the site of injury

By directly targeting COX-2 enzyme and PGE_2 production in invading macrophages at the site of injury, there was a subsequent decreased gene expression evident in Cd11b/Itgam and Cd18/Itgb2 beta-2 integrins when compared to sham control. Cd11b/Itgam and Cd18/Itgb2 are integrins that heterodimerize to form a complex known

as MAC-1 or CR3. It is normally present in an inactive confirmation in circulating monocytes, but is quickly activated to mediate leukocyte adhesion, migration and accumulation of cells at the site of inflammation[55]. Previous studies have shown that by blocking MAC-1 and its' ligands or the ablation of its genes encoding Cd11b or Cd18, leads to a decrease in severity of inflammation in animal models[55]. Given the attenuation in COX-2 activity and the reduction in PGE_2 production in CXB-NE targeted macrophages[48], the differential expression in Cd11b between CCI animals given drug versus drug-free CCI animals supports the observation that fewer macrophages are attracted to the site of injury. Here, we hypothesized that by inhibiting COX-2 and the production of PGE_2 in circulating monocytes and tissue macrophages, there would be a subsequent change in macrophage signaling, including integrins, cytokines, and the involvement of genes associated with other cell types that participate in releasing inflammatory mediators at the site of injury that leads to decreased pain behaviors when administered at a chronic pain state in rats. Additionally, macrophages functions are dynamic with a shift in polarity when given celecoxib-loaded nanoemulsion[46]. Our lab has previously shown there is a nearly 30% reduction of M1 macrophages in the ipsilateral sciatic nerve of pain treated (CXB-NE) animals on day twelve [46]. Temporally, there is multitude of surface markers used to identify macrophages after nerve injury[135] . A study by Lee and Zhang[58] showed that in injured nerves, macrophages exhibit heterogeneity, where a subpopulation identified by the MAC1 (CD11b/CD18) marker is cytokine/chemokine expressing and another subpopulation labeled by CD68 antibody is predominantly phagocytic (which is key for the regeneration process). Previously, our studies have shown that CD-68 positive macrophages are present in high number within

the damaged nerve (CCI DF-NE) compared to CCI animals receiving CXB-NE[46, 48]. We also demonstrated that the CD68 positive macrophages in the injured sciatic nerve can be distinguished as M1 (pro-inflammatory) and M2 (anti-inflammatory) by their expression of the costimulatory protein, Cluster of Differentiation 40 (CD40), or transferrin receptor (TFRC) respectively[46]. Utilizing the cytokine/chemokine secreting-specific antibody to CD11b, we were able to further identify additional phenotypically different macrophages in the CCI nerve. In a review by Ristoiu et al., (2013) they reported that in the sciatic nerve there is activation of CD11b-positive and CD68-positive macrophages after several neuropathy-induced animal models[52]. Our observation here is that at this moment in time (day 12 post CCI surgery), CD68-positive macrophages are found predominantly within the injured sciatic nerve, whereas CD11b/CD68-positive macrophages are found primarily in the epineurium surrounding the nerve fibers.

3.5.3 COX-2 inhibition in macrophages leads to a reduction in pro-inflammatory cytokine mRNA

Previous studies suggest that macrophage-derived PGE_2 alters neural activity, influences the milieu of cytokines, and changes gene expression at the site of injury, all of which contribute to the chronic pain state[46-48,51, 123, 136-139]. Nerve injury results in a significant increased expression of IL-6 in injured nerves [51,92,140]. IL-6 is also elevated in invading macrophages in vivo[51], ensheathing Schwann cells and increased in T cells in response to possible increased PGE_2 expression[130]. IL-6 is a pleiotropic cytokine where an increased production can be neurotrophic for neurons and can provide further signals that influence changes in neuronal and glial cell gene expression[130]. Consistent with

previous studies[127], we found that IL-6 mRNA expression is elevated post-CCI in the ipsilateral sciatic nerve. Expression of IL-6 also plays a role in axonal regeneration when overexpression of the protein and its receptor results in improved nerve regeneration[141-142].

The mRNA expression for cytokines IL-18 and IL-1β is increased in CCI DF-NE animal's sciatic nerve, with IL-1β responding to CXB-NE treatment, showing decreased expression when nanoemulsion drug therapy is used. This is consistent with the observation that both IL-18 and IL-1β exhibit elevated expression at the protein level in the sciatic nerve of CCI rats, and that the activation of the inflammasome combined with the dominant role exhibited by IL-18 during chronic inflammation contributes to chronic pain[20].

Tachykinins are a family of conserved peptides encoded by the Tac1 gene, which generates substance P, neurokinin A, neuropeptide δ, and neuropeptide γ [143,144]. These neuropeptides are mainly expressed in neuronal tissues in the central nervous system and in primary afferent neurons in the peripheral nervous system[144]. It has also been shown that substance P and neurokinin A are expressed in non-neuronal cells including macrophages and circulating monocytes[144]. Substance P is a neurotransmitter that has been implicated in chronic pain[145]. NMDA receptors like GRIN2b/NMDAR2 are present in primary afferents and evoke the release of substance P from their central terminals[145]. Interestingly, mRNAs encoding both substance P and GRIN2b/NMDAR2 are differentially expressed in the injured sciatic nerve and are responsive to CXB-NE. This suggests that the transcriptional regulation of GRIN2b/NMDAR2 as well as Tac1

mRNAs play a role in regulating pain transmission and that when COX-2 is attenuated in macrophages their co-regulation is similarly reduced.

3.5.4 mRNAs are differentially expressed in pain relief versus the untreated pain state

When comparing differential expression between the hypersensitive pain state (DF-NE) and the pain-relieved state (CXB-NE), there are 8 of the 84 genes that exhibit differential expression; five of which are known to be expressed in neurons [112, 146, 147]. Of these five, Grin2b/NMDAR2, Scn9a/Na_v1.7, and Maob are expressed in neurons[111,131, 146] and there is an increase in the mRNA expression for these five genes in the injured sciatic nerve during hypersensitivity. Furthermore, when COX-2 activity is attenuated by the targeted delivery of nanoemulsion loaded with celecoxib, there is a reduction in this over-expression. Changes in Na_v1.7/Scn9a, Maob, and Cacna1b mRNA expression in chronic pain is thought to be involved in the maintenance of chronic pain in the peripheral nervous system[148-150]. The role of Trpv3 is not well understood in peripheral neuropathy though its expression has been reported in mouse peripheral nervous systems[112] and the mRNA exhibited high expression levels in rat DRG in spared nerve injury models of neuropathic pain[76].

3.5.5 mRNAs at the site of injury contributing to anti-inflammation and regeneration

The neurotrophic factor GDNF is known to have neuroprotective function in L4 and L5 DRG neurons after axotomy[151]. Here we seen increased expression of GDNF between sham surgical sciatic nerve and CCI nerve treated with CXB-NE. GDNF is a survival promoting factor for nociceptive neurons and has been shown to have analgesic

properties when spinal nerve ligation injured mice are injected with GDNF-expressing lentivirus[152], suggesting GDNF mRNA have an anti-inflammatory role under neuropathic conditions. We also observed that β-actin (Act-β), which is associated and involved in growth cone formation [97,153], exhibited differential mRNA expression. Interestingly, β-actin is often and mistakenly used as a "housekeeping gene" with the thought that its expression would remain unchanged after most nerve injuries. Our study revealed that, in fact, β-actin mRNA expression is altered upon CCI injury, with increased expression evident in CCI DF-NE animals. Drug-treated animals (celecoxib) exhibited a significantly higher level of expression over what is evident in the DF-NE condition. This increase in actin expression may be in response to the activation of peripheral nerve regenerative processes[154].

Here we reported that the chemokine MCP-5 appears to play a role in neuropathic pain. MCP-1 is known as one of the main proteins that activates and attracts circulating monocytes to the injured nerve[54]. MCP-5 is similar to MCP-1 and is known to attract circulating monocytes and T cells[122]. Expression of MCP-5 can be induced by macrophages and possibly Schwann cells, but its overall role in neuropathic remains unclear. Our study showed a dramatic increase in MCP-5 mRNA in the pain state in the damaged sciatic nerve. When animals are given intravenous injection of CXB-NE, there is a significant reduction in MCP-5 expression, indicating a role for this gene at the site of injury in the CCI peripheral nerve.

3.5.6 Neuroinflammatory genes previously associated with cell bodies are differentially expressed at the site of injury

Exploration of differential expression of neuroinflammatory genes in previous studies has focused on changes in the dorsal root ganglia (DRG) and the dorsal horn. The chemokine, fractalkine, is thought to be present only in DRG neurons during the neuropathic pain response[155] with its receptor being expressed on a wide variety of cell types, including neutrophils, monocytes, CD8 T cells, Mast Cells, Natural Killer cells, fibroblasts, neurons, and endothelial cells[80, 90]. Interactions within the neuronal-glial-immune-cell triad results in amplification of sensory signals so that responsivity to noxious as well as innocuous stimuli is intensified in ways that contribute to the pain-like behavior[124]. Verge and colleagues[124] studied the fractalkine mRNA, showing that it is upregulated in DRG neurons as a result of CCI with a marked increase in expression of its G-Protein Coupled receptor, CX3CR1, in microglia as well as in neurons in the spinal cord. Here, we found that the mRNA expression of CX3CR1 is significantly increased in the periphery in the injured sciatic nerve in the drug-free nanoemulsion compared to sham. When treated with nanoemulsion loaded with celecoxib, the elevated expression of CX3CR1/GPR13 is reduced. Others have shown that when CX3CR1 is depleted by Diphtheria toxin treatment in CD11b-positive macrophages, 3 days following spinal nerve transection, no hypersensitivity was noted. By one week post-nerve injury, macrophages repopulated with no pain behavior evident[90]. When these same mice undergo the same nerve injury, neuropathic pain developed, suggesting that repopulated macrophages are able to engage in the development of inflammation leading to pain-like behavior[90].

In conclusion, the peripheral nerve response to injury involves complex responses from multiple cell types and it is for this reason we sought to profile mRNA expression for a specific set of genes involved in neuroinflammation by using mRNA derived from the site of injury. Our examination focused on the expression of genes involved in pain response modulation including those associated with inflammation, neurotransmitters signaling, neurotrophins, purinergic receptors, cytokines, and chemokines as well as products associated with the conduction of pain including ion channels, sodium channels, potassium channels, signal transduction/transcription, and synaptic transmission. We find differential expression of mRNAs in several of these categories in the pain-state as well as genes that are subsequently responsive to CXB-NE nanoemulsion drug therapy. Furthermore, analyzing gene expression in the sciatic nerve offers insight into how mRNA expression distal to the neuronal cell bodies may be of significant importance in establishing and maintaining chronic pain.

3.6 Supplemental Data

Table 5. Gene list of RT^2 Profiler Array: Neuropathic and Inflammatory Rat Pain (Qiagen). These genes have been implicated in the transduction, maintenance, and modulation of pain responses after tissue damage.

Ace	Cd200	Gch1	Il2	Mapk8	Pla2g1b	Scn11a
Adora1	Cd4	Gdnf	Il6	Ngf	Pnoc	Scn3a
Adrb2	Chrna4	Grin1	Itgam	Ntrk1	Prok2	Scn9a
Alox5	Cnr1	Grin2b	Itgb2	Oprd1	Ptger1	Slc6a2
Bdkrb1	Cnr2	Grm1	Kcnip3	Oprk1	Ptger3	Tac1
Bdnf	Comt	Grm5	Kcnj6	Oprm1	Ptger4	Tacr2
Cacna1b	Csf1	Htr1a	Kcnq2	P2rx3	Ptges	Tlr2
Calca	Cx3cr1	Htr2a	Kcnq3	P2rx4	Ptges2	Tlr4
Cck	Dbh	Il10	Maob	P2rx7	Ptges3	Tnf
Cckbr	Edn1	Il18	Mapk1	P2ry1	Ptgs1	Trpa1
Ccl12	Ednra	Il1a	Mapk14	Pdyn	Ptgs2	Trpv1
Ccr2	Faah	Il1b	Mapk3	Penk	Scn10a	Trpv3

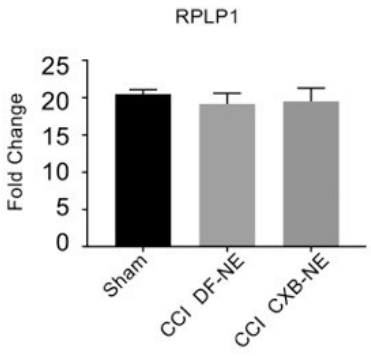

Figure 13. Normalization of genes to the housekeeping gene, Rplp1. Average CT value ranged from 18.5 to 20.1 in all samples. One-way ANOVA was not statistically significant amongst sham control, CCI drug-free (vehicle)-loaded nanoemulsion (DF-NE), or CCI celecoxib-loaded nanoemulsion (CXB-NE). P > 0.100.

Figure 14. Gene expression amongst controls. Student's t-test illustrated no statistically significant difference in the naïve and sham controls. All samples failed to express Actb (a neuronal marker) or the inflammatory mediator IL-18. P > 0.100.

AVERAGES	Rplp1	Actb	Il-18	Mcp-1
Naïve (n = 4)	24.21	Not detected	Not detected	30.36
Sham + CXBNE (n = 4)	22.88	Not detected	Not detected	27.88
Sham + DFNE (n = 4)	23.53	Not detected	Not detected	28.01

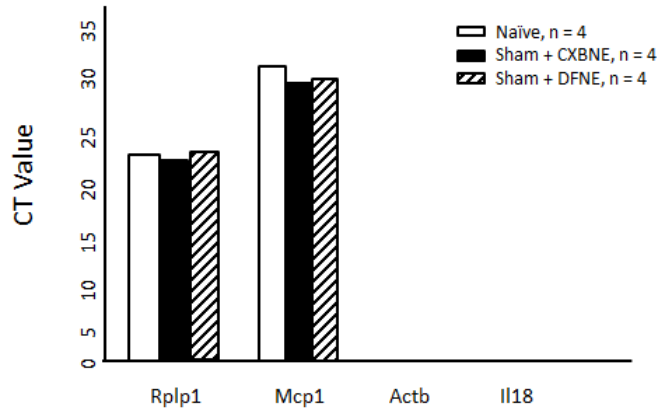

3.7 Funding

Funding includes acknowledgment for Confocal imaging which was supported with grants to J.A.P from the NSF DBI- 0400776, NSF DBI-1726368. NIR optical imaging was performed on Pearl® Small Animal Imaging System (Li-COR Biosciences) at Duquesne University (Supported by Pittsburgh Tissue Engineering Initiative Seed Grant). J.M.J. acknowledges support from NIDA award number 1R21DA039621–01, NIBIB award number R21EB023104–02 and AFMSA Award number FA8650-17-2-6836. J.A.P. and J.M.J acknowledge support from Pittsburgh Tissue Engineering Initiative Seed Grant. J.A.P also ac- knowledges the Hunkele Dreaded Disease Award, Samuel and Emma Winters Foundation, the Charles Henry Leach II Fund, the Commonwealth Universal Research Enhancement Award. Funding for D.B. was provided by the National Institutes of Health (NIH NINDS R25NS100118 PURE/NURE program). J.A.P and J.M.J. acknowledge support from the Duquesne University Inaugural Provost's Interdisciplinary Research Consortia Grant, which supports the Chronic Pain Research Consortium and a CPRC Starter Award.

Chapter 4. Targeted COX-2 inhibiting nanomedicine results in pain-relief and differential expression of RNA in the dorsal root ganglia of injured male rats

Submitted for publication in Molecular Pain – in press.

4.1 Contributions Statement

Andrea Stevens did all work in this chapter except where noted below:

Muzamil Saleem, Graduate Student in Dr. John A. Pollock's laboratory, dissected the dorsal root ganglia tissue from each animal.

Brooke Deal, Graduate Student in Dr. John A. Pollock's laboratory, constructed the heat map.

Jelena M. Janjic, Associate Professor in Graduate School of Pharmacy at Duquesne University and co-founder of Duquesne University's Chronic Pain Research Consortium, together with Dr. Pollock jointly designed the experimental approach for evaluating nanoemulsions in the CCI rat model for effects on neuropathic pain. Dr. Janjic conceived and designed the overall macrophage-targeted drug delivery approach with nanoemulsions, the nanoemulsion composition and processes for fabrication.

John A. Pollock, Professor of Biology and Principle Investigator, jointly designed the approach to assess the RNA transcriptome (with Andrea Stevens); all experiments were performed by Andrea Stevens under the guidance of John A. Pollock.

The University of Pittsburgh Genomics Research Core (Dr. Jeannette Lamb) and Genomics Analysis Core (Dr. Uma Chandran) performed the RNA sequencing and carried out the initial data analysis. Both provided substantial guidance in the technical aspects of the project.

Original draft preparation by Andrea Stevens, additional writing and review was by all authors.

4.2 Introduction

Peripheral neuropathy is characterized as damage or injury to the peripheral nervous system resulting in spontaneous pain, allodynia, and mechanical and thermal hyperalgesia. Peripheral neuropathy is characterized as damage or injury to the peripheral nervous system resulting in spontaneous pain, allodynia, and mechanical and thermal hyperalgesia. A key mechanism underlying peripheral neuropathy is neuroinflammation, which is thought to be more efficient at driving chronic pain than systemic inflammation[1] as it involves the induction of the innate immune response as well as activation of the nervous system. Interactions between injured neurons, glia and infiltrating immune cells result in the production of effector molecules known as inflammatory mediators, all of which contribute to the hypersensitive state. It is previously known that the release of inflammatory mediators contributes to the induction and maintenance of neuropathic pain leading to the alteration of neuronal function both at the site of injury as well as at the site of neuronal cell bodies in the dorsal root ganglia (DRG) [5, 20, 46,91]. Sensitization of the injured nerve and its associated neuronal cell bodies in the DRG may lead to long-term changes in gene expression in these cells, as suggested by RNA transcriptome studies[156-158].

We have utilized a neuropathic pain model in male rats known as chronic constriction injury (CCI) of the sciatic nerve[13, 14, 17, 18, 20, 46, 48, 49 159]. Within hours of CCI, activation of the inflammatory response occurs, resulting in cellular and molecular expression changes at and near the site of injury[20,160]. The production of inflammatory

mediators along with activation of immune-like glial and immune-cells leads to shifts in cellular phenotypes, which further results in changes in gene expression that signals hypersensitivity and chronic pain in CCI animals[94,160-162]. We have previously reported on gene expression changes that occur at the site of injury at the sciatic nerve for mRNAs involved in neuroinflammation as well as in the associated dorsal root ganglia[47,49]. For example, we have previously shown that CCI associated hypersensitivity is associated with GAP43, NPY and TRPV1 mRNA expression changes in the DRG and furthermore, that TRPV1 protein expression changes in specific CCI DRG cell bodies of neurons that innervate the affected foot (identified by DiD retrograde labeling)[47]. In other studies, qPCR of mRNA expression in the injured sciatic nerve for 84 neuroinflammatory genes revealed several distinct differences between naïve, CCI and CCI treated with COX-2 inhibition[49]. Changes in the expression of mRNAs for cytokines and chemokines is consistent with the inflammation and corresponding infiltration of macrophages at the site of injury. Furthermore, the expression of transcripts for integrins involved with selective macrophage adhesion, as well as changes in neuronal and glia expression profiles was observed in the sciatic nerve dependent on the pain or pain-relieved state[49]. Administration of a macrophage-targeted COX-2 inhibiting nanoemulsion (CXB-NE) revealed that by targeting the production of PGE_2 at the site of injury, pain relief is associated with a partial reversal of the gene expression profiles in the sciatic nerve when compared to tissue in a pain state[49]. Here we hypothesize that ultimately, the inflammatory milieu and tissue response at the site of injury is communicated to the DRG where changes in expression profiles are of particular importance given that these cells

are a component of primary sensory neurons, acting as the bridge between the peripheral and central nervous system.

RNA sequencing allows for the exploration of the molecular and biological mechanisms of neuropathic pain through the analyses of whole transcriptome changes after nerve injury. Using RNA sequencing, several studies have previously examined pain-associated changes in expressed RNA in the DRG [77,78, 79, 165, 166]. Here we report studying changes in the RNA transcriptome in the DRG when the CCI animal is experiencing significant pain as compared to a naïve animal and separately for animals that are treated with an anti-inflammatory nanoemulsion (COX-2 inhibiting Celecoxib-loaded nanoemulsion). The nanoemulsion pain-relieving therapy selectively targets the cyclooxygenase-2 (COX-2) in macrophages, which is normally produced by these infiltrating cells and other activated cells at the site of injury, triggering pain[29]. The non-steroidal anti-inflammatory drug (NSAID) Celecoxib (CXB) can be used to treat pain through the reduction of PGE_2 following selective inhibition of COX-2. We have previously shown that localized delivery of a single micro-dose (0.24 mg/kg) of Celecoxib in nanoemulsion, which is incorporated in circulating macrophages/monocytes that then naturally accumulate at the site of injury provides up to 6 days of pain relief [46, 48, 49,167]. An important feature is that the nanomedicine delivers drug to the affected injured nerve[46, 48, 49]. This creates a unique opportunity to assess drug effects on cellular expression of RNAs when the drug is present at the distal injury and virtually no other parts of the peripheral nervous system. With this approach, we have been able to reveal transcriptome changes in the DRG associated with CXB-NE. Results show that DRG

RNAs in CCI treated males exhibit differential expression in association with changes in neurons, activated glial cells and multiple immune cells.

4.3 Methods (See Chapter 2 and Appendix A for detailed methodology)

4.3.1 Blinding statement

In order to avoid bias, I was blinded to the tissue collected, wherein another investigator collected all tissues and labeled them. Tissue identities were not revealed until differential expression analysis

4.3.2 Statistics

Both raw P values and adjusted P values (also known as False Discovery Rate; FDR) were collected in this study using One-way ANOVA with Tukey's post-hoc testing (GraphPad Prism v8). The traditional 'raw P values' included ≤ 0.05 and ≤ 0.001 and the more stringent False Discovery Rate ('FDR') value ranged between ≤ 0.05 to 0.50. The FDR value's interpretation is that with a raw P value of ≤ 0.05, 5% of 100 of those are false positives. Although the traditional raw P values can still be reliably utilized, with the FDR, we can say with confidence that these values are not false positives and increases the statistical likelihood.

4.4 Results

4.4.1 Mechanical allodynia in CCI rats and relief from hypersensitivity with a microdose of celecoxib nanoemulsion

Consistent with previous studies, male rats experiencing sciatic nerve CCI [13, 46, 47, 49] exhibit peripheral neuropathy in the ipsilateral hindpaw, which can be demonstrated

with footpad stimulation by von Frey monofilaments of increasing diameter. Behavioral testing of animals in this specific study illustrates a behavioral baseline (before animals receive surgery) of no significant difference in pain-like behavior among the populations in this study (**Figure 6**). Mechanical allodynia testing was not conducted on the day of surgery (day 1), but was continued on days 2-12 following CCI surgery. All CCI animals used in this study exhibit behavior indicative of increasing hypersensitivity up to day 8 (**Figure 15**), at which time the population was divided into naïve (no injection treatment), those that receive intravenous injection of celecoxib-loaded nanoemulsion (CXB-NE) and those that receive an intravenous injection of drug-free nanoemulsion (DF-NE, vehicle). By day 10 (2 days post injection) animals receiving CXB-NE experience a statistically significant decrease in allodynia compared to those receiving vehicle (DF-NE) (**Figure 15**). There is no statistically significant difference between CCI CXB-NE behavior and naïve rats on days 11 and 12 indicating that the CCI animals were experiencing complete pain relief, whereas the CCI DF-NE animals continue to reflect significant hypersensitivity (**Figure 15**).

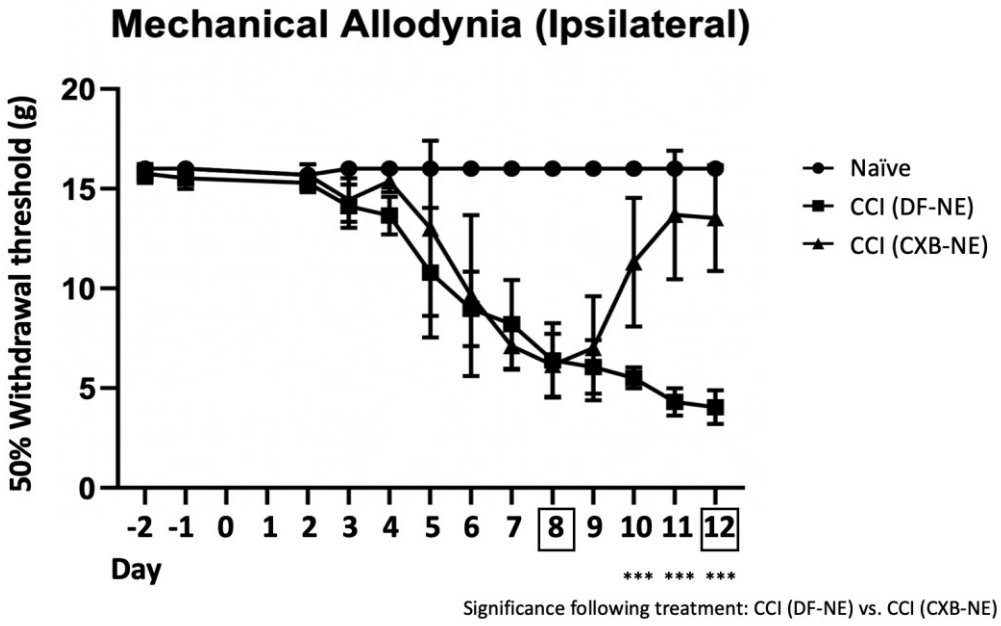

FIGURE 15: Pain relief behavioral testing of the animals used in this study and timeline of events following treatment. Celecoxib-loaded nanoemulsion (CXB-NE) reduces pain-like behavior in CCI animals within one day of administration compared to those receiving drug-free nanoemulsion as a vehicle (DF-NE). By day 12, injured rats given CXB-NE return to baseline behavior, whereas rats treated with CCI DF-NE continue to exhibit hypersensitivity (displayed as ****). Data are expressed as a mean +/- SD. Significance was determined by two-way ANOVA and post-hoc Tukey's multiple comparison test ($P < 0.0001$). Animals underwent mechanical allodynia on the ipsilateral hindpaw two days prior to surgery (days -2 and -1), a rest day on day 0 (day of CCI surgery) and day 1, and continued von Frey testing until euthanasia (day 12). Tail vein injection of nanoemulsion occurred as pain-like behavior plateaus on day 8. All animals were euthanized on day 12. Naïve n=3, CCI DF-NE n = 3, CCI CXB-NE n=4.

4.4.2 RNAseq Analysis

To identify transcriptional profiles of RNA in DRG experiencing peripheral nerve injury, high throughput RNA sequencing was performed on total RNA extracted from DRG recovered from animals on day12 post CCI surgery. Male rats were administered a single dose of nanoemulsion (0.24 mg/kg) intravenously on day 8 post-surgery, a time when pain-like behavior approaches a maximum. Total RNA was isolated from L4 and L5 ipsilateral dorsal root ganglia (and combined) for uninjured naïve rats as well as injured CCI (DF-NE) and CCI CXB-NE drug-treated rats. With alignment to the Rattus

norvegicus reference genome, overall, the RNA sequencing of the naïve animal DRG produced 18.8 million raw sequences of which 12.7 million sequences mapped to the reference genome representing 21,152 transcripts from 14,717 genes (**Table 6**). The sequencing from CCI DF-NE animals represented 20.2 million raw sequences, 13.4 million mapped to the genome corresponding to 21,218 transcripts for 14,753 genes (**Table 6**). The analysis of the RNA from CCI CXB-NE DRG found 26.1 million raw sequences, 18.8 million of which mapped to the rat genome, corresponding to 22,541 transcripts for 15,642 genes (**Table 6**).

The analysis shows that between 30-40% of the RNAs detected correspond to exonic elements that code for mRNAs that can be translated into protein (**Figure 16**). Non-coding base pairs comprising intronic and intergenic elements consists of the majority of the represented sequence elements that were detected. Intronic elements were expressed evenly in naïve and CCI DF-NE at 14%. A higher number of intronic sequences were detected for CCI CXB-NE at 21% overall (**Figure 16**). Intergenic elements dominated the detected RNAs; naïve 48%, CCI DF-NE 49%, and CCI CXB-NE 40% (**Figure 16**).

Table 6: Mean number of raw and mapped reads, transcripts and genes detected, and standard deviation.

Condition	*Naïve Control*	*CCI DF-NE*	*CCI CXB-NE*
Raw Sequences	$18.8 \times 10^6 \pm 1.2 \times 10^6$	$20.2 \times 10^6 \pm 2.9 \times 10^6$	$26.1 \times 10^6 \pm 1.1 \times 10^6$
Mapped Sequences	$12.7 \times 10^6 \pm 8.4 \times 10^5$	$13.4 \times 10^6 \pm 2.2 \times 10^6$	$18.8 \times 10^6 \pm 8.1 \times 10^5$
Transcripts Detected	21,152 ± 114	21,218 ± 524	22,541 ± 167
Genes Detected	14,717 ± 90	14,753 ± 375	15,642 ± 118

M, Millions; Mapped pairs is the total number of pairs for which both ends map; Transcripts/Genes Detected is the number of transcripts/genes with at least 5 reads.

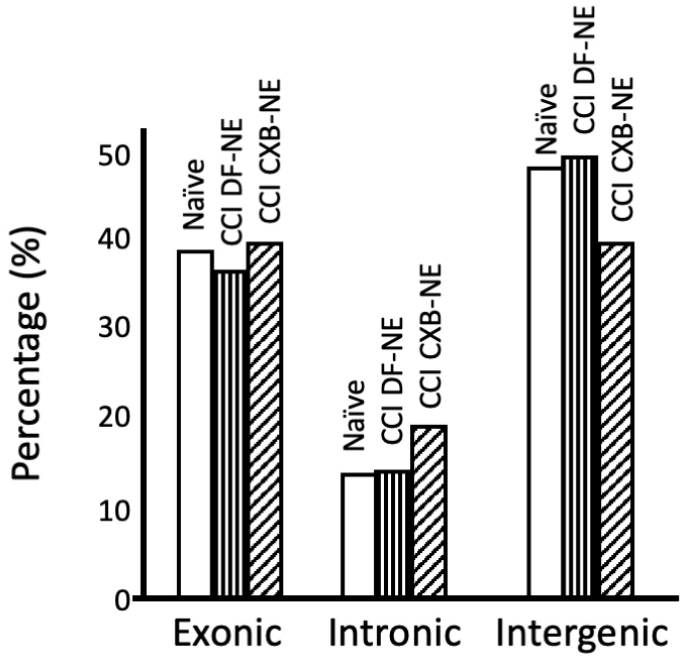

FIGURE 16: Distribution of gene elements. The mapped percentage of expressed exonic, intronic, and intergenic elements in naïve, CCI DF-NE, and CCI CXB-NE conditions. There is a significantly higher percentage of intronic reads in CCI CXB-NE compared to naïve and CCI DF-NE and a significantly lower percentage of intergenic reads. There is no significant difference in expression of exonic elements within conditions.

A comparison between RNAs detected in DRGs from vehicle (DF-NE), versus COX-2 inhibited (CXB-NE), and naïve shows that 8,948 distinct genes are expressed in all three conditions. Gene biotype analysis was performed for those RNAs that were differentially expressed showing that the majority of transcriptional changes were observed in protein-coding genes (94%). The remaining differentially expressed RNAs are considered non-coding, being composed of 111 (1.2%) RNAs of known long non-coding genes (lncRNAs), and as microRNAs (miRNAs; 0.07%). An additional 322 RNAs account for the remaining (2.79%) found within the samples but are not shown.

4.4.3 Chronic constriction injury of the sciatic nerve leads to differential expression of RNAs in the DRG

Table 7 shows the number of differentially expressed RNAs out of the 8,948 RNAs that were analyzed for statistically significant differences in the comparisons of control animals (naïve) versus CCI DF-NE (drug-free nanoemulsion) treated rats, control versus drug-loaded nanoemulsion (CXB-NE) treated CCI rats, and between the treated and untreated pain states. A comprehensive table of all statistical values studied are in **Table 7,** including the traditional 'raw P values' of ≤0.05 and ≤0.001 and the more stringent False Discovery Rate ('FDR') value ranging between ≤0.05 to 0.50. The FDR value is the adjusted P value, and its interpretation is that with a raw P value of ≤0.05, 5% of 100 of those are false positives. Although the traditional raw P values can still be reliably utilized, with the FDR, we can say with confidence that these values are not false positives. When compared to naïve-unoperated controls (pain free), CCI DF-NE (in pain) exhibited 183 total RNAs that were differentially expressed (raw P value ≤0.05)

and 16 with a raw P value ≤0.001. When the analysis calculates the adjusted P value (FDR ≤0.05) zero genes were revealed as significant; however, when the FDR value is increased to ≤0.50 and a raw P value ≤0.001, 16 genes are differentially expressed; 9 upregulated and 7 downregulated. Interestingly, these are the same genes within both statistical categorizations. When comparing naïve (unoperated, pain free) to CCI CXB-NE animals, 584 total RNAs are differentially expressed with a statistically significant raw P value <0.05 and 78 RNAs with a statistically significant FDR value (≤0.05). When comparing untreated injured animals, CCI DF-NE (pain) to CCI CXB-NE (COX-2 inhibiting nanoemulsion treated pain relieved) 675 genes differentially expressed were shown to be statistically significant (raw P value <0.05). Of those RNAs, 487 were upregulated in the pain relieved state (CCI CXB-NE), while 188 were downregulated (in CCI CXB-NE) (**Table 7**). When considering the adjusted P value (FDR) ≤0.05 for the comparison of CCI DF-NE (pain) to CCI CXB-NE (COX-2 inhibiting nanoemulsion treated pain relieved) 115 genes were found to be differentially expressed (**Table 7**). Of those 115 genes, 98 were upregulated in pain relief (CCI CXB-NE) and 17 were down regulated (in CCI CXB-NE) (**Table 7**). All further differential expression analyses in this work focuses on transcriptional differences amongst the pain state animals; all other data can be found in the Appendix B (**Tables 14-20**) section. Additionally, data reported in Appendix B includes all data with a significant P value (≤0.05).

Comparison of detected RNAs from CCI DF-NE (pain) to CCI CXB-NE (pain-relieved COX-2 inhibited) revealed significant changes in a total of 115 genes, 91 of which are considered protein-coding genes, 82 exhibiting elevated expression while pain is relieved, with 9 genes down regulated, and 24 representing non-coding transcripts; 57

of these genes are also shared with the naïve condition and their comparative expression levels visualized in **Figure 17**.

Table 7: Numbers of RNAs differentially expressed utilizing multiple statistical values. Upregulated and downregulated values represent the latter condition compared (CCI DF-NE genes up- and down-regulated when compared to naïve, CCI CXB-NE genes up- and down-regulated when compared to naïve; and RNAs of CCI CXB-NE up- and down-regulated when compared to CCI DF-NE).

	Naïve vs. CCI DF-NE	Naïve vs. CCI CXB-NE	CCI DF-NE vs. CCI CXB-NE
Raw P value Data			
Differentially Expressed (P≤0.05)	183	584	675
Upregulated Genes	110	514	487
Downregulated Genes	73	70	188
FDR Data			
Differentially Expressed (FDR≤0.05)	0	78	115
Upregulated Genes	0	72	98
Downregulated Genes	0	6	17
FDR Data			
Differentially Expressed (FDR≤0.10)	0	107	164
Upregulated Genes	0	97	141
Downregulated Genes	0	10	23
FDR Data			
Differentially Expressed (FDR≤0.50)	16	316	550
Upregulated Genes	9	287	487
Downregulated Genes	7	29	63
Raw P value Data			
Differentially Expressed (P≤0.001)	16	97	136
Upregulated Genes	9	88	116
Downregulated Genes	7	9	20

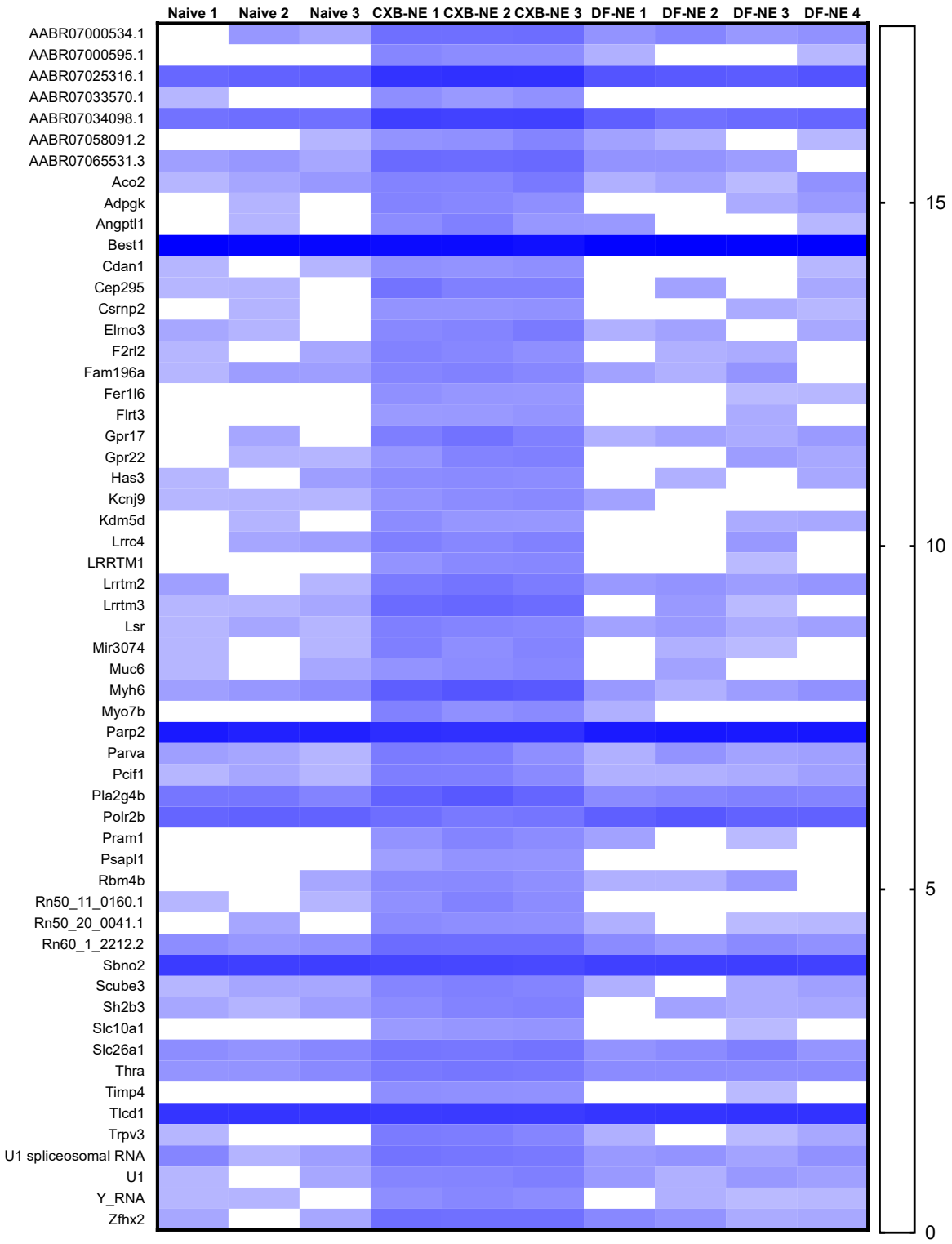

Figure 17. Heatmap showing $\log_2$ count per million (CPM) of the 57 genes shared across all three conditions with an adjusted P value (FDR) ≤ 0.05.

Table 8 illustrates the detailed information of the 25 up-regulated protein-coding genes with the greatest fold-change in expression along with their associated molecular function (NCBI database). During COX-2 inhibition (CCI CXB-NE), Prosaposin-like 1 (Psalp1) shows the highest expression change of 42-fold (essentially going from undetectable to expressed at a high level), with other notable genes including Leucine rich repeat transmembrane neuronal 1 (LRRTM1), transient receptor potential cation channel, subfamily V3 (TrpV3) and potassium voltage-gated channel subfamily J, member 9 (Kcnj9) exhibiting an increased expression after administration of the anti-inflammatory Celecoxib-loaded nanoemulsion (**Figure 17**). **Table 9** illustrates those significant down regulated protein-coding genes in CCI CXB-NE, having a raw P value <0.05, with their protein function as reported by NCBI. Of the 17 down-regulated transcripts (FDR ≤ 0.05) in the pain relief state (CCI CXB-NE) compared to the pain-state (CCI DF-NE), 9 of which are protein-coding (**Table 9**).

Of these differentially expressed genes in pain-state versus pain-relieved animals, 4 are previously annotated long non-coding RNAs (lncRNAs), all of which experience an increased expression after CXB-NE (**Table 10**). While these lncRNAs are annotated in ENSEMBL, there is however no known role ascribed to their pathogenesis in neuropathic pain.

Table 8: Top 25 upregulated protein-coding genes differentially expressed between CCI DF-NE and CCI CXB-NE rats with an FDR <0.05.

Gene Description	*Gene ID*	*Fold Change*	*FDR*	*ENSEMBL Gene ID*	*Molecular Function*
Prosaposin-like 1	Psalp1	42.204	0.00073	ENSRNOG00000006845	Neurotrophin/ Growth Factor
Anterior gradient 2	Agr2	33.680	0.03118	ENSRNOG00000005023	Adhesion
Anti-silencing function 1A histone chaperone	Asf1a	33.637	0.00734	ENSRNOG00000000415	Histone chaperone
Leucine rich repeat transmembrane neuronal 3	Lrrtm3	32.088	2.55E-24	ENSRNOG00000026466	Synaptic transmission
Nudix hydrolase 16 like 1	Nudt16l1	29.052	0.04646	ENSRNOG00000003224	Signal transduction
Membrane associated ring-CH-type finger 10	March10	27.061	0.04993	ENSRNOG00000007084	Ubiquitination
Myosin VIIb	Myo7b	23.855	3.40E-05	ENSRNOG00000015035	Adhesion
Myosin heavy chain 6	Myh6	22.701	4.00E-31	ENSRNOG00000025757	Adhesion
Transmembrane BAX inhibitor motif containing 1	Tmbim1	21.271	0.00016	ENSRNOG00000014797	Innate immune system
Leucine rich repeat transmembrane neuronal 1	LRRTM1	21.265	0.00011	ENSRNOG00000006093	Synaptic transmission
Arrestin 3	Arr3	17.859	0.00384	ENSRNOG00000002904	Signal transduction
Tissue inhibitor of metalloproteinase 4	Timp4	16.811	8.52E-05	ENSRNOG00000007955	Signal transduction
Codanin 1	Cdan1	16.177	0.00083	ENSRNOG00000047427	Cytoskeletal
Centrosomal protein 295	Cep295	14.559	3.40E-07	ENSRNOG00000010999	Centriole biosynthesis
Similar to Vomeromodulin	LOC690507	13.594	0.02271	ENSRNOG00000015637	Signal peptide for olfaction

Fanconi anemia, complementation group	Fancc	12.978	0.00461	ENSRNOG00000016889	Complement
AABR07000595.1	AABR07000595.1	12.822	0.00014	ENSRNOG00000030796	Unknown
MYC binding protein 2, E3 ubiquitin protein ligase	Mycbp2	12.429	0.0155	ENSRNOG00000010479	Axon guidance and Signal transduction
Solute carrier family 10 member 1	Slc10a1	12.363	0.0043	ENSRNOG00000005794	Ion channel
Leucine zipper protein 1	Luzp1	12.355	0.04913	ENSRNOG00000022402	Transcription factor
Transient receptor potential cation channel, subfamily V, member 3	Trpv3	12.111	3.32E-07	ENSRNOG00000019606	Ion channel
Sulfotransferase family 1A member 1	Sult1a1	11.715	0.03341	ENSRNOG00000019342	Neurotransmission
Mucin 6	Muc6	11.632	0.0074	ENSRNOG00000056817	Adhesion
Potassium voltage-gated channel subfamily J member 9	Kcnj9	11.274	0.0008	ENSRNOG00000007645	Ion channel
Single-minded family bHLH transcription factor 2	Sim2	11.092	0.0001	ENSRNOG00000054203	Transcription factor

Table 9: Top downregulated protein-coding genes differentially expressed between CCI DF-NE and CCI CXB-NE rats with an adjusted P value (FDR) ≤ 0.05.

Gene Description	*Gene ID*	*Fold Change*	*FDR*	*ENSEBML Gene ID*	*Molecular Function*
Histone H4 variant H4-v.11	Hist1h2ao	0.0308	0.04061	ENSRNOG00000058444	Nucleosome formation
U2 small nuclear RNA auxiliary factor 1	U2af1	0.0742	0.0218	ENSRNOG00000045860	Splicing factor
Poly (ADP-ribose) polymerase 2	Parp2	0.3284	2.58E-19	ENSRNOG00000008892	ADP-ribosylation

RNA polymerase II subunit B	Polr2b	0.3573	1.55E-05	ENSRNOG00000024779	RNA Polymerase
Bestrophin 1	Best1	0.5881	5.09E-05	ENSRNOG00000020346	Ion channel
Coiled-coil domain containing 152	Ccdc152	0.5883	0.01017	ENSRNOG00000039473	Unknown
ER membrane protein complex subunit 9	Emc9	0.6310	0.01652	ENSRNOG00000019162	Unknown
Strawberry notch homolog 2	Sbno2	0.7007	0.00027	ENSRNOG00000013987	Transcription factor
TLC domain containing 1	Tlcd1	0.7033	1.40E-08	ENSRNOG00000012579	Membrane assembly

Table 10: Differentially expressed annotated lncRNAs between CCI DF-NE and CCI CXB-NE rats with an adjusted P value (FDR) ≤ 0.05.

Gene Name	*Fold Change*	*FDR*	*ENSEBML Gene ID*
AABR07033570.1	50.95	.0001	ENSRNOG00000056730
AABR07033249.1	27.06	0.049	ENSRNOG00000055160
AABR07062800.1	15.77	0.0046	ENSRNOG00000054861
Rn60_1_2212.2	4.97	4.15E-12	ENSRNOG00000062127

4.4.4 Functional enrichment analysis

To further examine the mechanisms of differentially expressed RNAs within the pain states, Gene Ontology (GO, http://www.pantherdb.org) annotation and functional enrichment analyses were performed[168]. Gene Ontology relies on grouping known genes into categories of common function. The number of genes within each GO category encompasses all genes reported with significant enrichment (FDR ≤0.5) and that represent functional pathways already annotated (**Table 11**). This analysis shows that mRNAs exhibiting differential expression in this analysis are members of 14 functional pathways. We find there are up to ten differentially expressed mRNAs in the CCI pain state versus pain relief that are evident in these 14 distinct pathways (**Table 11**, Appendix B **Table 21**). Gene Ontology revealed the most significantly enriched 'biological processes' were the collection of "gene expression" (classified per its Gene Ontology

class as GO:0010467) and response to drug (GO:0042493) (**Appendix B Table 21**). The most significantly enriched 'molecular functions' include molecular transducer activity (GO:0060089) and signaling receptor activity (GO:0038023) (**Appendix B Table 21**). The more specific, GO Slim analysis of molecular function reveals G-protein coupled receptor activity (GO:0004930) and transmembrane signaling receptor activity (GO:0004888), both of which are noted in GO molecular function as well. Twenty statistically enriched cellular components are shown in the pain state when CXB-NE and DF-NE animals are compared. Notable cellular components include membrane-bounded organelle (GO:0043227), intracellular membrane-bounded organelle (GO:0043231), and cytoplasmic part (GO:0044444) (**Appendix B Table 21**).

KEGG signaling pathway analysis comparing 675 differentially expressed genes (raw P value ≤0.05) amongst CCI DF-NE and CCI CXB-NE conditions displays a single statistically significant KEGG pathway of Calcium signaling (KEGG:04020). When drug is present (CCI CXB-NE versus naïve) between the 584 differentially expressed genes (raw P value ≤0.05), cell cycle (KEGG:04110) show KEGG pathway expression, however no significant KEGG signaling pathways between CCI DF-NE and naïve conditions are noted. Reactome pathway (www.reactome.org) analysis[169] shows that when COX-2 is inhibited in macrophages, there is a statistically significant activation of two pertinent Reactome pathways: neutrophil degranulation (R-RNO-6798695) and the innate immune system (R-RNO-168249). Furthermore, PML-RAR alpha-regulated adapter molecule 1, Pram1, is known to be involved in neutrophil degranulation and has a fold change of 8.73 in the COX-2 inhibiting Celecoxib-loaded nanoemulsion (CXB-NE) pain relieved state. Expression changes in Importin 7 (Ipo7) and Strawberry Notch

Homology 2 (Sbno2) are two genes involved in the activation of the innate immune system. Sbno2 is reduced in expression when CXB-NE is present (fold change 0.70) and Ipo7 is increased (6.9 fold change).

Table 11. Gene Ontology (GO) Panther functional pathway analysis. The number of genes within the previously annotated functional pathways with significant enrichment (FDR ≤0.5. Includes genes differentially expressed between CCI DF-NE and CCI CXB-NE animals. Displays genes with an FDR ≤0.05 or genes with an FDR ≤0.5 and exhibits more than 4 genes per pathway.

Functional Pathway	Genes Involved
5HT2 type receptor mediated signaling pathway (P04374)	Gna11, Slca4, Plcd3, Cacna1c, Htr2b
Angiogenesis (P00005)	Pla2g4b, Fos, Pld2, Apc, Angpt2, Sphk2, Cryab
Blood coagulation (P00011)	F2rl2
Cytoskeletal regulation by Rho GTPase (P00016)	Myh6
FAS signaling pathway (P00020)	Parp2
Gonadotropin-releasing hormone receptor pathway (P06664)	Gna11, Ptger1, Fos, Cacna1c, Itpr2
Heterotrimeric G-protein signaling pathway (P00026, P00027)	Kcnj9
Huntington disease (P00029)	Rhog, Fos, Htt, Grin3b, Dync1h1, Optn, Arf6
Inflammation mediated by chemokine and cytokine signaling pathway (P00031)	Myh6, Pla2g4b, Gna11, Rhog, Myh7b, Camk2g, Adcy5, Ifngr1, Itpr2
Integrin signaling pathway (P00034)	Parva, Arhgap26, Lama5, Actn3, Col10a1, Arf6, Parva, Lama3, Col5a3
Muscarinic acetylcholine receptor 2 and 4 signaling pathway (P00043)	Kcnj9
Oxidative stress response (P00046)	Pla2g4b
Nicotinic acetylcholine receptor signaling pathway (P00044)	Myh6, Myo7b, Myo19, Myo18b, Myh7b, Chrnb1, Cacna1c
TCA cycle (P00051)	Aco2
VEGF signaling pathway (P00056)	Pla2g4b
Wnt signaling pathway (P00057)	Arr3, Myh6, Gna11, Wnt4, Myh7b, Apc, Pppr2r5b, Myh6b, Cdh15, Itpr2, Arr3, Smarcd3

4.4.5 Genes previously implicated in neuroinflammation

Several genes that have been previously reported to exhibit differential expression in neuroinflammation and/or the neuropathic pain were independently revealed in our analysis as summarized in **Table 12 and Table 13. Table 12** illustrates mechanism-specific genes expressed in the pain state compared to pain relief after injection of COX-

2 inhibiting CXB-NE, with upregulation and downregulation noted with arrow symbols. **Table 13** shows previously identified cell-specific expression with specific changes following CXB-NE. Based on gene ontology analysis using the Gene Expression Database[34], genes with overlapping expression in the pain and immune responses include; the purinergic ligand-gated calcium channel P2rx4, the G-protein coupled PGE_2 receptor, Ptger1, and IL-16, a pro-inflammatory cytokine that is chemotactic for CD4+ T-lymphocytes. Genes that normally exhibit neuronal expression and that are involved with the overall neuroinflammatory response include the sodium channels Scn8a/Nav1.6 and Scn11a/Nav1.9; the calcium channels Trpv1, Trpv3; and the NMDA receptor Grin3b/NMDAR3b. Significant expression changes occur when celecoxib (CXB) is administered in the pain-state and include mRNAs associated with axonal growth cone (Flrt3), growth cone (LRRTM1), axon guidance (Flrt3), regulation of axon guidance (Mycbp2), response to axon injury (Flrt3), and axonogenesis (Map1a, Dst). Molecular expression of genes involved in the immune response are noted including the β-arrestin 2 (Arrb2). Transforming growth factor β receptor signaling pathway activation including importin 7 (Ipo7) involved with the innate immune response, strawberry notch 2 (Sbno2) involved with macrophage activation, and PML-RAR alpha regulated adaptor molecule 1 (Pram1) a component of integrin-mediated signaling as well as T cell receptor signaling, regulation of neutrophil degranulation, and lysine (K)-specific demethylase 5D (Kdm5d), which is involved with T cell antigen processing and presentation. SH2B adaptor protein 3 (Sh2b3) a component of the cellular response to chemokines and negative regulation of chemokine-mediated signaling pathways and Fanconi anemia complementation group C

(Fancc) involved in myeloid cell homeostasis. All differentially expressed gene ontologies are listed in **Appendix B Table 21.**

Table 12: Differentially expressed genes in CCI DF-NE versus CCI CXB-NE involved in underlying neuroinflammatory pain mechanisms categorized using molecular functions. Increased and decreased expression is noted with arrow symbols ↑ and ↓.

	Ion channels	Signal transduction	Synaptic transmission	Cell adhesion and migration	Neurotrophins/ Growth factors	Inflammatory signaling/ Inflammation	Eicosanoid metabolism	Transcription factors	Other
Pain response	↑Nav1.6 ↑Nav1.9 ↑Cacna1c ↑Cacna1d ↑Kcnj9 ↑Trpv1 ↑Trpv3 ↑Ncald	↑P2rx4 ↑Arrb2 ↑Mycbp2	↑Grin3b	None	↓Ntrk1	↑Ifngr1 ↑IL-16 ↑Tnfaip8l2	↑Ptger1 ↑Pla2g4b ↓Ptgds	None	None
Nerve regeneration		↑Gpr22 ↑Arhgap26 ↑Plce1 ↑Arhgef11 ↑Itpkc ↑Nkiras1 Mycbp2	↑LRRTM1 ↑LRRTM2 ↑LRRTM3 ↓Cotl1	↑Dst ↑Flrt3 ↑Lrp2bp ↑Parva	↓Ntrk1 ↑Gdf11 ↓Ltbp4 ↑Psapl1	↑Map1a ↑Fkbp3	↑Pla2g4b ↓Cotl1	↓c-Fos	None
Immune response	↑Trpv1 ↑Trpv3	↑P2rx4 ↑Nkiras1 ↑Arrb2 ↑Gpr17	Epb41l3	Elmo3 ↓Card14 Tcaim	None	↑Ipo7 ↑Pram1 ↑Fancc ↑Irgq ↑F2rl2 ↑Sh2b3 ↑Scube3 ↓Sbno2 ↑Ilf3 ↑Ifit1 ↑IL-12rb2 ↑IL-12 ↑IL-16 ↑C8a ↑Ahsa2 ↑AC127605 ↓Ctsa	↑Pla2g4b ↑Ptger1 ↓Ptgds	None	↓Nbeal2

Cytokine production	↑Itpr2	↑Sema4c	None	None	None	↑Angpt 1 ↑IL-12 ↑IL-12rb2 ↑IL-16 ↑Ilf3 ↑F2rl2 ↑Hmox 2	↓Ptgds	None	None
Unknown role in CCI	↓ Best1	↑Atxn10 ↑Htt ↑Timp4	None	↑Acan ↑Agr2 ↓Ltbp 4	↑Vasn ↑Psapl1	None	None	None	↑Optn ↓ Fxn ↑Apo b

Table 13: Cell-specific expression of differentially expressed genes in the pain state compared to pain relief. Increased and decreased expression is noted with arrow symbols ↑ and ↓.

	Ion channels	**Signal transduction**	**Synaptic transmission**	**Cell adhesion and migration**	**Neurotrophins/ Growth factors**	**Inflammatory signaling/ Inflammation**	**Eicosanoid metabolism**	**Transcription factors**
Neuronal	↑Na_v1.6 ↑Na_v1.9 ↑Scn3b ↑Cacna1c ↑Cacna1d ↑Kcnj9 ↑Kcnmb1 ↑Kcnt1 ↑Kcne3 ↑Kcnab1 ↑Trpv1 ↑Trpv3 ↑Ncald ↑Clcn7	↑P2rx4 ↑Arrb2 ↑Mycbp 2 ↑Camk2 g	↑Grin3b ↑Stx18 ↑Syt5 ↑LRRTM1 ↑LRRTM2 ↑LRRTM3	↑Flrt3 ↑Dst	↓Ntr k1	↑Map1a	↑Pla2g 4b	None
Glial cells	None	↑Arr3	None	↑Omg ↑Syne2	None	None	None	None

Macrophages	↑Trpv1 ↑Scl22a2↑Sclc2a8 ↑Scl26a ↑Scl51a ↑Scl7a4 ↑Scl6a4 ↑Slc10a ↑Slc9a8	↑Wnt4		↑Myo7b ↑Myo9b ↑My019 ↑Thbs3 ↑Adgrg6 ↑Adgrg5 ↑Sphk2 ↑Muc6 ↑Muc15 ↑Elmo3		↑Ifngr1 ↑Fancc ↑Fanca ↑C8a ↑Card14 ↑Ilf3 ↑Ifit1 ↑IL-12rb2 ↑IL-12 ↑IL-16	↑Pla2g4b ↑Ptger1 ↓Ptgds	↓c-fos ↑Jmjd1c ↓Jmjcd8 ↑Ncor1 ↑Ncoa2 ↑Nr2c2
Circulating monocytes	None	None	None	↑Itgb1bp1 ↑Thbs3	None	↑IL-12rb2 ↑IL-16 ↑Sh2b3	None	None
Neutrophils	None	↑Abr	None	↑Myo7b ↑Myo19 ↑Myh6 Myh10 ↓Myl12b ↑Myh7b ↑Itgb1bp1 ↑Thsb3	None	↑Pram1 ↑Ipo7 ↑F2rl2	None	None
Mast cells	None	↑Pld2	None	↑Snx17 ↑Sphk2 ↑Thbs3	None	↑Unc13d ↑Pram1	↑Pla2g4b	None
T Cells	None	None	None	↑Muc6 ↑Muc15 ↑Tcaim	None	↑Il12rb2 ↑IL-12 ↑IL-16	None	↓c-Fos
Endothelial cells	↑Itpr2	↑Gna11 ↑Adcy5 ↑Pld2 ↑Angpt2 ↑Sphk2	None	None	None	↓Cryab	↑Pla2g4b	None

*Genes with a statistically significant raw P value or FDR value ≤0.05 are included.

4.4.6 Validation of genes by qPCR

Quantitative reverse transcription PCR was conducted on RNA purified from DRG amplified with primers for TrpV3, Scn8a, Pram1, IL-16, Ipo7, Flrt3, and Ifngr (**Figure 18**). All of these genes exhibited elevated RNA expression in the CCI DF-NE pain-state as compared to naïve when using RNA sequencing. All of these mRNAs when individually assessed by qPCR also exhibited elevated expression in the CCI CXB-NE pain-treated state compared to when the animals are in a pain state (CCI DF-NE). These results confirm the observation that there is a shift in expression for these transcripts when CXB-NE is present.

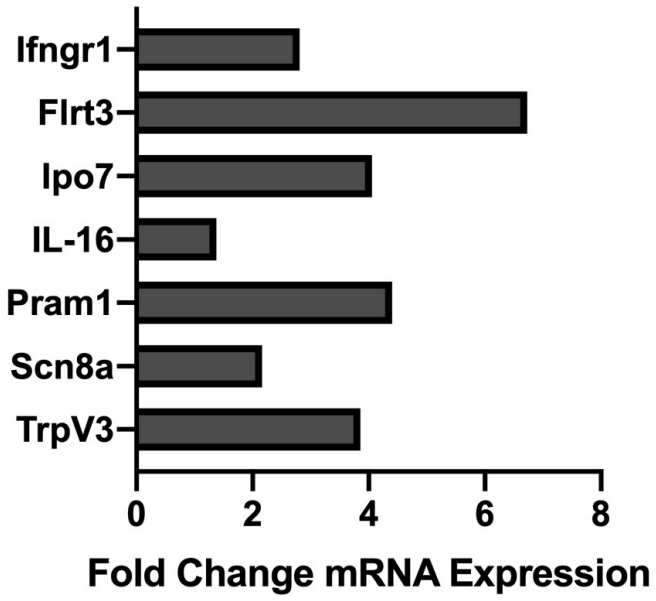

Figure 18. Individual qPCR analysis of distinct genes showing differentially expressed in the pain (CCI DF-NE) compared to the pain-relieved (CCI CXB-NE) state. CCI animals given CXB-NE exhibit increased expression of 7 known neuroinflammatory genes consistent with the RNAseq analysis.

4.5 Discussion

RNA sequencing allows for the exploration of an aspect of the molecular and biological mechanisms underlying neuropathic pain through the analyses of transcriptome changes. Identifying gene expression changes in the pain state (CCI DF-NE) is important in defining the mechanism of neuropathic pain and the sustained chronic pain response that ensues long after injury has occurred. Up until recently, relevant gene expression studies have been limited to individual genes and subset of genes via quantitative PCR and microarrays[47, 49, 160]. Although these techniques are vital in gene expression studies, they can only be utilized to identify known RNA transcripts. RNA sequencing differs in that it allows for the identification of expressed RNAs not previously known. Thus, researchers have begun to reveal RNA transcriptome changes in the affected tissues underpinning pain in small animal models [157,158, 163, 164, 166]. Mounting evidence indicates that differential expression of transcripts in the DRG coding for ligand-gated ion channels, cell signaling molecules, G-protein coupled receptors, and neuroimmune-specific precursors are all involved in the establishment of the perceived pain[158,164, 165]. We sought to further this analysis by assessing whole transcriptome changes in the DRG for animals experiencing pain relief from a state of modelled neuropathic pain as a result of treatment with the COX-2 inhibiting NSAID, celecoxib (CXB) packaged in nanoemulsion. The effective dose of celecoxib is a micro-dose, delivering COX-2 inhibiting CXB-NE to the site of injury. We reveal a novel drug effect on the differential expression of RNAs associated with neurons, activated glial cells, and multiple immune cells in the proximal dorsal root ganglion. Additionally, we use

PANTHER Gene Ontology and functional enrichment analyses to reveal 14 distinct pathways implicated when CXB-NE is given to CCI animals. Reactome pathway analysis indicates an altered neuroinflammatory response with changes in neutrophil granulation and the innate immune system within the cell bodies of injured rats. Moreover, we use qPCR to explore a subset of genes that show elevated expression in CCI rats experiencing a state of pain-relief following administration with CXB-NE, compared to those in a pain state (drug-free nanoemulsion). This subset of genes has been previously reported in the literature to be involved in neuroinflammation [20,49,79,165,80,240]. RNAs revealed in this current study are inclusive of both protein-coding (mRNAs) and non-protein-coding, including recently annotated long non-coding RNAs (lncRNAs). Overall, the impact of a precise drug inhibition of COX-2 and the corresponding reduction in PGE_2 production at the site of injury is to broadly influence RNA expression in multiple cell types of the corresponding DRG.

The main achievement of this study is the demonstration that treatment of neuropathic pain in animals achieved by targeted inhibition of COX-2 in macrophages leads to changes in gene expression profiles throughout the affected peripheral nervous system; not just confined to the site of injury[49] or within infiltrating macrophages. For context, previous studies using systemically, intrathecally, or subcutaneously delivered celecoxib demonstrated a decrease in PGE2 and moderate attenuation of allodynia in CCI animals[241, 242], whereas upon intraneural injection hypersensitivity persisted as well as PGE2 levels[48]. Our studies use a theranostic nanoemulsion, which an anti-inflammatory NSAID component (Celecoxib) utilized for treatment and a near infrared fluorescent dye (NIRF) to localize the nanoemulsion in vivo [46,48,49]. Nanoemulsion is readily cleared from

the bloodstream and introduced to the DRG by infiltrating macrophages[48, 73, 196, 243]. We hypothesize that the observed gene expression changes in the DRG is due to targeted COX-2 in infiltrating macrophages upon phagocytosis of the nanoemulsion from the bloodstream[46,48,49]. In accord with previous studies, a single dose (~0.24 mg/kg) of Celecoxib-loaded nanoemulsion (CXB-NE) one week after CCI surgery leads to in a change in the number of infiltrating macrophages, revealing on day 12 while the DRG has infiltrated macrophages, the density is 40% of what is seen in the injured sciatic nerve[46]. Also, while 63% of the macrophages in the sciatic nerve have nanoemulsion, only 19% of the macrophages in the DRG carry nanoemulsion[46]. From a behavioral standpoint, in CCI CXB-NE animals, there is a reduction in hypersensitivity within a day of intravenous injection and a near reversal in hypersensitivity by day 12, at which time tissue collection occurred[46,48,49]. Furthermore, our group (Saleem et al 2019) [46] have shown that peak pain-relief occurs on the third and fourth day after CXB-NE treatment and persists up to 6 days after administration[46]. Although gene expression changes were examined on day 12, it is likely that different subset of genes will be expressed beyond this time point. Saleem et al.[46] also demonstrated shifts from M1 to M2 phenotypes within the injured nerve when CXB-NE is administered compared to CCI animals receiving drug-free nanoemulsion (DF-NE), revealing an increase in the number of M1 macrophages in CCI DF-NE animals on day 12 [46]. Alternatively, the number of M2 macrophages is significantly increased in injured animals receiving CXB-NE on day 12, with a parallel production on day 18 in both pain-treated and untreated pain states[5]. At day 12, there are nearly twice as many infiltrating macrophages in the injured sciatic nerve than the corresponding DRG; interestingly, about 60% of the sciatic nerve

macrophages have nanoemulsion, whereas in the DRG only about 20% carry nanoemulsion[46]. When CXB is present, the number of macrophages at day 12 in the in sciatic nerve is nearly halved, but is unchanged in the DRG[46]. By day 18, the number of macrophages in the DRG increases about 3-fold, while it remains unchanged in the injured nerve[46]. Given that analgesia persists until around day 15, this may indicate the induction and persistence of gene expression that influences the milieu of cells at the DRG long term.

Clearly transcriptional changes are not restricted to changes in expression of genes associated with the production of PGE_2 in macrophages, instead transcriptional changes are evident for other neuroinflammation-associated genes and genes expressed in other cell types. The 25 genes with the greatest increase in expression are protein-coding genes associated with CCI CXB-NE pain relief (compared to CCI DF-NE) are illustrated in **Table 8,** however, the biggest differences may not be the most important in terms of underlying biology. **Tables 12 and 13** refer to genes previously implicated in neuropathic pain and neuroinflammation, which display varying degrees of altered expression in this study. Genes known to be involved in neuroinflammation and found to be responsive to drug therapy in this study are listed in **Tables 12 and 13**. Among the differentially expressed RNAs, Phospholipase A2 Pla2g4b (involved in the hydrolysis of phospholipids in the membrane), G-protein coupled Prostaglandin E receptor type 1 Ptger1 and Prostaglandin D2 Synthase Ptgds are involved in the production of PGE_2 after breakdown of the cell membrane. We also find differences in Coactosin-like (COTL1), which binds to F-actin and interacts with 5-lipoxygenase in leukotriene biosynthesis. All of these are associated with the metabolism of arachidonic acid and eicosanoids, which

are associated with COX-2 inhibition; and they show differential expression when CXB-NE is present in CCI animals.

We also know that on day 12, day of tissue collection, CCI animals are known to be undergoing peripheral nerve regeneration[46,76]. Our data shows that genes involved in this process are affected when drug-loaded nanoemulsion is applied to the pain state, possibly leading to an increase in factors contributing to nerve regeneration. Fibronectin leucine rich transmembrane protein 3 Flrt3, and leucine rich repeat transmembrane neuronal proteins LRRTM1, LRRTM2, and LRRTM3 are all differentially expressed and are known to be involved in axon outgrowth and synapse formation[170].

One way to think of these observations is in terms of a potential shift in cell fate, which may be occurring among several cell types during the chronic inflammatory state. The transition to chronic pain relies on significant changes in gene expression. Similarly, when COX-2 is inhibited in macrophages during the neuroinflammatory response, the shifts in RNA expression can represent realignment of cellular function representing pain-relief and possibly shifts in cell fate as was seen in the macrophage transition from M1 to M2 in the sciatic nerve in response to CXB-NE[46]. Transcriptional and protein changes are noted in both the damaged sciatic nerve and the dorsal root ganglia[46,47, 49, 244]. We have previously shown that intravenous injection of CXB-NE one week post injury, results in differences in macrophage expression at the injured sciatic nerve and in the lumbar DRGs[46] as well differential expression of a subset of mRNAs in the sciatic nerve compared to the DRGs[49]. Here we show when COX-2 is inhibited, there is an increased expression in inflammatory molecules (pro-inflammatory cytokines IL-12, Il12rb2, IL-16) and other RNAs known to be involved with cells associated with the neuro-

inflammatory response including Unc13d involved in intracellular trafficking and exocytosis, also Pram1 an adaptor protein involved with T-cell receptors mediated signaling, Sh2b3 an adaptor protein involved with regulating signaling pathways and Ipo7 a nuclear transport protein. In addition, there is a down-regulation in ion channels in CCI DF-NE (Scn8a, Scn11a, Scn3b, Clcn7, Kcnj9, Kcnt1, Kcnmb1, Kcne3, Kcnh6, Kcnab1, Trpv1, Trpv3, Cacna1c, and Cacna1d) ranging from a fold change of 2.5 to 20.7, when the raw P value is ≤ 0.05. Given these changes, it appears that select RNAs associated with neuronal expression in the DRG shift from a normal sensory neuron to a hypersensitive pain-responding neuron after chronic constriction injury. Even after a pain-relieving behavioral change is evident after CXB-NE is given, RNAs typically associated with inflammation continue to exhibit increased expression on day 12. In comparison, to the injured sciatic nerve, when given CXB-NE, neuroinflammatory-associated RNAs show downregulation, with a decreased expression of Scn9a and TrpV3 and an increase expression in Cacna1b[49]. Interestingly a comparable RNA sequencing studying examining sex differences at the DRG after CCI revealed a modest upregulation of Scn9a[79]. It is important to note that gene expression differences exist in the DRG and sciatic nerve after CCI. We have shown previously that IL-6, IL-1β, Scn9a/Nav1.7, Grin2b/NMDAR2b, Itgam/Cd11b, Moab, Tac1, and Trpv3 are all downregulated in the injured sciatic nerve after CXB-NE administration, whereas Cacna1b is upregulated[49]. Similarly, some genes and their homologs exhibit differential expression in the DRG under nanoemulsion treatment. For example, in the DRG, there is an increased expression of the Calcium channel Cacna1b and sodium voltage gated channels Nav1.6 and Nav1.8 after treatment with CXB-NE. A recent study in mice explored how DRG

macrophage activation may influence sensory neurons and found a significant upregulation of IL-1β only in CD11b macrophages, with no evidence of IL-1β expression in satellite cells or sensory neurons[244]. In addition, there is a shift in RNA expression typically associated with Schwann cells, macrophages, and mast cells in their inflammatory functions. RNA expression changes in cell adhesion molecules (Flrt3, Elmo3, Card14, Dst, Parva, Myo7b, Myo19, Itgb1bp1, Thsb3) is also seen, suggesting the extracellular milieu for the cells in the DRG, including the primary sensory neurons, is changing. An increase in expression of Flrt3 in the DRG has been noted in previous RNA sequencing studies[79]. Furthermore, Mast cells may be in a degranulating state in the pain-relieved state, as indicated by an increase in Pram1 and Unc13d expression. We have previously shown a decrease in Mcpt1 mast cell degranulation at the site of injury when COX2 is inhibited by nanoemulsion CXB-NE [46,49].

This study shows decreased expression of TrpV3 RNA in the DRG while in the pain state (DF-NE) as compared to animals with COX2 inhibited by CXB-NE that are experiencing pain relief. Interestingly, we have previously shown the opposite effect in the sciatic nerve where a significant decrease in TrpV3 gene expression is evident in CCI CXB-NE animals[49]. One interpretation is that TrpV3 expression at the injured sciatic nerve is prominent due to its activation by arachidonic acid metabolites in inflammatory conditions. A 2006 study by Zhu and colleagues[114] shows that TrpV3 is potentiated by unsaturated fatty acids such as the activation of arachidonic acid, which is targeted specifically by CXB. Furthermore, a study by Freichel (2012)[171] and colleagues demonstrated that activated mast cells exhibit increased expression of Trp proteins, associated with pain and degranulation.

Neuro-immune cross-talk may be associated with the increased expression of F2rl2 a 7-Transmembrane G-Protein coupled receptor, Pram1, which is associated with T-cell receptor mediated signaling, and Ipo7 a nuclear transport protein. These observations are consistent with the REACTOME analysis, displaying activation of neutrophil degranulation (R-RNO-6798695) and activation of innate immune system (R-RNO-268249) pathways. Neuroimmune signaling further mediated by the purinergic receptor P2rx4 (expressed by neurons and immune cells) may lead to the increase in neutrophil and M1 macrophage infiltration after nerve injury as seen when given a systemic COX-2 inhibitor[245]. Although we have previously reported in vitro and in vivo specificity of the nanoemulsion to monocytes[72], activation of the innate immune system may lead to an increased neutrophil response after CCI. Within injured sciatic nerve tissues, we have previously identified pain and CXB-NE pain-relief shifts in M1 and M2 macrophage phenotype and mast cell degranulation activity using the same experimental conditions at day 12 [46]. Considering all of the RNA expression data from both the injured sciatic nerve[15] and associated DRG cell bodies reported here, we observe that due to the CCI damage of the associated axons and surrounding cells in the sciatic nerve, RNA expression changes are apparent at not only the injured sciatic nerve [46,48,49], but also in the cells of the DRG.

In addition to differential expression of protein-coding RNAs expressed in the DRG, non-coding RNA expression changes was investigated. The role of non-coding RNAs remains an important aspect of pain research as these RNAs, actively participate in processes that coordinate gene expression[172]. One class of non-coding RNAs are long non-coding RNAs (lncRNAs), which are greater than 200 nucleotides in length, highly

abundant and multi-functional. lncRNAs have the capacity to regulate gene expression[173]. Interestingly, we have identified 4 lncRNAs that are differentially expressed when celecoxib-loaded nanoemulsion is administered (**Table 10**). Each of these lncRNAs exhibit significant expression changes ranging from a nearly 5-fold increase to a 50-fold increase in CCI- CXB-NE (**Table 10**) and have only been recently annotated in ENSEMBL.

In summary, peripheral nerve injury resulting in behavioral hypersensitivity causes changes in RNA expression at the site of injury[49], as well as differential RNA expression evident in the corresponding cell bodies of the dorsal root ganglia. We also demonstrate that introducing CXB-NE not only reduces hypersensitivity[46,48,49], and reduces inflammation at the site of injury[46,48,49], the drug therapy is associated with widespread changes in the transcriptome of various cell types at the site of injury and the cells of the corresponding dorsal root ganglia. Even though celecoxib specifically attenuates COX-2 activity in the associated macrophages, the influence extends far beyond.

Chapter 5. Discussion, Conclusions and Future Directions

As adapted from:

A. Stevens, L. Liu, D. Bertovich, J.M. Janjic, J.A. Pollock. Differential expression of neuroinflammatory mRNAs in the rat sciatic nerve following chronic constriction injury and pain-relieving nanoemulsion NSAID delivery to infiltrating macrophages. *International Journal of Molecular Sciences* 2019; 20(21): 5269. Doi.org/10.3390/ijms20215269.

A. Stevens, M. Saleem, B. Deal, J.M. Janjic, J.A. Pollock. Targeted COX-2 inhibiting nanomedicine results in pain-relief and differential expression of RNA in the dorsal root ganglia of injured male rats. *Molecular Pain In Press* 2020.

M. Saleem*, **A. Stevens*,** B. Deal, L. Liu, J. M. Janjic, J. A. Pollock. A new best practice for validating tail vein injections in rat with near infrared labeled agents. *Journal of Visualized Experiments* 2019; e59295. *Co-authors contributed equally.

5.1 Discussion

5.1.1 Neuropathic injury involves a dynamic inflammatory response involving the neuro-immune triad

I have hypothesized that neuropathic conditions will elicit RNA expression changes representative of neuroinflammation, the pain response, and the underlying neuroimmune cross-talk. Specifically, these expression changes would be apparent at the site of injury within the inflamed sciatic nerve and its' connection to the central nervous system, the cell bodies of the dorsal root ganglia (DRG) as well as within other aspects of the neuro-immune triad, including neurons, glial cells and immune cells such as macrophages and

Schwann cells. We have demonstrated that altered RNA expression profiles, inclusive of protein-coding and non-coding molecules, occurs in both site of the injured nerve as well as in the DRG. Although we cannot say for certain whether these specific RNAs are found within a given cell type within the sciatic nerve or DRG tissue, we can speculate on their expression based on associations established in the literature. More studies are required to determine which cell type is expressing each given RNA and is discussed in the Future Studies subsection.

It is previously known that neuropathic injury involves a dynamic inflammatory response mediated by multiple cell types both at the site of injury (in the sciatic nerve) and in the DRG[19,27]. There is an increased dialogue between immune cells, neurons, and glia that results in behavioral hypersensitivity interpreted as pain. The resultant neuroimmune cross-talk at and near the site of injury perpetuates its effects in two ways. Firstly, the sutured chronic injury of the nerve leads to a change in the microenvironment causing a local neuroinflammation[19]. Neuroinflammation consists of both phenotypic and structural changes to resident immune, glial and neuronal cells as well as the activation of infiltrating immune cells[91]. Each cell type is able to influence the neuroinflammatory response through the production and release of inflammatory mediators such as cytokines, chemokines, neurotrophic factors, Substance P, and prostanoids and the increased expression of ion channels and cell surface receptors[91]. Second, there is subsequent healing and axonal regeneration of the injured peripheral nerve fibers[12,174]. This overall process is initially marked by a degeneration phase, known as Wallerian degeneration, within 3-5 days of injury[174], promptly followed by an extensive period of regeneration. During each of these phases, both immune and glial cells undergo

phenotypic shifts assisting in the initial degradation and phagocytosis of debris at and surrounding the site of injury followed by neuroimmune signaling of pro- and anti-inflammatory mediators[12]. One of the major goals of our study is to explore the underlying neuroimmune response, in terms of RNA expression changes, following nerve injury caused by chronic constriction (CCI).

Differential expression of RNA within the injured sciatic nerve as well as in the cell bodies of the DRG is evident 12 days after injury. Assessment of the differential expression of mRNAs in CCI sciatic nerves was performed by quantitative PCR for several genes previously identified as associated with neuroinflammation. We found many that mRNAs exhibited differential expression associated with CCI pain as well as pain relieved states. The injured sciatic nerve exhibited an increased expression of macrophage-related genes in the pain state (CCI DF-NE) compared to the sham control and pain relieved animals (CCI CXB-NE) (as discussed later in Section 5.1.2). Other immune-cell related genes exhibit differential expression when compared to the sham control and between the CCI conditions including T cell marker Cd4, cytokines IL-6, IL-18 and IL-1β. Chemokine receptor Cx3cr1, Toll-like receptor 2 Tlr2, and Tumor necrosis factor Tnf1.

Helper T cell marker Cd4 gene exhibited an elevated expression in the injured nerve (fold change 8.3) as compared to the un-injured control. When pain is relieved, Cd4 mRNA expression was still elevated, though reduced slightly (fold change of 7.3) relative to un-injured control state. Although not a statistically significant difference in expression, there is a downregulation of Cd4 in CXB-NE pain-relieved animals, possibly indicating that fewer T cells were present at the site of injury after the attenuation of

COX-2 in macrophages. This may be a significant finding as a number of studies have implied a role of helper T cells in the pathogenesis of pain[35-37], with a more significant interplay in the neuroimmune triad in female animals[167, 193] (see Section 5.2 for future studies).

Differences in RNA expression are noted between CCI DF-NE and sham controls, illustrating that numerous genes alter their expression in response to the neuroinflammation caused by CCI. Notable changes include the pro-inflammatory cytokines associated with multiple cell types (neurons, macrophages, Schwann cells) including IL-6, IL-18 and IL-1β. IL-1β, a pain-induced cytokine, exhibits a significant (18 fold) increase compared to the sham control. IL-1β is a tightly regulated cytokine produced predominantly by myeloid cells[218]. It is synthesized as an inactive precursor molecule that must be cleaved to initiate biological activity involved in the immune response[130]. Pattern recognition receptors interact with damage-associated molecular patterns (DAMPs) secreted in response to tissue injury, leading to the cleavage of IL-1β to its active form[130]. Okamoto and colleagues[128] examined cytokine mRNA expression in the sciatic nerve at several time points following nerve injury. They found that at day 14, IL-1β was upregulated (30 - fold increase) in expression in the CCI pain state. Although the relative expression is much higher in the Okamoto[128] study than what is observed here, we nonetheless found that IL-1β exhibited elevated differential expression. The differences between our procedure and that of Okamoto and co-workers can account for the differences in observed expression levels, where methods of RNA isolation and extraction as well as experimental parameters for the qPCR reaction can account for the observed differences in the results.

Both IL-1β and IL-18 are involved in inflammasome signaling upon activation of the innate immune response. This response is mediated by pattern recognition receptors that are able to recognize danger-associated molecular patterns (DAMPs) upon nerve injury[134], inducing gene transcription and translation of IL-1β and IL-18 inactive precursors (pro- IL-1β and IL-18)[236]. When DAMPs are recognized, IL-1β and IL-18 are produced by inflammasomes[219,234]. As noted earlier, this study shows that both of these genes exhibit an elevated RNA expression after nerve injury. Vasudeva et al.[20] established an increase in protein expression after CCI of both IL-18 and IL-1β. Their work also demonstrated, using Bayesian network analysis, that IL-18 acts as a central node involved in inflammatory signaling in the CCI pain response. This represents a unique activation of the inflammasome. The inflammasomes are a group of multimeric protein complexes that are triggered by a range of substances during tissue damage[93]. Inflammasomes were first described in 2002[239] as a cytosolic caspase-activating protein complex in macrophages, but now are known to be found in multiple cell types including neutrophils, mast cells, and T cells[236]. It is currently known that inflammasome activation, in turn, leads to the activation and proteolytic cleavage of IL-18 and IL-1β [219]. While our research illustrates that genes involved in inflammasome activation and signaling are being expressed nearly two weeks after nerve injury, these results do not directly address whether or when the inflammasome is activated. However, this may be indicative of inflammasome signaling being a pertinent player involved in the ongoing maintenance or persistence of pain.

An extensive cross-talk is thought to be occurring between the nervous and immune systems, in which specifically activated nociceptors and immune- and immune-like glial

cells engage in multi-directional signaling, possibly leading to the persistence of pain[137]. Signaling occurs through the local and persistent production and release of a milieu of inflammatory mediators by neurons, macrophages, monocytes, neutrophils, mast cells, Schwann cells, and satellite glial cells. Our results show that mRNA expression in the injured sciatic nerve is altered for mRNAs typically associated with neurons, including Actin-β Actb, receptors for inflammatory mediators Calca, Ntrk1, Comt, endothelin receptor Ednra, glutamatergic receptors Grm1 and Grm5, ion channels Kcnj6, Kcnq, Scn9a/Nav1.7, TrpV3, and Cacna1b/Cav2.2. In addition, a subset of genes previously associated with multiple cell types and neuroinflammation showed marked expression differences when drug therapy is present, including the inflammatory mediators Glial cell derived neurotrophic factor GDNF (associated with Schwann cells and neurons), cytokines IL-18, IL-1β, IL-6 (associated with circulated monocytes, macrophages, Schwann cells, and neurons) , monoamine oxidase B Maob, and tumor necrosis factor Tnf as well as their associated receptors (Chemokine C-X3-C motif receptor Cx3cr1)[49]. Our RNAseq study further demonstrates an altered expression of RNAs previously associated with neuroinflammation (Trpv1, TrpV3, Scn8a, Scn11a, Kcnj9, Cacna1c, IL-12, IL-16) as well as nerve regeneration (Flrt3, LRRTM1, LRRTM2, LRRTM3)[49].

Cx3cr1 is a single ligand, membrane-tethered chemokine CX3CL1 (fractalkine)[53]. All circulating monocytes express the fractalkine receptor and it is known to exhibit elevated expression in the pain state[220], particularly in the dorsal root ganglia and spinal cord as well as in macrophages in the periphery following injury[221]. The Cx3cr1 gene exhibits no significant difference in expression in sham relative to CCI CXB-NE but is significantly downregulated when CXB-NE is present. A fold change in pain-relieved animals

decreases nearly 5-fold compared to pain state animals (CCI DF-NE). This data suggests that by inhibiting COX-2 in macrophages, there is a subsequent decrease in fractalkaline signaling and a reduced production of its receptor Cx3cr1 in the periphery.

Ensheathing Schwann cells (as well as neurons and macrophages) at the site of injury are known to actively secrete IL-6[127]. We found that IL-6 mRNA expression is elevated post-CCI in the drug-free ipsilateral sciatic nerve. However, IL-6 is recognized as a marker in nerve regeneration[122]. With a significant downregulation of IL-6 when COX-2 inhibiting nanoemulsion is present in macrophages at the sciatic nerve, we would assume less nerve regeneration is occurring when drug is present. However, it is clear that IL-6 is not the only inflammatory mediator produced that is involved in regulating axonal regeneration.

In terms of the role of neurons in the neuro-immune triad, we have also successfully demonstrated that neuronal injury in the periphery leads to changes in gene expression at the site of injury and in the corresponding ganglia, which may be distinct. Peripheral sensory axons of the sciatic nerve have their cell bodies in the DRG, but it is at the distal axon, centimeters away from the DRG cell-bodies, which are injured and thus the source of noxious stimulation. Knowing that pain signals begin as noxious stimuli detected by nociceptors in peripheral nerve fibers of DRG primary sensory neurons, which are then transmitted to the central nervous system, DRGs act as a bridge between pain sensation in the periphery to response in the spinal cord and brain that are interpreted as pain. It appears that depending on whether the RNA is being produced to function within the cell bodies or is being transported to the distal nerve fibers for various functions, RNA expression may be different. This observation is supported with the results on the

production of the voltage transient receptor potential 3 (TrpV3) mRNA in both the sciatic nerve and DRG. TrpV3 is downregulated in both neuronal tissues after administration of CXB-NE, suggesting it may be actively transported from the nucleus of the DRG to the distal axons in similar levels in response to nerve injury. Another gene typically associated with neurons includes the tachykinin pain molecule precursor gene, Tac1. Tac1 leads to the generation of substance P, neurokinin A, neuropeptide δ, and neuropeptide γ [143,144] which are mainly expressed in neuronal tissues in the central nervous system and in primary afferent neurons in the peripheral nervous system[144]. However, it has also been shown that substance P and neurokinin A are expressed in non-neuronal cells including macrophages and circulating monocytes[144]. This suggests an interplay between the inflamed sciatic nerve tissue and the COX-2 inhibited macrophages after CXB-NE administration.

Another facet of the study RNA profiles within the injured nerve tissue would include the differentiation of sensory and motor neurons within the studied samples. As stated earlier, the sciatic nerve contains a mixed population of motor and sensory axons, whereas the corresponding cell bodies of the DRG are purely sensory. The corresponding motor components are found within the ventral nerve root. Vasudeva et al. conducted a study on CCI used DiD retrograde labeling from the footpad to the nervous system to identify the presence of anatomical structures within the labeled neuronal pathway to the lumbar level 5 (L5) DRG[47]. RNA sequencing of the ventral nerve root could be conducted in order to determine the role of motor sensation and RNAs associated with motor movement and muscle within the CCI NSAID-loaded nanoemulsion model used in the second aim of my study.

Differences in expression of RNAs associated with the DRG and the injured sciatic nerve can be accounted for, mainly due to their anatomical and functional differences. The injured sciatic nerve contains axons and supporting cells that together are involved in propagation of action potential and signaling, whereas the primary sensory neurons contain the nuclei, where transcription is actively occurring. In both the DRG and the sciatic nerve the distinct cells have a wealth of cell surface receptors and signaling mechanisms that help to interpret cell-cell communication in the local environment. The cell bodies extending axons into the sciatic nerve are located in the L4-L6 DRGs, with most innervation being in L4 and L5 DRG. Once these primary sensory neurons are activated by axonal injury at the sciatic nerve, they are likely to modify their RNA production in response to nerve injury. Studies have shown that after multiple axonal injuries in the periphery, the DRG become primed and thus are likely to regenerate distal axons more rapidly in response to subsequent lesions[181-183]. In addition to this response, retrograde signaling sent from the site of injury to the cell body occurs[184] may help to initiate transcriptional changes in the nucleus that increase production of molecules involved in neuronal regeneration[185, 186]. Simultaneously, this retrograde signaling also contributes to the altered gene expression of the surrounding cells and milieu of inflammatory mediators around the injured neurons[10,183,186, 187]. Taken together, our studies revealed altered RNA expression in the injured sciatic nerve as well as the corresponding DRGs with differential expression appearing to be evident in multiple cell types in both locations.

CXB-NE tends to exert its effects in a different manner in the affected DRGs, than at the site of injury in the sciatic nerve. For example, the receptor to cytokine interleukin

12, IL-12rb2, as well as IL-16, are both upregulated in the DRG after administration of COX-2 inhibiting nanoemulsion. Furthermore, IL-12 is produced by antigen-presenting cells such as macrophages and can exert an effect on T cells, such as stimulating production of IFN-γ [178]. Additionally, IL-16 production is associated with mast cell activation following prostaglandin synthesis[179]. Saleem et al.[46] has shown the presence of degranulating mast cells at the DRG in CXB-NE treated rats. In the inflamed sciatic nerve, however, we have showen there is a differential expression of IL-18, also highly involved in the production of IFN-γ[20]. Interestingly, IL-18 RNA expression was not detected in the DRG 12 days post-surgery.

By dampening the neuroimmune cross-talk provoked by production of inflammatory mediators, we have demonstrated COX-2 attenuation in tissue-differentiated macrophages not only leads to a decrease in PGE2 production[46, 48] but also leads to changes in RNA expression of genes both known to be implicated in neuroinflammation as well as other novel ones. Interestingly, although our study only targeted COX-2 production in macrophages, gene expression changes associated with other cell types were modulated when drug therapy is present. Furthermore, injured animals exhibited differential expression of multiple RNAs within the injured sciatic nerve and in the corresponding cell bodies within the DRG.

5.1.2 COX-2 inhibiting nanomedicine modulates RNA expression that has been altered by nerve injury in macrophages and other cells involved in neuroinflammation

Overall, under neuropathic conditions, we know that CXB-NE is altering the activity of COX-2 and the production of PGE2 in macrophages. We anticipated that RNA expression changes may too be occurring in these targeted cells. However, our data reveals that the impact of this pain-relieving therapeutic extends beyond the macrophages to influence changes in RNA expression in other cell types. Furthermore, while pain is known to alter gene expression within the neurons in the dorsal root ganglia (DRG), there is an observed similar effect at the site of injury, involving multiple cell types based on previous studies of RNA expression corresponding to a given cell type.

We know that macrophages are recruited to the site of injury within three days after surgery where they begin to phagocytose myelin debris and biproducts of damage formed as a result of nerve injury[56,176]. Previous studies by our laboratory have established that there is a reduction in number of infiltrating macrophages in CCI CXB-NE animals associated with a reduction of COX-2 activity and the subsequent production of PGE2[46, 48], and thus it is expected that RNA expression changes may too be occurring in these targeted cells as well. In fact, we have found that in the damaged sciatic nerve, several macrophage-associated genes as well as genes responsible for coding pro-inflammatory cytokines exhibit altered RNA expression. A study by Bausbaum et al. (2020)[250] utilized a spinal nerve ligation (SNL) model and fluorescence-activated cell sorting to distinguish CX3CR1-positive macrophages within the injured DRG and found that the CX3CR1-positive cell population in the L4 and L5 DRG was increased by nearly 3 fold compared

to the unoperated, contralateral side 4 days after injury. Based on this study, Bausbaum and colleagues[250] were able to conclude from DRG macrophages are a major contributor to the initiation and maintenance of pain, and via other cell-sorting and transgenic mouse line experimental techniques, that macrophages outside of the DRG may not be as important as once thought[250]. However, data generated within my laboratory has shown that on day 12, while the DRG has infiltrating macrophages, the density is 40% of what is seen at the injured sciatic nerve[46]. When CXB-NE is present, the number of macrophages at day 12 in the sciatic nerve is nearly halved, but unchanged in the DRG[46]. This may indicate that the gene expression profiles associated with an increase in neuroinflammation are occurring moreover at the site of injury than the corresponding DRGs 12 days post-injury. Overall, mRNAs associated with neuroinflammation demonstrated a reduction at the injured sciatic nerve when CXB-NE was administered compared to DF-NE in CCI animals. On day 12 in the DRG, RNA expression profiles associated with neuroinflammation demonstrated a partial reversal in expression with some prominent neuroinflammatory genes showing an upregulation in pain-treated (CCI CXB-NE) animals compared to those without treatment (CCI DF-NE). This could possibly be attributed to an ongoing effect of the CXB-NE on long-term gene expression changes. Coinciding with behavioral data, in which analgesia persists until day 15 [46], this may indicate the induction and persistence of gene expression that influences the milieu of cells at the DRG are long-term and may be occurring later. After all, even after administration of a pain-relieving drug (CXB-NE) is evident, RNAs typically associated with inflammation continue to exhibit increased expression on day 12 in the DRG. In order to explore this phenomenon further, an increased time point study is required where

tissues are dissected later than 12 days and the same RNA expression profiles are assessed.

Itgam/Cd11b and Itgb2/Cd18 form the integrin MAC-1 complex, which is responsible for the recruitment and adhesion of leukocytes to the site of injury[55,121]. Similarly, Mcp5 serves to recruit circulating monocytes to the site of injury comparable to Mcp1, a better studied homolog[122, 223]. Each of these genes produce proteins that are involved in macrophage recruitment to the site of injury and showed a decrease in RNA expression when directed COX-2 inhibition occurred in macrophages 4 days after intravenous injection of CXB-NE. This may signify that by inhibiting COX-2 and a subsequent decrease in PGE_2 production at the site of injury in macrophages, there is an attenuation of the recruitment of signaling for new infiltrating macrophages. In the sciatic nerve, other mRNAs typically associated with macrophages and circulating monocytes exhibited increased expression when compared to the sham control but not a major difference between the pain and pain relieved state. These genes include Adrb2 (adrenergic beta-2 receptor), Ccr2 (chemokine C-C receptor 2), Cnr2 (cannabinoid receptor 2), and Ptgs2 (prostaglandin E synthase 2). Given this attenuation in COX-2 activity in macrophages, our data suggests that by inhibiting this enzyme and its biproducts, there is a subsequent change in macrophage signaling, including integrins and cytokines that can potentially affect surrounding cells.

Gene profiles of macrophage-related genes also exhibit differential expression after injury following CXB-NE. M1, pro-inflammatory, macrophages are induced by interferon gamma, IFN-γ, amongst other activators[176]. At day 18 in the DRG, there is an increase in the number of M1 macrophages in CCI CXB-NE relative to CCI DF-NE by

56% compared to day 12 [46]. As we know, activated M1 macrophages mainly secrete pro-inflammatory cytokines, which promote debris removal, and may assist in the healing process[176]. Furthermore, it is thought that anti-inflammatory and axonal healing promoting-M2 macrophages infiltrate the site of injury after M1 macrophages have fulfilled their phagocytic, pro-inflammatory role[176]. Our study showed a distinct increase in expression of the interferon gamma receptor (Ifgnr) RNA within the DRG after animals experienced pain-relief (CXB-NE). This is consistent with other studies as IFN-γ has been shown to directly polarize macrophages toward an M2 phenotype[176]. M2 Macrophages are also known to promote angiogenesis[177], which provides nutrition for the repair of the nerve tissue, an important step in nerve healing[176]. It is possible that an increase in Ifgnr mRNA in the cell bodies of the DRG is involved in the repair process associated with the polarization of macrophages both in the DRG as well as near the site of injury in the sciatic nerve.

Additionally, a heightened increase of monocyte chemoattractant protein 1 and 5 (Mcp1 and Mcp5) are noted in both the sciatic nerve and DRGs after chronic constriction injury (**Figure 18**). Mcp1 is a mediator in the immune response, it is involved in binding to the surface of circulating monocytes helping to recruit them to the site of injury[122]. Mcp5 is thought be homologous to human MCP-1, but little is known about the

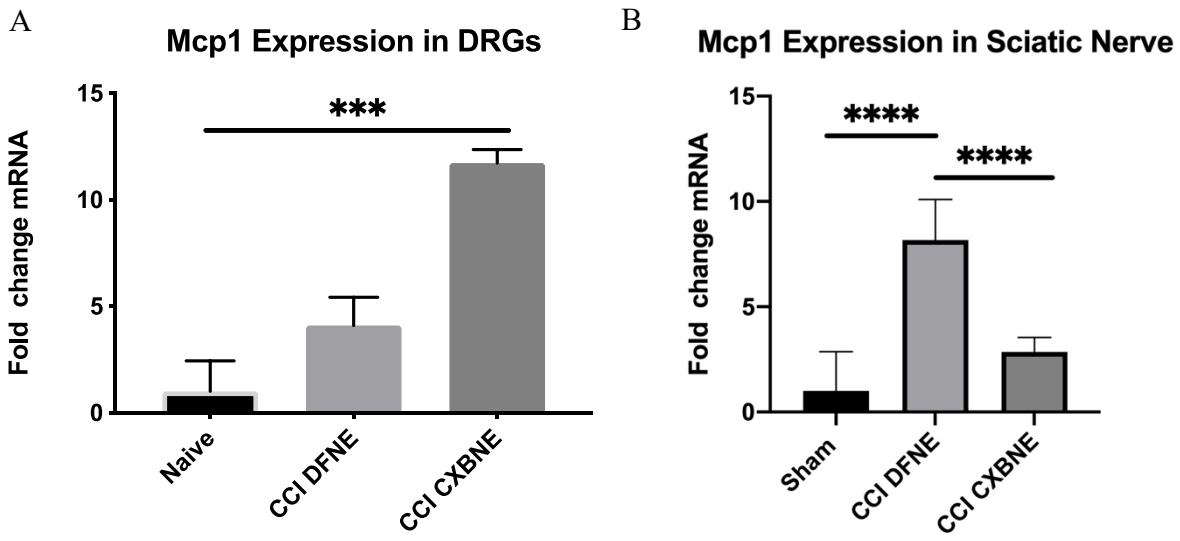

Figure 19. Differential expression of Mcp1 mRNA in the sciatic nerve and DRG on day 12 post-surgery. qPCR was performed on Mcp1 mRNA from (A) L4-L5 DRG and (B) injured sciatic nerve. In the injured sciatic nerve tissue, there is significant expression differences in the naïve control and CCI animals. In the DRG, there is no statistical difference in Mcp1 of CCI CXB-NE and naive animals, but there is between CCI CXB-NE and CCI DF-NE as well as sham and CCI DF-NE. Note that although two different controls are reported (sham and naïve) they are statistically the same. One-way ANOVA and Tukey's multiple comparison was performed between conditions. **** $P < 0.0001$.

molecule in the pain response in animals. As noted in **Table 2**, mRNA expression differences exist in the different neuronal tissue. In the DRG, there is a large increased expression of Mcp1 mRNA in the CXB-NE pain-relieved animals compared to pain state animals (**Figure 19**). In the corresponding sciatic nerve, there is a slight increase in Mcp1 in the CCI CXB-NE pain-relieved animal. Surprisingly, the CCI animals treated with DF-NE, which are still exhibiting pain-like behavior, have a slightly elevated expression of Mcp1 in the DRG, whereas at the corresponding site of injury, the Mcp1 expression in the sciatic never is very high, even higher than that observed in the pain-relieved sciatic nerve (**Figure 19**). Although, Mcp1 is known to be expressed during CCI and spinal nerve ligation models of pain in animals by small and large neurons as well as

in the axon terminals[223], Celecoxib-loaded nanoemulsion seems to have a differential effect on these two anatomical areas as observe with these two different techniques. This is expected as the dorsal root ganglia contain the cell body where RNA is being actively transcribed, whereas the axons may contain differing amounts of RNA, depending on the needs of the distal nerve fibers.

Of note, Mcp1 mRNA expression levels were compared to different negative controls – whereby naïve tissue was utilized in the DRG studies and sham tissue in the sciatic nerve studies. This is consistent throughout Specific Aim 1 (Chapter 3) and Specific Aim 2 (Chapter 4), in which main analyses of RNA expression in the sciatic nerve was compared to sham negative controls (Chapter 3) and RNA expression in the DRGs were compared to naïve negative controls (Chapter 4). As noted in the supplemental section of Chapter 3, multiple negative controls were initially used (included naïve and sham) in the study but because of cost-restrictions, only sham data was further analyzed. Only ipsilateral tissues were assessed throughout the study for the purposes of consistency and to keep costs as low as possible not all possible negative controls were considered. Naïve controls were utilized of ipsilateral sciatic nerve and DRG tissues, in which the animals received no surgery or nanoemulsion. Gene expression in naïve controls in the sciatic nerve were comparable to sham (**Figure 14**) negative controls(in which these animals' sciatic nerves are exposed during surgery, but no sutures are placed on the nerve to create CCI), thus only sham controls were utilized in running the RT^2 PCR Arrays, as they were expensive. For individual qPCR analysis of sciatic nerve tissues, only sham controls were included to keep the analyses consistent between individual genes and those within the RT^2 arrays. In terms of behavior, both naïve and sham animals exhibited similar behavior

patterns, with the exception that sham animals experienced pain 1-3 days after surgery (**Figure 15**), most likely due to post-operative pain. When compared in terms of mRNA expression within the injured sciatic nerve, no statistically significant mRNA difference was revealed on day 12 between naïve or sham negative controls in a subset of genes including the neuroinflammatory genes (IL-18, IL-1β, IL-10 MCP-1, MCP-5; **Figure 14**). As for the DRG, no statistically significant difference was noted between the two negative controls in a smaller sample size on day 12 for a subset of housekeeping (Gaphd, Rplp1) and neuroinflammatory genes (IL-18, IL-1β, MCP-1, MCP-5) and naïve negative controls to limit time and cost involved in animal surgeries.

In terms of CCI-induced gene expression changes (without administration of any nanoemulsion), differential expression of RNA within the injured axons of sciatic nerve as well as the cell bodies 12 days after injury were noted when compared to CCI animals receiving any form of nanoemulsion. CCI animals administered drug-free nanoemulsion (DF-NE) were expected to exhibit similar gene expression profiles to CCI only animals (those receiving no nanoemulsion), as they exhibit the same mechanical allodynia behavioral patterns (**Figure 6**) and are assumed to be comparable in terms of underlying molecular physiology of CCI only animals. We found this for the most part to be true, however, animals given no nanoemulsion at all (CCI only) exhibited much higher increases in several neuroinflammatory-related genes than CCI DF-NE animals in the sciatic nerve (**Table 14**), with a particular increase in expression of Cd18, Mcp5, and Cx3cr1 in the CCI only (no nanoemulsion) animals. This is of interest, and will require further exploration, as each of these are macrophage-associated genes and it may be possible that the nanoemulsion itself, although inert, could be activating the immune

response as it phagocytosed by circulating monocytes[46-49,71-73]. Inclusion of these controls were not used in the publications (Chapters 3 and 4) as they require a much further investigation and are considered outside of the scope of the goals of the studies.

Table 14. Fold change of mRNA expression compared for each of the CCI conditions normalized to the pain-free sham animals. The mRNA expression in the two hypersensitive conditions is distinct. Relative comparison of mRNA between the experimental group and sham control is shown based on the fold change using the Livak method ($p \leq 0.05$).

Gene	CCI Only (No nanoemulsion) Pain-like behavior Hypersensitive	CCI DF-NE Pain-like behavior Hypersensitive	CCI CXB-NE Pain-relieved
Cd18	31.9	11.5	6.8
Cd11b	11	9.5	4.0
Mcp5	41.3	11.9	4.3
Mcp1	12.4	8.2	2.9
IL-10	0.9	1.4	1.1
IL-1ß	11.2	18.4	7.1
Cx3cr1	19.1	5.4	3.5

Surprisingly, RNA expression changes involved in the production of prostaglandins, specifically PGE_2, were limited in both the injured sciatic nerve and DRG tissues. Of the 8 of the 84 genes differentially expressed in sciatic nerve tissue comparing CCI CXB-NE to CCI DF-NE animals, these include mRNAs associated with neurons (Tac1, Grin2b, Maob, Scn9a), pain (Tac1), macrophages (Cd11b), and inflammatory mediators (IL-6), but do not show any statistically significant difference in mRNAs associated with COX-2 or the subsequent cascade involved in PGE_2 production. For instance, beyond the RT^2 PCR array containing 84 known neuropathic and inflammatory genes, Ptgs2 (prostaglandin E synthase 2) and Ptgds (prostaglandin D2 synthase), Ptger2 (prostaglandin E receptor 2) were each individually assessed in both CCI conditions as well as naïve and sham animals, with no significant differences seen in expression.

Within the DRG tissues, there was, however, a decrease in Ptgds when Celecoxib-loaded nanoemulsion (CXB-NE) was administered to CCI rats.

Beyond neuron or macrophage differences in expression, our studies have demonstrated that other cell types' transcripts are likely affected following CXB-NE therapy. Our data has shown that the impact of drug reaches beyond the macrophages to influence changes in gene expression in a way that would include cells other than the macrophages carrying the nanoemulsion; these changes in RNA expression are evident at both the site of injury and the DRGs. RNA sequencing analysis of the DRG transcriptome has revealed the activation of two prominent immune-related Reactome pathways: neutrophil degranulation involving PML-RAR alpha-regulated adapter molecule 1 Pram1, and the innate immune system, which involves Importin 7 (Ipo7) and Strawberry Notch Homology 2 (Sbno2). Pram1 is expressed by granulating myeloid cells and may be associated with increased expression of multiple myeloid cell types in the DRG and at the site of injury. Importins mediate the nuclear import and export of activated signaling proteins involved in axonal regeneration[175]. Although not much is known regarding Ipo7 or its role in chronic constriction injury or its linkage to COX-2 inhibition, its related to importin-beta, a well understood importin that has been localized to injured sciatic nerve and DRGs after nerve injury[175]. The transcription factor Sbno2 contributes to the anti-inflammatory effects associated with M2 macrophages[180]. Pram1 and Ipo7 expression are increased when CXB-NE is present, whereas Sbno2 is reduced in expression when CXB-NE is present. This suggests a potential difference in the neuroimmune crosstalk relative to expression changes occurring at the actual site of injury within the sciatic nerve.

5.1.3 Nanoemulsion NSAID therapeutic treatment relieves pain-like behavior, reduces inflammation, and reduces macrophage infiltration at the site of injury.

Acting as a theranostic, the nanoemulsion has the ability to both deliver a therapeutic (in this case the non-steroidal anti-inflammatory drug, Celecoxib) as well as contain an imaging modality that allows us to track inflammation. The nanoemulsion contains a near infrared fluorescent (NIRF) dye, DiD, that can be used for in vivo imaging studies. Initial neuroimaging studies have revealed in the chronic constriction injury (CCI) model, that NIR fluorescence is concentrated in the area of the affected sciatic nerve on the ipsilateral hindleg[47]. Furthermore, when the nanoemulsion carries another distinct imaging agent, 19^F MRI, the fluorescent signal was localized on the ipsilateral sciatic nerve as well[47]. We have confirmed that treatment with CXB-NE results in a decrease in inflammation at the sciatic nerve on day 11 in the same area after CCI[46, 48,49]. This concurrent decrease in inflammation as indicated by RNA, protein, and NIRF signal is occurred by a reduction and near reversal of pain-like behavioral changes measured by von Frey mechanical allodynia testing. A multitude of behavioral assays and tools can be used to assay pain-like behavior in injured rats, wherein I chose to use von Frey testing as it has been established in the Pollock laboratory as a reliable and accurate tool to assess neuropathic pain-like behavior[20, 46-49]. Mechanical allodynia measures withdrawal responses to von Frey filaments of increasing gram force in both the injured (ipsilateral) and uninjured (contralateral) hindpaws. In addition, observed licking behaviors, lack of ipsilateral hindpaw use, and other biting or scratching at the site of injury were conducted and noted throughout all experiments. Other assays that can be explored in future experiments include the grimace scale (which uses time-lapsed

videography to measure rat facial expressions indicative of pain-like behavior), Hargreave's testing (measures latent thermal hypersensitivity), or walking gait analysis (measures whole animal pain-like behavior).

Correlating to the NIRF imaging in the live animals, histologically, there was a marked reduction in the number and type of macrophages present at the site of injury when CXB-NE treatment was employed[46,48,49]. Saleem et al. also demonstrated that 63% of the macrophages in the sciatic nerve carry nanoemulsion on day 12, whereas only 19% of the macrophages in the DRG carry nanoemulsion on that day. By day 18, macrophages carrying nanoemulsion in CCI CXB-NE and CCI DF-NE equalizes at around 12% [46]. With only drug-free nanomeulsion (DF-NE), there is a marked increase in CD68 positive macrophages at the affected sciatic nerve that coincides with injury on day 12[47]. Further analysis of CD68 macrophage infiltration at the corresponding dorsal root ganglia (DRG) reveals no significant change in macrophage infiltration on day 12, whereas on day 18, there is a substantial and nearly equivalent increase in CD68 positive macrophages in the DRG as there is in the sciatic nerve[46].

In past studies, we have also demonstrated that CD68 positive macrophages at the site of injury and the corresponding ganglia can be further distinguished based on the cell surface markers. Saleem et al.[46] was able to distinguish M1 (pro-inflammatory) and M2 (anti-inflammatory) macrophages by their expression of the costimulatory protein Cluster of Differentiation 40 (CD40) or transferrin receptor (TFRC). Based on these protein co-localization studies, on day 12 within the damaged sciatic nerve, CD68 and CD40 positive macrophages of CCI animals administered CXB-NE exhibited roughly 55% M1 macrophages whereas DF-NE animals express a significant increase with nearly 20%

more[46]. In the same study, DF-NE expressed only 36% M2 macrophages (CD68 and TFRC positive cell surface markers), whereas CXB-NE animals expressed 60% [46]. This is important as it reveals there is a shift in macrophage phenotype when injured animals are given the NSAID-loaded nanoemulsion. Switches in macrophage have both the potential to influence the production of inflammatory mediators as well as lead to changes in axonal regeneration[178,181].

Beyond M1 and M2 differentiation, macrophages are also pleiotropic under inflammatory conditions, having the ability to exert their influence in multiple ways[52]. As discussed earlier, in conjunction with our mRNA studies, we have observed a change in expression in the highly abundant α_M and β_2 integrins, CD11b (ITGAM) and CD18 (ITGB2). mRNA analysis at the injured sciatic nerve has revealed a significant increase in CD11b expression in the pain state compared to the pain-relieved state and a 3-fold increase in expression of CD18. In their protein form, together, these molecules form a heterodimer known as Mac-1, which is normally present in an inactive precursor in circulating monocytes that is known to be rapidly activated to assist in leukocyte adhesion, migration and accumulation at the sites of inflammation[55]. In a review by Ristoiu et al.[52], they describe the markers used for cell subtypes across the pain literature. They found that in the sciatic nerve, activation of CD11b- and CD68-positive macrophages were detected at different time points after partial spinal nerve ligation (PSNL), CCI and sciatic nerve crush, but they did not show a distinctive spatial distribution inside the nerve[52]. However, our studies have shown CD68 positive macrophages are found predominantly within the injured sciatic nerve, whereas CD11b positive macrophages were found primarily in the epineurium surrounding the nerve

fibers[49]. In the DRG, CD11b and CD68 macrophages invaded the tissue and either remain scattered between neurons or they formed perineuronal rings around medium and large neurons after injury[52]. Moreover, these two cell surface receptor specific macrophage markers are known to differ in their structure and functionality. In accord with our findings, CD11b macrophages are small, round shaped and distributed around the lesion site, whereas CD68 macrophages are large, irregular, foamy shaped and found amongst the damaged nerve fibers[58]. CD11b macrophages are known to be cytokine/chemokine expressing, whereas CD68 antibody is predominantly phagocytic (which is key for the regeneration process)[58]. Zhang and colleagues[58] were also able to demonstrate temporal differences between the two macrophage subtypes. They reported CD11b positive macrophages existed only at early time points after injury (not beyond day 14), whereas CD68 macrophages persisted for at least 3 months post-injury[52]. With our mRNA data, this suggests that CD11b positive macrophages contribute to the initiation of neuropathic pain by increasing cytokine/chemokine signaling and CD68 positive macrophages contribute to the ongoing maintenance of hypersensitivity via other mechanisms. It is possible that these phagocytic CD68 macrophages may be involved in axonal regeneration.

5.1.4 Attenuation of COX-2 in macrophages affects peripheral nerve regeneration

Multiple cell types are engaged during the axonal regeneration of the injured neurons following neuropathic injury. Neuronal regeneration can be thought of as a transcription and translation dependent process where the cell bodies changes gene expression patterns in response to injury at the axonal level[175]. In addition, neutrophils are the first cell type recruited to the injured nerve[56], followed by the recruitment of circulating monocytes (as

tissue macrophages), breakdown of the blood-nerve-barrier through the endothelium[104] and activation of Schwann cells, accompanied by degeneration of the distal axon and ultimately expression of regeneration-associated RNAs within the cell bodies[56]. This is subsequently followed by formation of a growth cone within the injured axon[56]. After the first 48 hours post-injury, Wallerian degeneration is marked by a phenotypic shift in resident and activated Schwann cells, in which they no longer serve to primarily myelinate the axon, but instead they dissociate and begin acting like macrophages, phagocytosing injured axonal debris and secreting inflammatory mediators[56, 89]. as time proceeds, it could serve as an important indicator. Behavioral assays assessing axon regeneration can be utilized to explore regeneration over time. An example being walking gate analysis of a rat on a treadmill belt using DigiGait technology. DigitGait software generates digital hindpaw prints and dynamic gait signals, representing the temporal record of paw placement on the belt as the injured animal walks, indicating pain detection based on gait[249]. This technology can be used in both assessing neuropathy as well as recovery due to axonal regeneration[249]. This would be a helpful tool in detecting axonal regeneration as on day 12 the regenerative process is robust. In addition, by blocking COX-2 activity in macrophages, there is essentially an attenuation of overall inflammation which may contribute to the recovery process, in which axonal regeneration plays a key role. Beyond day 12, further studies are required to assess the extent of axon regeneration occurring at the injured sciatic nerve, however, studies using the NSAID ketorolac, have shown histological changes to axon and myelin diameter over a period of 42 days following sciatic nerve crush injury, revealed an increase in axonal regeneration and a recovery in pain-like hypersensitivity in these animals[253].

In the DRG, a number of RNAs are differentially expressed when COX-2 is inhibited in infiltrating macrophages, including those known to be previously involved in axonal regeneration. Neurotrophic growth factors are thought to attract cell machinery to the injured nerve to promote axon regeneration, assist in degrading cellular debris and the guiding and activation of genes to the injured stump. The neurotrophin, nerve growth factor (NGF), is involved in pain signaling upon binding to Neurotrophic receptor tyrosine kinase A, Ntrk1/TrkA[109]. The NGF-TrkA complex is internalized and transported from peripheral axons to sensory cell bodies in the DRG[109], where it may play a role in pain signaling. Consistent with nerve regeneration and repair involving administration of CXB-NE, Ntrk1/TrkA shows decreased expression in the DRG after drug therapy compared to CCI DF-NE.

Certain transcription factors involved in axonal regeneration signal transduction are expressed when CXB-NE is present in the DRG, including c-Fos. c-Fos is essential for the reprogramming of myelinating Schwann cells to non-myelinating Schwann cells[33], which aid heavily in the regenerative process. Genes expressed involved in signaling include Fkbp3, , Gpr22, Arhgap2, Plce1, Arhgef11, Itpkc, Nkiras1, and Mycbp2. The extracellular signaling kinase Mapk1 (mitogen-activated kinase 1) is activated by c-Fos and has been implicated in nerve injury in the dedifferentiation of Schwann cells as well as activation of MCP-1[33]. On the other hand, Notch signaling involving decreased Rassf1 expression after CXB-NE in the DRG and this gene is known to contribute to demyelination[33]. Given this gene's expression is assessed on day 12, a decrease in expression makes sense, as demyelination occurs during the earlier Wallerian degeneration phase. Preliminary immunohistochemistry staining of the general Schwann

cell marker S100 (Dako, 1:100) in the distal stump has shown increased staining in CCI CXB-NE compared to CCI DF-NE, possibly indicating a heavier axonal regenerative process occurring (data not shown). In addition, the roles of growth-associated protein 43 (GAP-43) and F-actin protein expression on CCI animals receiving drug-free and celecoxib-loaded nanoemulsions has recently been examined in a pilot study[238]. GAP-43 has been shown to have involvement in nerve regeneration[89,] whereby protein levels are increased in the injured sciatic nerve following administration of CXB-NE on day 8 (as compared to DF-NE)[238]. The study by Alyssa Brauckmann also examined F-actin, a growth cone marker that protrudes from the distal ends of damaged axons[238,] demonstrating a significant increase between naïve/CCI DF-NE conditions and CCI-CXBNE on day 12, with highest expression in the pain-relieved state[238]. Exploration of potential axonal regeneration mRNAs in the injured sciatic nerve were limited to the genes found within the qPCR array (Qiagen) used. Only β-actin (Act-β) showed differential expression in the sciatic nerve. Act-β is involved in growth cone formation[97,153], and when CXB-NE is present, Act-β exhibits a higher level of expression compared to their CCI DF-NE counterparts. This increase in actin expression may be in response to the activation of peripheral nerve regenerative processes[154].

Other genes that may be involved in axonal regeneration include fibronectin leucine rich transmembrane protein 3 Flrt3, and leucine rich repeat transmembrane neuronal proteins LRRTM1, LRRTM2, and LRRTM3; all of which are differentially expressed and are known to be involved in axon outgrowth and synapse formation[170]. LRRTM1, LRRTM2, and LRRTM3 exhibit an increase in expression when CXB-NE is present. Other similar genes involved in recruiting cells to the cell body microenvironment

involved in axonal regeneration include fibronectin leucine rich transmembrane protein 3, Flrt3, also shows an increase in expression after CXB-NE in the DRG. Given the extensive RNA changes occurring within the DRG, I propose that it is the cell bodies that are preparing and defining which RNA transcripts will be made and shipped to the injured axons within the sciatic nerve to be later translated into proteins for use by the targeted cells. Use of anterograde transport allows for the translocation of RNA transcripts to the axon, whereby mRNAs may be translated into protein given their need or involvement in axonal regeneration or ncRNAs (non-coding RNAs) may act as regulators of protein and other RNA functions.

Future experiments centered around the pro-healing response and possible role of CXB-NE in axon regeneration need to be conducted. Including repeated and later-set dosing experiments in future work may reveal even stronger data on the role of selective COX-2 inhibition on activated macrophages and their role in axonal regeneration. As pain-like behavior begins to reappear (around day 15)[46], a repeated dose of 0.24 mg/kg could be administered and then possibly again after day 18, as this is the day established within previous data demonstrating distinct differences in macrophage and nanoemulsion infiltration at the sciatic nerve and DRGs[46]. Furthermore, it would be interesting to administer CXB-NE beyond the established day 8 administration, to explore the possibility that a later administration may or may not affect expression levels of RNAs and proteins previously involved in the axonal regenerative process.

5.1.5 Long non-coding RNAs may be implicated in pain

Non-coding RNAs (ncRNAs) have the ability to influence pain pathogenesis as they act as transcriptional regulators with the ability to modify the expression of mRNAs and protein targets[224]. ncRNAs include the smaller microRNAs (miRNAs) which are less than 200 base pairs in size and long non-coding RNAs (lncRNAs), which are greater than 200 base pairs. Each of these have been implicated in chronic pain[224-227]. lncRNAs comprise 90% of human total RNA and are uniquely expressed in all cell types, wherein at least 50% of lncRNAs have been reported in the nervous system[228]. With their ability to modulate gene expression of other RNA transcripts, they may have the ability to influence pain pathogenesis with greater strength than originally thought. In this study, of the 675 transcripts statistically significantly expressed in the DRG of CCI animals given CXB-NE relative to those given DF-NE, only a mere 26 include known ncRNAs, whereas 611 were mRNAs. This is most likely because most ncRNAs have yet to be annotated and explored in mammalian genomes. Additionally, those 26 miRNAs and lncRNAs in our dataset have only been recently annotated, with little known about each of them in regard to their molecular function.

miRNA undergo a complex biogenesis that was first described in 2015 by Lin and Gregory[229]. Initially, within the nucleus, a primary miRNA transcript is cleaved to a precursor miRNA approximately 70 base pairs in length followed by further processing into a 22 base pair duplex miRNA once exported out of the nucleus. One strand of the duplex miRNA is loaded onto the RNA-induced silencing complex (RISC) to form a functional mature miRNA. Mature miRNAs bind to the 3' untranslated region of target genes to silence them by either translational repression or mRNA degradation[224]. In our

DRG RNA sequencing study, of interest, the miRNA miR-3074 which shows a 30 fold increase in expression when CXB-NE is present in CCI animals on day 12, has been studied in the spinal cord and shown to act primarily to inhibit cell proliferation and neuronal differentiation through transcriptional regulation in an oligodendrocyte precursor cell transplantation study in rats after spinal cord injury[230]. The only other expressed ncRNA studied in the literature to do date is miR-3065, which has shown involvement in breast cancer development[231]. Future studies should focus on those 14 miRNAs expressed in this study and their role in neuropathic pain, as previous studies have shown miRNAs exhibit differential expression based on the given injury model and cell type in which they are expressed[224]. Conflicting reports about the regulation of a given miRNA has been shown to differ depending on which pain model is utilized, the animal being studied, and tissue RNA is extracted from[224], therefore miRNA profiling should be evaluated in a way specific to our given study. For instance, validation studies using uniquely generated primers can be designed to look for specific miRNAs in a given DRG (or sciatic nerve). Furthermore, in vitro studies of macrophage expression of miRNAs shown to be differentially expressed should be conducted. Both of these studies could help reveal if in fact and how much the given miRNA is expressed in the DRG after CCI injury and drug therapy as well as if macrophages are directly involved in generating these transcripts.

Other tools available for studying miRNA expression include those that explore when and how a given ncRNA is regulated in its expression as these regulatory mechanisms may reveal the potential roles of miRNA in injury and their associated action of the pain-relieving therapy. Such tools include those that have the ability to

affect miRNA expression in vivo such as chemically modified anti-miRNA oligonucleotides that inhibit endogenous miRNA expression by binding to and sequestering the targeted miRNA and consequently rendering it useless for RISC complex incorporation[224]. However, these chemical agents proved inefficient in inhibiting targeted mRNA in DRG following intrathecal injection in small animal models[224]. Another tool that can be used to study miRNA expression includes the use of miRNA mimics. miRNA mimics are double-stranded RNA molecules that mimic endogenous miRNAs on cellular uptake where the strand containing the targeted mature miRNA sequence (known as the active strand) is preferentially incorporated into the RISC complex, and the other strand (known as the inactive strand) is degraded[224]. By conjugating a fluorescent tag to the active strand, localization following uptake into peripheral sensory neurons can be established. Although each of these tools can reveal the potential location of these molecular transcripts, it is still necessary to understand their function. Function studies involving ncRNAs are important as ncRNAs have the ability to target and affect specific mRNAs as well as other RNA transcripts. Most of these tools lie in miRNA target-prediction computer algorithms that explore the validity of predicted miRNA-mRNA pairs to treat cells or in vivo tissue with mimics or inhibitors of dysregulated mRNAS, extracted from affected tissues[224].

In addition to quantitative PCR (qPCR) to quantify the differential expression of a given ncRNA, other tools are commonly used. Northern blotting was once considered the gold standard in ncRNA research but is limited in its use in pain studies due to technical limitations[224]. Fluorescent in situ hybridization (FISH) studies can be utilized to explore cell specific expression of each of the ncRNAs. This would be particularly

helpful for long non-coding RNAs (lncRNAs) as research involving them in CCI-induced neuropathic pain remain limited. lncRNAs have been implicated in multiple physiological and pathological processes throughout the body and nervous system[225] but the literature has been limited to understanding the molecular mechanisms of only a handful of lncRNA and their involvement in neuropathic pain models [228, 232]. One potential lncRNA that may be involved in our studies is Scn9a NAT, an antisense lncRNA that targets the mRNA Scn9a. Although we have shown decreased of this voltage-gated sodium channel Scn9a/Na_v1.7 in the injured sciatic nerve, a recent study has explored its expression and relation to its antisense lncRNA in the DRG[232]. These two genes show an opposing pattern of expression in the DRG, with higher levels of Scn9a mRNA and lower levels of Scn9a NAT[232]. However, our RNAseq studies in the DRG only show differential expression of the sodium voltage-gated channels Scn8a/Na_v1.6 and Scn11a/Na_v1.9 when CXB-NE is administered in the pain state and did not detect Scn9a. We did however detect Scn9a/Na_v1.7 in the inflamed sciatic nerve tissue (but not in the DRG). There could be potential antisense lncRNA Scn8a/Na_v1.6 and Scn11a/Na_v1.9 transcripts found within the DRG as well as the presence of Scn9a NAT in the injured sciatic nerve that could be explored using qPCR and FISH techniques. The FISH technique can be very challenging as the ncRNAs can be expressed at a relatively low level to have their desired effect.

5.1.6 Genes implicated in neurodegenerative disease are differentially expressed when CXB-NE is present in CCI

Although the protein-coding mRNAs explored in the sciatic nerve were those previously established in the literature as involved in neuropathic and inflammatory pain (Qiagen Array), genes implicated in non-pain disease states were implicated when sequencing the entire transcriptome of injured rats' DRGs. RNA sequencing analysis revealed a cluster of key genes involved in other pathological processes, including Htt in Huntingtin Disease, Apolipoprotein B (Apob) in Alzheimer's disease, ataxin 10 (Atx10) in spinocerebellar ataxia, frataxin (Fxn) in Friedrich Ataxia, and optineurin (Optn) involved in optic neuropathy. Htt shows a 3 fold increase in expression when CXB-NE is given, Apob a nearly 10 fold increase, Atx10 a fold increase, Fxn a 0.04 fold decrease and Optn a 5 fold increase. Interestingly enough, each of these genes have some involvement in neurodegeneration and this may explain their expression profiles after CCI. Conducting further experiments to study which cells are producing these given genes using fluorescent in situ hybridization (FISH) could reveal further potential interaction of the neuro-immune triad involved in both neuropathic pain and the axonal regenerative responses. Antibodies that would be examined may include IL-6, IL-18, Itgam/Cd11b, Act-β, and potentially Flrt3 as potential neuroinflammatory genes in which expression spans throughout the neuro-immune triad of cells.

5.2 Future Studies

Recent studies and requirement by the National Institutes of Health are now requiring all pain studies involving small animals to include both males and females[190]. Beyond

studying both sexes due the clear anatomical differences, pre-clinical pain studies have already shown neuroimmune differences[191,192]. Inclusion of female data may elucidate differences in adaptive versus innate immune responses using this pain model and what may be different when nanoemulsion drug therapy is used to inhibit COX2. Pain literature is currently establishing the major roles of the innate and adaptive immune systems based on sex differences. Although both systems work together to respond to chronic pain, each may differ in their underlying molecular mechanisms given the sex in which it is responding. Innate immunity involves the immediate response that recognizes foreign bodies or injury, mounting a mostly monocyte-derived neutrophils and macrophages, mast cells, T cells, glia, and inflammatory mediators like cytokines/chemokines. On the other hand, the adaptive immune response is characterized by a later, cell-mediated, acquired and specific immunity to given foreign bodies or injury markers involving primarily T cells and the humoral B cell response. Expression of inflammatory mediators, macrophages and T cells is the major underlying cellular differences in males and females. Although helper T cells are intricately involved in the innate immune response, they are too involved, with cytotoxic and regulatory T cells, in the adaptive immune response, as well as the production of inflammatory mediators. The central T-cell mediated adaptive response was first seen in female mice after induction of the neuropathic pain spinal nerve ligation in 2015 by Sorge and colleagues[193]. Their studies revealed that female mice might preferentially use adaptive immune cells instead of microglia to produce allodynia after nerve injury, and in the absence of adaptive immune cells, female mice then will use the male, microglia-dependent pathway instead[193].

This is an important concept to address, as the Janjic laboratory designed nanoemulsions we use target the innate-monocyte-derived macrophage response. Since this may be different in females than males, the nanoemulsion will likely cause a different effect in terms of gene expression and thus needs to be studied more in depth. Furthermore, our RNA sequencing study a prominent role of the innate immune system using Reactome analysis in male rats given CXB-NE compared to those receiving DF-NE. A study by our colleagues Liu and Janjic et al. [167] using the sameCOX-2 inhibiting nanoemulsions directed to monocyte derived macrophages shown in a Complete Freund's Adjuvant (CFA) of pain in male and female mice revealed a more distinct nanoemulsion near infrared red fluorescent (NIRF) signal distributions in CD68 positive macrophages in males compared to females[167]. Repeat RNA sequencing studies of CCI and the effect of CXB-NE on transcriptome expression in males and females rats in currently underway by Brooke Deal in our laboratory.

A major part of this study relies on previous literature in which given RNAs are associated with a given cell type. As discussed earlier in Section 5.1.5, more experiments exploring RNA expression in a given cell type are required. Fluorescent in situ hybridization (FISH) studies would allow future researchers to explore cell-specific RNA expression of protein-coding genes explored in this study. An advantage of this technique is that it uses paraformaldehyde-fixed tissues, commonly collected in the Pollock laboratory, providing results consistent with the work done in my research. In addition, multiplex FISH is a newer technique which allows for enables the detection of multiple targets with multiple fluorophores in a single sample. FISH also uses highly specific probes and distinct fluorophores that can be imaged via confocal microscopy to

detect a given RNA. Another technique that can be used to identify cell-specific identities within a sample is fluorescence activated cell sorting (FACS)[250]. FACS is a commonly used immunotechnique that identifies cells within a sample using fluorophore-attached antibody staining. Beyond exploring the major cells of the neuroimmune triad, subsets of macrophages could be revealed with FACS. A study by Botchwey and colleagues[251] explored the differential expression of classical versus non-classical monocyte markers after tissue injury utilizing FACS and markers used in this study to identify them (CX3CR1, CD11b, IL-6, and IL-1β). The major disadvantage of this technique is that it requires viable (not fixed) samples, and as you begin to dissociate the cells for sorting, a subsequent change in RNA expression may occur, leading to changes that could lead to altered gene expression from the NSAID-loaded, macrophage-targeted treatment applied. Another technique that could provide insights in cell-specific gene expressions would utilize another form of RNA sequencing data, the major technique performed in the second aim of my study. Cell-lineage specific data allows for the recovery of cell type specific expression profiles from RNA sequencing data, however, given cost- and time-limitations, this analysis was not performed on my data set.

5.3 Conclusions

Studying CCI in rats and the effects of a targeted theranostic nanoemulsion may have implications in human health. CCI mimics neuropathic pain[13], which is a common complication of diabetes mellitus, chemotherapeutic use, and nerve trauma, amongst others. In particular, diabetic neuropathy is found in at least half of the affected population and is characterized by distal-to-proximal nerve damage leading to

neuropathic pain symptoms[188] and is further associated with a mortality rate of 25-50% within 5-10 years following the onset of diabetic neuropathy[189]. Understanding the mechanisms of neuropathic pain in rats has shown that a prevailing neuroimmune response contributes to the major neuroinflammation-causing pain-like behavior in the laboratory. Even more so by utilizing laboratory animals and techniques to explore the underlying genetics and subsequent pathogenesis of neuropathic pain may be useful in understanding the drivers of neuropathic pain in humans. In addition, by studying a clinically relevant nanoemulsion to illustrate the molecular cell biological responses, it is possible that this particular theranostic will one day be used to treat patients in clinic with the same disease symptomology.

With the advent of RNA transcriptome sequencing and quantitative PCR to analyze, quantify and compare gene expression in the pain state, we now have the ability to look at the molecular genetics in first animals, then humans in a clear way. Studying neuropathic pain in humans has many limitations (pain being subjective, collecting tissue, sample size issues, and analyzing meta-analyses where pain is measured using different parameters) that can be bypassed in animals, helping to establish the fundamental patterns of gene expression of neuropathy. A metanalysis focusing on combining only pain cohorts who have harmonization amongst them (used the same neuropathic pain definition and similar subjects) identified 28 genes that show association with the presence of neuropathy in humans[233]. These genes have involvement in neurons (specifically in ion channels and neurotransmission), cytokine production, metabolism and the immune response, each consistent with our findings in our CCI rat neuropathic pain studies. In particular, overlapping genes in the meta-analysis of humans and our

studies include Scn9a and Scn11a, Comt, Gch1, Slc11a2, and IL-6. This is important as our studies have revealed that these genes, both found to be differentially expressed in the sciatic nerve or the cell bodies of the DRG, can be influenced by the NSAID celecoxib-loaded nanoemulsion in animals suffering from peripheral neuropathy.

With this, altered gene expression of RNA is apparent within the entire peripheral nerve, including the injured sciatic nerve and L4 to L5 DRGs. Specifically, by attenuating COX2 activity specifically in infiltrating macrophages, there is a subsequent change in expression of mRNAs associated with neuroinflammation in the injured sciatic nerve as well differential RNA expression in the corresponding cell bodies of the dorsal root ganglia. Based on previous gene-cell localization studies, this change in expression is not limited to macrophages, but also genes associated with other cell types at the site of injury (neurons, Schwann cells, T cells, and endothelial cells). The products of some of these genes are known to contribute to increased infiltration of immune cells, activation of immune-like glial cells at the site of injury, and the production of inflammatory mediators as well as production of mRNAs that influence axonal regeneration. Furthermore, mRNAs generally associated with the cell bodies in the DRGs such as the Calcium channel genes Cacna1b and TrpV3 are found to be differentially expressed in the injured sciatic nerve. Overall, with the utilization of celecoxib-loaded nanoemulsion, this targeted inhibition of COX2 and reduction PGE_2 in macrophages, in turn has a much broader influence on gene regulation and expression throughout the sciatic nerve after peripheral nerve injury in male rats. By introducing CXB-NE not only is there a reduction in hypersensitivity[46, 48, 49], but there is an overall reduction in inflammation at the site of injury[48,49] and the drug therapy is associated with widespread changes in the

transcriptome of various cells at the site of injury as well as the cells of the dorsal root ganglia. Even though celecoxib specifically attenuates COX-2 activity in the associated macrophages, the influence extends far beyond.

Appendix A. Tail vein injection protocol.

Based on the publication:

M. Saleem*, **A. Stevens***, B. Deal, L. Liu, J. M. Janjic, J. A. Pollock (2019) A new best practice for validating tail vein injections in rat with near infrared labeled agents. JoVE - J. Vis. Exp., e59295. *Co-authors contributed equally.

Contribution Statement:

A.S. performed optimization of tail vein injections when designing the protocol, LiCOR imaging, wrote the protocol and initiated the publication.

M.S. wrote the introduction, results and conclusions of the publication and created the figures.

J.A.P. overseen the entire publication and contributed to the concept and design of the publication and protocol. J.A.P and J.J. jointly designed the experimental approach for evaluating nanoemulsions in chronic constriction injury rate model for neuropathic pain.

B.D. assisting in filming of the video's protocol and publication.

J.J. and L.L. contributing to editing the manuscript and designed and developed the nanoemulsion. L.L.

B.D., L.L., M.S, and J.A.P. were all involved in filming of the publication.

A.1 Intravenous Tail Vein Injections

As adapted from:

M. Saleem*, **A. Stevens*,** B. Deal, L. Liu, J. M. Janjic, J. A. Pollock. A new best practice for validating tail vein injections in rat with near infrared labeled agents. *Journal of Visualized Experiments* 2019; e59295. *Co-authors contributed equally.

A.1.1 Summary

Here we present a method to validate tail vein injections in rats by utilizing near-infrared fluorescence imaging data from dyes incorporated into agents or biological probes. The tail is imaged before and after the injection, the fluorescent signal is quantified, and an assessment of the injection quality is made.

A.1.2 Abstract

Intravenous (IV) administration of agents into the tail vein of rats can be both difficult and inconsistent. Optimizing tail vein injections is a key part of many experimental procedures where reagents need to be introduced directly into the bloodstream. Unwittingly, the injection can be subcutaneous, possibly altering the scientific outcomes. Utilizing a nanoemulsion-based biological probe with an incorporated near-infrared fluorescent (NIRF) dye, this method offers the capability of imaging a successful tail vein injection in vivo. With the use of a NIRF imager, images are taken before and after the injection of the agent. An acceptable IV injection is then qualitatively or quantitatively determined based on the intensity of the NIRF signal at the site of injection.

A.1.3 Introduction

The route of administration of agents into small animals serves as a critical point of many experiments. It determines where the agent is to be delivered and, subsequently, what will happen to the agent thereafter. Although other routes can be used for agent administration[194], the intravenous route of delivery is a preferred route for certain agents. IV injection allows agents to be directly injected into the bloodstream, bypassing first-pass tissue effects and the need for extraneous solute absorption[194]. This also allows for targeting cells in the bloodstream[48, 72] and direct delivery to all tissues within the circulatory system. In rodents, several veins can be considered, including the jugular, the saphenous, and the tail vein.

In this method, a NIRF dye containing a biological probe—in this case, a nanoemulsion (**Figure 20A**)[71-73,195]—is injected into the lateral tail vein of rats. This particular NIRF-containing nanoemulsion has been used previously to image and track neuroinflammation in vivo and ex vivo[196,197] in a rat model[13] of neuropathic pain[20, 47,71-73, 48, . Imaging is conducted before and after the injection with a preclinical NIR fluorescence imager. This serves as a tool to validate the quality of the agent administration. Imaging prior to the tail vein injection serves as a basis for obtaining a baseline image.

Increasingly in animal studies, intravenously administered nanoemulsions are being utilized as biological probes and targeting agents[198-201]. It is a proven challenge to administer an agent via the tail vein[203, 204]—be it a drug, a viral vector, or another probe—and to ensure that the entire contents of the injection have successfully entered the bloodstream and not the surrounding tissues[203]. Therefore, a method of visualizing and evaluating the quality of a successful injection is beneficial.

Typically, a heat lamp or warm water is used to warm the tail, which causes dilation of the vein, permitting its visualization prior to injection. While this ensures easier entry into the vein, there is not a quantitative way to discern whether the compound has entered the bloodstream in its entirety[204-207]. This becomes more difficult still in strains of animals where the vein contrasts faintly with the skin, such as in black mice. Typically, the investigator can gauge a failed injection by experiencing resistance during the injection and, in some cases, visualizing a bulge on the tail, indicating a subcutaneous leakage of the agent[208, 209].

In this study, NIRF imaging of the nanoemulsion injected into the lateral tail vein of live rats is performed on a small-animal NIRF imaging system. Rats are fed a special purified diet to reduce nonspecific gut fluorescence. Simultaneous image acquisition of white light and 800 nm fluorescence is captured using the NIRF imager and associated software. The relative fluorescence intensity is measured on the tail at the pre-injection and post-injection states. The fluorescence intensity for the region of interest (ROI) at the site of injection is recorded and divided by the area of the ROI. Qualitative assessments can be made on which injections are acceptable. Optionally, further quantitative analysis can be performed by setting thresholds for acceptable injections and assigning ROI measurements into groups, at which point statistical significance can be calculated.

By utilizing this validation strategy following tail vein injections, the standard of a research study improves due to increased consistency of agent administration. This method of assessing the quality of tail vein injection can be easily customized for different injectable agents to include infra-red fluorescent probes provided commercially by several companies.

A.1.4 Protocol

All protocols were performed in accordance with the guidelines in the Guide for the Care and Use of Laboratory Animals of the National Institutes of Health and Institutional Animal Care and Use Committee (IACUC) at Duquesne University.

A.1.4.1 Preparation and anesthesia

NOTE: Aseptic techniques are used for the entirety of the procedure. Only new sterile materials and autoclaved sterile instruments are to be used. Personal protective equipment (sterile gloves, hair bonnet, surgical mask, scrubs) needs to be worn to avoid contamination.

Use adult male Sprague-Dawley rats weighing 250–300 g. Acclimate the rats to standard living conditions, keep them on a 12 h light/12 h dark cycle, and provide food and water ad libitum. House the animal socially, keep them on paper bedding, and provide a special diet to avoid autofluorescence during imaging.

With the use of a properly placed heating pad, anesthetize the animal under an initial 5% isoflurane in 20% oxygen, followed by a maintenance level of not less than 1.5% isoflurane and not more than 3%, unless the animal wakes up or retains feeling.

Confirm proper anesthesia via a lack of response to tail pinches. Monitor the blood flow as well via vital signs throughout the procedure.

A.1.4.2 Pre-injection

Image the animal in a preclinical NIR fluorescence imager by positioning the animal laterally to expose the injection site on the lateral tail to establish a baseline of

fluorescence in the tail (**Figure 20C,E**).

Following imaging, move the animal back to the surgical table, and place it under anesthesia for the tail vein injection. Note: Continue monitoring the rat's vital signs and recheck proper anesthetization via tail pinch.

A.1.4.3 Tail vein injection with NIRF-containing agent

With the animal in the prone position, orient the tail with the dorsal side facing up. Dilate the tail vasculature in warm water for a minimum of 1 min. Orient the tail vein so the lateral side (either right or left) is turned 30° (clockwise or counterclockwise) to expose the right or left tail vein (**Figure 20B**).

Once a lateral tail vein has been located (which appears dark-colored upon dilation), sterilize the entire tail with alcohol pads, repeating 2x.

At an appropriate dosage based on the study design, begin injections in the distal coccygeal vertebrae region of the tail and moving more proximal if proper needle placement fails.

Insert a 25–27 G sterile needle, bevel up, into the lateral tail vein, with the tail at a 180° angle, inserting the needle parallel to the lifted tail. Observe blood flashback in the rim of the needle to ensure correct placement. If no flashback is apparent, slowly move the needle tip (without removing it from the tail) to find vein insertion. If placed subcutaneously, no blood flashback will occur.

Insert the syringe with the injectable materials into the rim of the needle. When proper placement is achieved, the injectable fluid will not incur resistance upon injection. The injection will advance smoothly and easily. Once injected, remove the needle and the

syringe, apply pressure with sterile gauze for at least 1 min to ensure clotting, and mark the spot of injection with a pen on the tail, ensuring it is visible on the white light image. Note: No hematoma or lesion will be visible at the site of injection.

If the needle tip moves during the syringe insertion, remove the needle and retry the needle entry procedure more proximal on the ipsilateral tail vein. Do not reuse the same needle if a different reentry point is tried. Note: Alternatively, the injection can be performed with an IV catheter. This has the benefit of visual confirmation of the catheter during venipuncture. Insert the catheter, bevel side up, at the angle previously described. Observe prompt flashback in the entire length of the needle and the catheter to ensure correct placement. Slight back pressure can be used to pull blood into the syringe to confirm proper placement in the vessel before injecting. Again, no resistance will be felt.

A.1.4.4 Post-injection

Perform quality assessment after the tail vein injection in a preclinical NIR fluorescence imager in the same orientation as the pre-injection image. Increase the isoflurane anesthesia to 3% for several minutes and move the animal to the imager. Ensure the animal is still properly anesthetized.

Quickly, orient the animal on its lateral side to expose the injection site (as marked) on the lateral tail. Check to see if a NIRF signal is present only at the site of injection as this is the most optimal injection, indicating a successful tail vein injection (**Figure 20D**). Note: If the signal is sparse but still within the proximal vicinity of the tail vein injection, the injection is acceptable and can be considered as a successful tail vein injection. If the signal is dispersed throughout the entire tail, it is considered to be subcutaneous and, thus,

unsuccessful (**Figure 20F**). **Figure 21** shows additional examples of failed injections.

A.1.4.5 Image quantification

Note: Image quantification can be performed in the imaging software that accompanies the NIR imager, if this is a function of the software. Alternatively, other commercially available imaging software may be used[25]. In the post-injection image, draw an ROI around the area of fluorescence at the injection site and clone it in all animals in order to compare[2,6]. Perform a simultaneous image acquisition of white light (body view) and 785 nm excitation for 820 nm emission using the NIRF imager and associated software, with linked lookup tables (LUT). Perform a one-way analysis of variance (ANOVA) as a statistical analysis for the entire set of conditions revealing a treatment effect with a statistically significant p-value of 0.0024.

Measure the area and relative fluorescence intensity and record the measurement of the area/intensity. Note: The researcher can decide on thresholds that discriminate good from bad injections or assign a percentage of quality to the injection.

A.1.5 Representative results

Rats were injected with NIRF-containing nanoemulsion into the lateral tail vein, and pre- and post-injection images were taken with the small-animal imager as described in the protocol. Post-injection images are qualitatively assessed for injection quality and placed into ‘good injection’ (n = 7) and ‘bad injection’ (n = 4) groups. Qualitative assessment was carried out by observing the post-injection area fluorescence intensity. In an optimal injection, the NIRF signal is confined to the site of injection. No signal will be seen if the injection is successful because the agent has been fully displaced into the

bloodstream. A bad-quality injection displays a NIRF signal that is dispersed along the length of the tail.

Images were analyzed with the accompanying NIRF imager software. ROIs were drawn at the site of pre-injection images (**Figure 20C, E**) and around the area of fluorescence in post-injection images (**Figure 20D, F**). Images where fluorescence was visible throughout the length of the tail were deemed unacceptable and removed from the analysis (**Figure 21**). Measurements of the area and fluorescence intensity were recorded. Values for area/fluorescence intensity were calculated and plotted (**Figure 20G**). A significant difference in fluorescence intensity between pre- and postinjection images was observed in the 'bad injection' group (**Figure 20G**) ($p = 0.0024$).

A.1.6 Figures and Legends

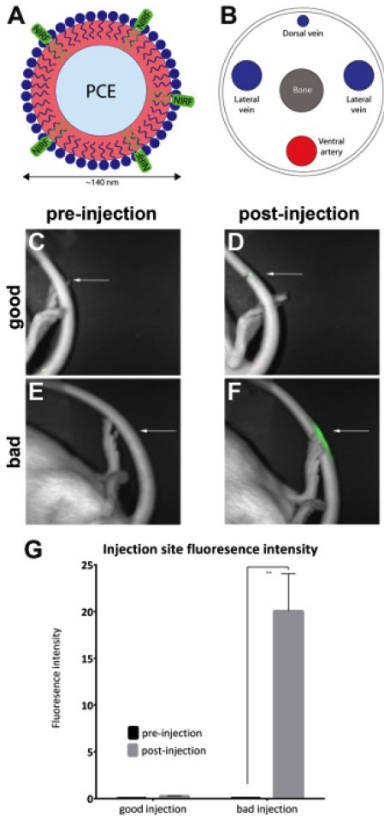

Figure 20. NIRF based nanoemulsion and images of tail vein. (A) A nanoemulsion-

based biological probe containing NIRF dye was injected into (B) the lateral tail vein and imaged in a NIRF imager. (C and D) Pre- and post-injection images of a good injection. (E and F) Pre- and postinjection images of a bad injection. White arrows indicate the point of injection. It is possible to qualitatively assess the success of a good injection compared to a bad injection by assessing the extent of the NIRF signal at the site of injection. Unacceptable injections display fluorescence throughout the length of the tail and were removed from the analysis (Figure 20). (G) The images can also be analyzed to reveal a quantitative measure of fluorescence intensity, with thresholds for injection quality assigned by the investigator. The error bars on the graph reflect the SEM. For the 'good injection' group, n = 7. For the 'bad injection' group, n = 4. There is a statistical difference in fluorescence intensity in the 'bad injection' group when comparing pre- and post-injection images (unpaired t-test; p = 0.0024).

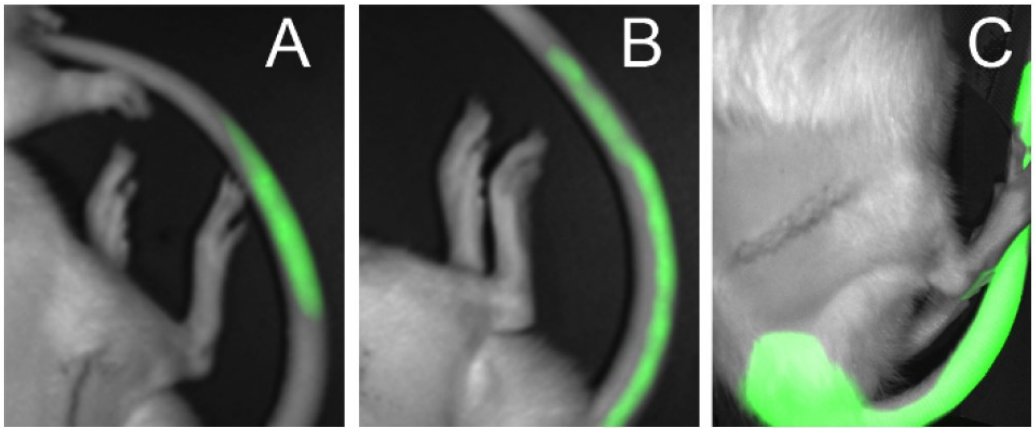

Figure 21. Examples of bad injections. (A) Fluorescent signal seen in part of the tail. (B) Fluorescent signal seen over the full length of the tail. (C) Fluorescent signal dispersed heavily in the entire tail and caudal area of the animal's body.

A.1.7 Discussion

Research laboratories incur significant costs as a result of the misadministration of testing agents. Tail vein injections are a difficult technique to master to attain consistent success rate, with the most experienced of technologists often incurring misadministration errors. There is no reliable way to confirm a successful injection. This protocol offers a solution to this problem by giving researchers a qualitative and quantitative method to validate the success of a murine tail vein injection. Here, a NIRF-labelled nanoemulsion[196,197,209] incorporates the agent of choice (in this case, a drug) and is imaged

at the site of injection in a NIRF small-animal imager. There is also the option to develop a non-nanoemulsion-based agent and use the same principle of NIRF imaging by incorporating commercially available infra-red dyes. Additionally, ready-to-use imaging agents with a variety of applications, such as tumor imaging, metabolic imaging, cell trafficking, and apoptosis are also commercially available. An injection is performed either by using a sterile needle or, alternatively, an IV catheter; this depends on the preference of the researcher. In addition, automated tail vein injectors[211] have been used to assist in this process and are compatible with this methodology. However, this technology has not yet become commercially available.

There are important steps in the tail vein injection method that ensure a higher rate of correct agent administration. First, the tail should be cleaned with ethanol to remove any dirt or debris, allowing researchers to better visualize the vein. Dilating the vein by submerging the tail in warm water is also a very important step in the method, as it allows a greater surface area for injection. Injecting at a more distal point on the tail vein allows for some error, in the event that multiple attempts are required. Injection should be attempted at a more proximal position in the tail as the tail vein increases in size as the caudal aspect of the animal's body is approached. In addition, the contralateral tail vein can be used if needle placement fails in more than three to five sites on the ipsilateral tail vein.

A successful administration of a test agent results in little to no NIRF signal at the point of injection. If no resistance is felt during the administration of the injection and there is little to no fluorescence at the tail, then the injection can be recorded as successful. If resistance is felt during injection and there is a trail of NIRF signal along some length of

the tail, then the injection is recorded as unsuccessful and is likely partly subcutaneous. Fluorescence images are taken pre- and post-injection, and the quality of the injection is assessed by observing qualitatively or analyzing quantitatively the fluorescence signal at the site of injection. The software accompanying the NIR fluorescence imager is often capable of performing this analysis.

The method can be adapted in several ways. It is applicable to tail vein injection in both mice and rats. Most small-animal NIR fluorescence imagers will be capable of accommodating murine rodents. Levels of anesthesia need to be adjusted depending on the weight of the animal, in accordance with the research laboratory's IACUC protocol. Another possible modification is the preparation of a non-nanoemulsion-based probe either by incorporating an infrared dye into the researcher's formulated agent or by purchasing a ready-to-use imaging agent, tailored to a specific biological application.

If a rat is relatively large, it can often be difficult to position it in the small-animal imager. It is thus recommended that a test image is taken with the animal in the drawer before injecting, and a field of view ascertained where the tail is visible. It is helpful to tape the tail to the drawer of the imager, to ensure it does not move during imaging.

Alternative methods seeking to assess the quality of tail vein injections in small animals are limited to the utilization of labeling reagents that do not interfere with concurrent experimental procedures and require euthanasia of the animals postinjection[198,199]. Some reagents may impact study outcomes and the therapeutic assessment of the animals involved, so care in experimental design is recommended.

This method can, in the future, be refined with advances in small-animal imaging technology, as well as improvements in infrared fluorescent probes. Biological probes with

an incorporated infrared dye, designed for a variety of different applications, can be used at the agent administration stage of a study design to validate the quality of an injection, as outlined in this method[48,72, 212-217].

Appendix B. RNA Sequencing Master dataset.

Contributions statement: The University of Pittsburgh Genomics Research Core (Dr. Janette Lamb and colleagues) performed RNA sequencing of L4-L5 DRG RNA for the three conditions tested.

The University of Pittsburgh Genomics Analysis Core (Dr. Uma Chandran and colleagues) performed differential expression of data obtained from RNA sequencing. Experiment design, analyses, and preparation of tables was performed by Andrea Stevens under the supervision of Dr. John A. Pollock.

Note: Datasets include only genes differentially expressed with a raw P value ≤ 0.05 from Chapter 4 (RNA sequencing of DRG tissues).

Table 15. CCI DF-NE versus naïve differential expression data (protein-coding genes). Includes differential expression data using one-way ANOVA analyses of pooled L4-L5 DRGs from RNA sequencing.

Gene	Fold Change	Raw P value	FDR	Gene	Fold Change	Raw P Value	FDR
Tmcc2	0.05	0.0168	1.0000	Kirrel	0.059	0.024	1.00
Pdzk1	1.52	0.0459	1.0000	Tln1	0.537	0.048	1.00
Cplx2	4.94	0.0204	1.0000	Epb41l3	2.387	0.001	0.39
Slc9a6	0.69	0.0275	1.0000	Telo2	5.993	0.009	1.00
Smurf1	14.23	0.0295	1.0000	Extl1	16.812	0.029	1.00
Fbxw8	3.11	0.0186	1.0000	Fancc	9.116	0.004	1.00
Pcbp3	3.44	0.0180	1.0000	Atrnl1	10.855	0.001	0.47
Clip1	0.05	0.0083	1.0000	Nudt6	0.289	0.033	1.00
Rcc1l	0.06	0.0242	1.0000	Tubb2b	0.375	0.020	1.00
St3gal6	0.04	0.0139	1.0000	Cltb	0.197	0.017	1.00
Dvl3	0.07	0.0451	1.0000	Usp3	0.065	0.047	1.00
Exoc1	0.06	0.0274	1.0000	LOC108348250	4.282	0.018	1.00
Lnx1	0.15	0.0237	1.0000	Tpbgl	3.906	0.028	1.00
Galnt10	10.00	0.0013	0.5899	Ubap2l	6.426	0.045	1.00
Mat2b	14.24	0.0331	1.0000	Apbb1	3.544	0.011	1.00
Col3a1	0.42	0.0070	1.0000	Syt5	3.356	0.020	1.00
LOC103690141	3.33	0.0427	1.0000	Pde4dip	6.048	0.030	1.00
Trove2	0.16	0.0405	1.0000	Rabep2	8.274	0.028	1.00
Toml12	3.30	0.0471	1.0000	Iffo1	6.487	0.027	1.00

Pkmyt1	1.44	0.0071	1.0000	Stat5b	0.037	0.002	0.80
Hmox2	3.48	0.0036	1.0000	Pik3r2	0.066	0.040	1.00
Col1a1	0.59	0.0234	1.0000	Hipk1	0.098	0.001	0.56
Aldh9a1	0.16	0.0352	1.0000	Mpv17l2	1.826	0.000	0.36
Ano3	7.37	0.0127	1.0000	Dag1	2.066	0.037	1.00
Nalcn	7.35	0.0388	1.0000	Zmynd15	0.341	0.007	1.00
Arhgef25	6.49	0.0286	1.0000	Ino80e	2.146	0.025	1.00
Scn8a	3.93	0.0015	0.5938	Wbp1l	0.159	0.039	1.00
Vsnl1	5.50	0.0128	1.0000	Rhog	24.850	0.001	0.59
Rab3ip	14.24	0.0290	1.0000	Gsk3a	2.131	0.041	1.00
Ngfr	1.91	0.0465	1.0000	Htra1	4.002	0.008	1.00
Lyz2	0.34	0.0237	1.0000	Fxyd3	0.497	0.023	1.00
Snap25	3.32	0.0052	1.0000	Tnfaip8l2	14.214	0.046	1.00
Dync1h1	1.47	0.0364	1.0000	Nrxn2	3.114	0.016	1.00
Trim37	2.32	0.0139	1.0000	Dnaaf5	14.237	0.040	1.00
Klhl9	14.20	0.0352	1.0000	Pusl1	2.070	0.040	1.00
Srgap3	3.62	0.0294	1.0000	Fkbp5	0.051	0.013	1.00
Borcs6	0.05	0.0135	1.0000	Zdhhc2	13.429	0.000	0.29
Il12rb2	3.58	0.0194	1.0000	Col6a6	0.047	0.007	1.00
Slit3	5.47	0.0104	1.0000	Lrtomt	6.527	0.034	1.00
Pcnx1	0.32	0.0113	1.0000	Fancf	0.059	0.023	1.00
Nckap1	7.44	0.0263	1.0000	Cbarp	0.158	0.027	1.00
Mcam	0.16	0.0499	1.0000	Mrps21	3.330	0.034	1.00
Tagln2	0.69	0.0144	1.0000	Ppp1r1c	3.069	0.028	1.00
Nefh	1.68	0.0000	0.1236	Mars	3.902	0.030	1.00
Parp2	0.74	0.0071	1.0000	Abhd1	1.280	0.008	1.00
Mtss1	0.12	0.0075	1.0000	Tril	4.419	0.043	1.00
Trappc12	3.20	0.0456	1.0000	Gga3	1.461	0.049	1.00
Sez6	0.07	0.0399	1.0000	LOC684988	2.166	0.014	1.00
Tmem59	0.18	0.0075	1.0000	Wdr1	2.959	0.045	1.00
Dync1i2	4.21	0.0078	1.0000	Kif26b	0.059	0.034	1.00
LOC100362176	14.24	0.0322	1.0000	Cyp2t1	2.176	0.041	1.00
Kcnh2	9.93	0.0048	1.0000	Ormdl2	7.382	0.018	1.00
Ttc17	14.24	0.0290	1.0000	Dhx16	2.619	0.001	0.56
Kank2	0.07	0.0424	1.0000	Ttll7	4.129	0.002	0.59
Lama3	4.22	0.0099	1.0000	Tmem42	0.047	0.007	1.00
Rab11a	6.00	0.0161	1.0000	Uqcrc1	3.169	0.004	1.00
Tbck	14.26	0.0353	1.0000	Dot1l	0.084	0.000	0.36
Vat1l	2.54	0.0287	1.0000	Prdm2	5.980	0.011	1.00
Ifngr1	27.47	0.0005	0.3568	Mt-nd3	3.511	0.009	1.00
Slirp	1.72	0.0328	1.0000	Apc2	2.190	0.049	1.00
Adk	9.07	0.0052	1.0000	Uqcrc2	7.365	0.013	1.00
Tnik	0.15	0.0025	0.8654	Fam227b	14.254	0.037	1.00
Kif13b	3.22	0.0324	1.0000	Exoc3	3.015	0.036	1.00
Wwc2	0.23	0.0462	1.0000	Chmp2b	14.226	0.031	1.00
Tm9sf3	0.10	0.0036	1.0000	Marveld1	0.043	0.009	1.00
Cela2a	5.34	0.0495	1.0000	Ncald	24.816	0.001	0.59
Nefl	1.98	0.0005	0.3568	AABR07002068.1	2.541	0.042	1.00
Large1	3.73	0.0264	1.0000	Klhdc8b	14.236	0.029	1.00

Nefm	1.70	0.0030	0.9613	AABR07000534.1	0.356	0.027	1.00
St5	4.04	0.0337	1.0000	Ptrh1	1.333	0.015	1.00
Acat2l1	0.62	0.0261	1.0000	Gtf3a	0.280	0.009	1.00
Plekhb2	0.34	0.0219	1.0000	Fbln5	2.958	0.047	1.00
Map1a	1.67	0.0004	0.3568	Nrn1	1.978	0.044	1.00
Slc35g3	3.62	0.0258	1.0000	Card9	14.237	0.029	1.00
Atxn10	4.95	0.0345	1.0000	Cox11	2.006	0.046	1.00
Prune2	2.01	0.0270	1.0000	Ywhah	1.319	0.002	0.63
Gal	0.05	0.0101	1.0000	AABR07025316.1	0.586	0.000	0.29
Jup	0.20	0.0029	0.9459	Ttll13	0.026	0.000	0.25
Serinc4	0.64	0.0001	0.1588	Mast2	16.873	0.016	1.00
Polr2c	1.81	0.0283	1.0000	Nek9	19.637	0.013	1.00
Rap1gds1	0.06	0.0397	1.0000	AABR07073400.1	16.990	0.046	1.00
Hmgcr	0.06	0.0228	1.0000	Kat5	0.131	0.029	1.00
Gtf3c1	0.25	0.0151	1.0000	LOC103694857	0.014	0.009	1.00
Cotl1	0.17	0.0394	1.0000				

Table 16. CCI DF-NE versus naïve differential expression data (non-coding genes). Includes differential expression data using one-way ANOVA analyses of pooled L4-L5 DRGs from RNA sequencing.

Gene	Gene Biotype	Fold Change	Raw P value	FDR value
Gm22953	miRNA	0.801	0.0204	1.00
AC120291.1	miRNA	0.562	0.0424	1.00
AC130391.2	miRNA	0.444	0.0084	1.00
AC099089.1	miRNA	0.701	0.0006	0.39
AABR07072559.1	miRNA	0.413	0.0224	1.00
AC114096.2	miRNA	0.305	0.0000	0.12
AC105645.3	miRNA	0.544	0.0143	1.00
AABR07027752.3	miRNA	0.489	0.0067	1.00
AABR07043167.3	miRNA	1.925	0.0317	1.00
AABR07027811.3	miRNA	0.380	0.0004	0.36

Table 17. CCI CXB-NE versus naïve differential expression data (protein-coding genes). Includes differential expression data using one-way ANOVA analyses of pooled L4-L5 DRGs from RNA sequencing.

Gene	Fold Change	Raw P Value	FDR	Gene	Fold Change	Raw P value	FDR
Tmcc2	18.95	0.029	0.62	Celsr1	10.161	0.003	0.17
Slc26a1	3.03	0.000	0.01	Tmem91	5.486	0.040	0.70
Zbtb24	5.76	0.007	0.30	AABR07073181.1	2.658	0.015	0.46
Pln	3.78	0.008	0.31	Pptc7	0.120	0.042	0.71
Numa1	4.51	0.001	0.09	Reln	2.672	0.007	0.30
Scube3	6.35	0.000	0.00	Wfikkn1	4.886	0.033	0.63
Marcks	0.22	0.050	0.77	Kmt2e	2.727	0.017	0.49
RT1-S3	5.06	0.002	0.12	Atp8b5p	4.943	0.039	0.69
Pdap1	32.54	0.001	0.11	Tecr	3.373	0.026	0.58
Ankrd61	9.13	0.002	0.16	Uba6	16.773	0.045	0.74
Stard13	8.59	0.005	0.24	Cabp4	26.904	0.039	0.69
Fam207a	16.70	0.031	0.62	Lrrc19	23.362	0.016	0.46
Clip1	34.66	0.000	0.04	Primpol	16.722	0.045	0.74
Gper1	8.60	0.007	0.30	Dennd4b	30.317	0.002	0.16
Il3ra	16.77	0.045	0.74	Flrt1	23.227	0.016	0.46
Mcm7	6.49	0.020	0.53	Fkbp5	30.359	0.003	0.17
Slc8b1	21.22	0.032	0.63	Tmem126a	2.965	0.023	0.56
Hip1	28.48	0.006	0.28	Evi2a	3.806	0.024	0.56
Kif13a	16.62	0.041	0.71	Ccser2	0.415	0.025	0.58
Rcc1l	21.19	0.009	0.33	Hjurp	4.039	0.010	0.36
Hoxd4	0.44	0.020	0.53	Ppp2r3a	4.040	0.004	0.22
Cct8	28.07	0.007	0.30	Pmel	2.886	0.037	0.69
St3gal6	27.95	0.008	0.32	Sec61a2	6.002	0.025	0.58
Kalrn	23.78	0.033	0.63	LOC500300	10.799	0.002	0.11
Eif4a2	4.94	0.047	0.75	Ahctf1	5.987	0.026	0.58
Ube2l3	18.91	0.018	0.51	Sned1	6.512	0.012	0.40
Serpind1	4.94	0.039	0.69	Ppp2r3c	2.254	0.048	0.75
Alcam	2.80	0.006	0.28	Plec	1.514	0.035	0.66
Tmem50b	5.47	0.025	0.57	Man2b1	4.943	0.039	0.69
Usp46	0.06	0.037	0.68	Ggn	23.425	0.004	0.22
Sod1	4.62	0.044	0.73	Aco2	5.280	0.000	0.01
RGD1311575	7.56	0.013	0.42	Pcna	0.229	0.047	0.74
Exoc1	25.65	0.012	0.40	Senp6	18.784	0.030	0.62
Fam175a	25.64	0.006	0.29	Kif20a	3.248	0.003	0.17
Clock	32.51	0.002	0.15	Klhl34	2.950	0.001	0.09
Adcy5	7.84	0.001	0.10	Nup50	28.295	0.010	0.36
Lnx1	8.65	0.010	0.36	Ppm1e	21.190	0.008	0.31
Eprs	3.98	0.023	0.56	Polr2b	0.443	0.000	0.01
Slc30a10	2.63	0.044	0.73	Mrps21	0.208	0.007	0.31
Gpatch2	5.49	0.045	0.74	Nnat	43.409	0.002	0.12
Ero1b	3.26	0.025	0.57	Gpr183	64.230	0.000	0.00
Mtmr1	18.99	0.023	0.56	Nup188	6.619	0.003	0.19
Fstl1	0.58	0.046	0.74	Lrrc8a	32.253	0.001	0.09

Fam104a	2.75	0.005	0.25	Gpr171	18.917	0.018	0.51
Myo19	3.85	0.008	0.31	Fer1l6	48.109	0.000	0.00
Klhl20	16.70	0.031	0.62	Mars	0.294	0.039	0.69
Alg1	2.08	0.046	0.74	Nsun7	6.505	0.032	0.63
Arr3	4.43	0.013	0.42	Jph4	16.732	0.035	0.66
Sdhc	0.32	0.019	0.51	Zfhx2	19.604	0.000	0.00
Hexim1	3.41	0.007	0.30	Abhd1	0.716	0.001	0.06
Nudt16l1	30.01	0.003	0.16	Gpr17	22.117	0.000	0.00
Tp53bp2	16.70	0.042	0.71	Myh6	17.310	0.000	0.00
Trove2	5.93	0.036	0.68	Set	1.894	0.012	0.41
Pnpt1	7.07	0.019	0.52	Gp1ba	16.703	0.031	0.62
Hn1	4.94	0.039	0.69	Pex1	3.443	0.044	0.73
Enam	18.95	0.016	0.46	Gbf1	3.395	0.036	0.67
Wdr26	25.50	0.011	0.38	Morn5	0.684	0.015	0.46
Flrt2	16.77	0.044	0.73	Adpgk	20.121	0.000	0.00
Clgn	6.53	0.020	0.53	Ap2a1	3.069	0.046	0.74
Nit1	7.04	0.023	0.56	Iqcg	21.602	0.039	0.69
Sgca	21.14	0.018	0.50	Syt7	18.946	0.016	0.46
Tmem94	50.68	0.000	0.01	Lrrtm3	25.058	0.000	0.00
Ptger1	2.07	0.027	0.60	LOC102555377	4.871	0.020	0.54
Vasn	10.72	0.002	0.12	Pmpca	1.777	0.018	0.50
Dnah9	32.34	0.001	0.07	Disp2	4.575	0.021	0.54
Eml5	2.75	0.036	0.68	LOC690784	30.084	0.002	0.11
Cox20	3.24	0.001	0.09	Usp54	3.093	0.042	0.72
Dcn	0.13	0.046	0.74	Gga3	0.607	0.014	0.44
Cacna1b	6.54	0.024	0.56	RGD1562319	32.404	0.000	0.05
Ofd1	7.56	0.014	0.44	Ctsw	4.942	0.039	0.69
Angptl1	18.84	0.000	0.01	Sez6l2	4.565	0.042	0.72
Ano3	0.12	0.022	0.54	Fbxl2	21.190	0.008	0.31
Arid2	16.73	0.039	0.69	RGD1359290	9.120	0.006	0.28
Flrt3	41.38	0.000	0.01	AABR07060293.1	9.687	0.006	0.28
Erbb3	2.74	0.002	0.12	Rtel1	3.811	0.024	0.56
Agr3	21.32	0.014	0.45	Ssx1	7.559	0.013	0.42
Agr2	34.79	0.001	0.09	Ankrd11	4.175	0.008	0.31
Csdc2	5.98	0.043	0.72	Cdh15	4.585	0.040	0.70
Kcnmb1	21.13	0.010	0.37	LOC684988	0.340	0.002	0.13
Apob	8.00	0.022	0.54	Arhgef18	6.523	0.015	0.46
Btbd11	16.62	0.041	0.71	Mki67	23.453	0.005	0.24
Slc10a1	43.62	0.000	0.01	Sh2b3	4.912	0.000	0.01
Ctnna1	0.20	0.045	0.73	Myrf	27.866	0.007	0.30
Skp1	5.46	0.044	0.73	Gnl3	7.591	0.019	0.52
Snap25	0.35	0.008	0.32	Zc3h18	6.007	0.027	0.60
Ezh2	3.54	0.010	0.36	Ctns	4.326	0.000	0.01
Rfx1	5.88	0.000	0.04	Dgat1	16.844	0.049	0.76
Steap2	16.70	0.031	0.62	Vps9d1	16.703	0.031	0.62
LRRTM1	74.86	0.000	0.00	Eppin	4.911	0.029	0.62
Stx18	5.47	0.001	0.10	RT1-S2	21.343	0.023	0.56

Trim37	0.44	0.021	0.54	Rasa1	28.105	0.005	0.24
Wwp1	40.71	0.007	0.29	RGD1563145	4.943	0.039	0.69
Snf8	5.93	0.049	0.76	Robo1	16.702	0.031	0.62
Borcs6	16.74	0.043	0.73	Letmd1	3.586	0.049	0.76
Crbn	2.46	0.047	0.75	Grina	3.273	0.018	0.50
Fndc9	2.76	0.040	0.70	Adck5	3.022	0.025	0.58
Pzp	3.65	0.018	0.50	AABR07000595.1	77.364	0.000	0.00
Neb	4.09	0.027	0.60	Mt-nd2	2.181	0.012	0.41
Sema4f	5.05	0.003	0.19	Mab21l2	7.028	0.020	0.53
Psapl1	43.60	0.000	0.01	LOC100361645	4.215	0.011	0.39
Casq1	43.59	0.003	0.17	Pcdh10	23.644	0.010	0.37
Vamp2	18.95	0.041	0.71	Pogk	39.078	0.000	0.02
Slc3a1	1.35	0.045	0.73	Acsm3	11.739	0.000	0.05
March10	27.95	0.003	0.17	Dot1l	6.500	0.046	0.74
Xpot	18.89	0.020	0.53	Scrib	8.158	0.006	0.28
Cacna1c	35.10	0.002	0.12	Ptprt	4.572	0.032	0.63
Nrdc	4.40	0.024	0.57	Dysf	6.621	0.033	0.63
Ndrg1	0.31	0.028	0.61	Mab21l1	4.016	0.012	0.41
Pla2g4b	3.49	0.000	0.00	Pdzd7	16.618	0.041	0.71
Tmem132e	0.05	0.048	0.75	AC127605.1	34.445	0.001	0.10
Kcnj9	6.28	0.000	0.04	Zrsr2	16.703	0.031	0.62
Mcam	8.04	0.013	0.42	Cacna2d1	2.546	0.049	0.76
Atg101	0.05	0.044	0.73	Osbpl9	2.658	0.021	0.54
Usp1	5.98	0.031	0.62	Fam196a	4.328	0.000	0.04
Mpdz	4.94	0.042	0.71	Ube2d4	32.346	0.002	0.14
Timp4	59.32	0.000	0.00	Cfap126	0.315	0.012	0.40
Tmem30b	21.19	0.008	0.31	Rps27a	18.722	0.034	0.66
Atp8a2	2.97	0.024	0.56	Ifit2	16.703	0.031	0.62
Ccne2	2.26	0.001	0.10	Fscn2	3.069	0.016	0.46
Lrrc4	6.38	0.000	0.01	Uqcrc2	0.201	0.022	0.54
Appl2	8.55	0.022	0.54	Atp6v0a1	5.499	0.034	0.65
Orc3	5.48	0.030	0.62	Abhd12	5.979	0.026	0.58
Slc9a8	3.82	0.026	0.58	LOC100360933	16.702	0.031	0.62
Myo1f	5.49	0.049	0.76	Hyi	3.028	0.045	0.73
Bsg	0.60	0.002	0.12	Erich4	30.070	0.002	0.12
Gpr22	12.18	0.000	0.01	Spidr	7.535	0.001	0.07
Eid1	4.99	0.002	0.12	Pram1	74.621	0.000	0.00
Nkiras1	16.70	0.031	0.62	Ccdc152	0.653	0.004	0.21
Smad3	8.60	0.009	0.33	Rab26	2.493	0.001	0.09
Angptl3	32.40	0.000	0.05	AABR07006480.1	2.969	0.021	0.54
Nefh	0.67	0.002	0.12	Ahdc1	18.948	0.022	0.54
Pnisr	3.00	0.000	0.05	Cep192	18.849	0.031	0.62
Orc1	8.56	0.016	0.46	AABR07005040.1	25.676	0.004	0.21
Adamts10	5.96	0.030	0.62	U2af1	0.119	0.036	0.68
Parp2	0.44	0.000	0.00	Ralgapa1	0.180	0.027	0.59
Pcdh17	8.11	0.011	0.37	Znf750	23.638	0.013	0.42
Foxj2	16.65	0.039	0.69	AC133403.1	0.725	0.022	0.54

Mtss1	9.13	0.004	0.21	Thyn1	2.231	0.021	0.54
Thra	3.11	0.000	0.00	Lrrtm2	12.724	0.000	0.00
Atp6v1d	5.47	0.042	0.71	Cdan1	7.537	0.000	0.04
Sez6	25.68	0.002	0.13	AC115420.2	2.063	0.020	0.53
LOC102552055	5.86	0.001	0.07	Mdn1	7.038	0.043	0.73
Tas1r1	4.94	0.050	0.77	Olr338	18.920	0.019	0.53
Lgals1	0.71	0.026	0.59	Cyp2ac1	8.806	0.011	0.38
LOC100151767	0.65	0.001	0.10	Myo18b	3.242	0.020	0.53
Smarcd3	3.17	0.023	0.56		11.486	0.000	0.00
Azi2	19.13	0.031	0.62	AABR07000534.1	14.005	0.000	0.00
Eps15	6.02	0.031	0.62	Pdss1	7.018	0.016	0.47
Ipo7	4.18	0.004	0.20	Kdm4b	6.055	0.008	0.32
Mycbp2	10.17	0.004	0.22	Adamtsl4	2.854	0.030	0.62
Smarcd2	2.90	0.025	0.57	Sh3gl1	3.711	0.003	0.18
Megf11	43.25	0.000	0.04	Dnajc19	2.060	0.031	0.62
Plekhh1	7.05	0.009	0.34	Gtf3a	3.143	0.026	0.58
E2f5	23.43	0.005	0.24	Nrn1	0.290	0.001	0.09
Arrdc4	4.94	0.039	0.69	Dopey2	5.787	0.013	0.42
Nfe2l3	32.41	0.000	0.05	Col10a1	3.804	0.023	0.56
Bmp1	7.51	0.018	0.50	AC132720.1	6.040	0.037	0.69
Pigh	4.17	0.004	0.20	Exosc8	18.946	0.016	0.46
Has1	8.61	0.004	0.22	Slc24a1	5.471	0.023	0.56
Cep295	21.31	0.000	0.00	AC132539.1	0.048	0.046	0.74
Ank2	1.85	0.010	0.36	Ahsa2	4.016	0.012	0.41
Tenm4	16.81	0.047	0.75	Arhgef40	2.058	0.001	0.06
RGD1359634	2.16	0.016	0.46	Ak3	2.924	0.045	0.74
Lrp2bp	21.19	0.008	0.31	Itpr3	2.176	0.010	0.36
Tfdp2	21.17	0.036	0.67	AC130391.3	0.746	0.030	0.62
Masp2	7.72	0.000	0.00	Slc48a1	16.702	0.031	0.62
Slc37a4	18.95	0.016	0.46	AC103090.1	1.704	0.014	0.44
Kif3c	3.81	0.033	0.63	Lama5	21.189	0.008	0.31
Ccdc39	3.71	0.002	0.15	B3gnt9	41.051	0.000	0.04
Arfgef3	5.73	0.011	0.39	Sim2	3.603	0.031	0.62
Ap3m1	4.60	0.000	0.02	Ywhah	0.667	0.000	0.00
Psip1	1.94	0.032	0.63	AABR07025316.1	10.187	0.000	0.00
Gcsh	21.19	0.008	0.31	AC141521.2	2.607	0.017	0.48
Rnf146	4.57	0.023	0.56	Fam46b	18.946	0.016	0.46
Dusp4	25.98	0.027	0.60	Gls	2.389	0.031	0.62
Galnt7	18.92	0.019	0.53	Ttll13	83.654	0.000	0.00
Col17a1	18.95	0.016	0.46	LOC102552324	25.761	0.003	0.17
Dst	1.59	0.005	0.24	Alas1	4.937	0.042	0.71
Slirp	0.51	0.014	0.43	Muc6	6.490	0.000	0.04
Unc45a	18.85	0.022	0.54	Scn3b	3.716	0.010	0.37
Glyatl2	32.53	0.001	0.10	Adamts5	3.082	0.013	0.42
Tnik	7.27	0.001	0.07	Pfkm	4.574	0.031	0.62
Cemip	19.05	0.029	0.62	AABR07020815.1	0.426	0.026	0.58
Tlcd1	0.76	0.000	0.00	Plcb2	16.641	0.038	0.69

Gpr18	4.84	0.001	0.11	Cfap99	2.497	0.032	0.62
Espl1	23.71	0.012	0.41	RGD1562378	0.042	0.008	0.31
Uaca	21.21	0.009	0.33	Srrm2	2.998	0.001	0.10
Mov10	3.73	0.002	0.14	AC106292.2	1.337	0.026	0.58
Metap1	8.08	0.007	0.31	Fbxl3	8.605	0.004	0.22
Lrig1	4.87	0.028	0.61	Has3	5.143	0.000	0.04
Atpif1	0.18	0.019	0.53	Itgb1bp1	23.479	0.006	0.26
Ccdc150	4.94	0.039	0.69	Cc2d2a	19.044	0.024	0.56
Tm9sf3	10.16	0.005	0.23	AABR07035428.2	4.359	0.002	0.14
Ralbp1	4.08	0.038	0.69	AABR07059140.1	23.474	0.005	0.26
Nefl	0.63	0.024	0.56	Ypel4	3.806	0.030	0.62
Megf10	18.79	0.036	0.67	Kdm5d	12.288	0.000	0.04
Tnip2	16.70	0.031	0.62	AC128154.1	3.819	0.030	0.62
P2ry14	32.42	0.001	0.07	Rnf114	18.789	0.029	0.62
Gpr87	21.28	0.019	0.52	AABR07058091.2	16.464	0.000	0.01
Sbno2	0.63	0.000	0.00	Kmt2d	4.274	0.000	0.05
Jade1	19.21	0.040	0.70	Plxnb3	18.992	0.036	0.67
Kifc3	21.50	0.022	0.54	Rbm4b	9.898	0.000	0.01
Omg	16.22	0.001	0.07	Myo1e	23.340	0.012	0.41
Evi2b	3.80	0.045	0.74	Cfap100	18.946	0.016	0.46
Tns1	0.49	0.048	0.75	F2rl2	8.160	0.000	0.00
P2ry1	16.70	0.031	0.62	Slc26a2	18.915	0.021	0.54
Capn5	3.14	0.031	0.62	Acadvl	4.797	0.000	0.00
Josd1	16.84	0.049	0.76	Abca1	3.029	0.044	0.73
Nav2	6.51	0.015	0.46	Slc16a4	34.649	0.000	0.03
Plcxd3	19.10	0.033	0.64	Mgat4a	25.644	0.015	0.46
Btbd6	3.41	0.005	0.25	Aak1	4.189	0.020	0.53
Chrnb1	4.94	0.039	0.69	Prpf18	3.597	0.001	0.11
Tmbim1	4.32	0.003	0.16	Apoe	0.665	0.022	0.54
Zfyve28	7.03	0.024	0.56	Prr14	16.720	0.033	0.63
Mas1	34.61	0.000	0.04	Iffo1	0.228	0.039	0.69
Myo7b	84.51	0.000	0.00	Pprc1	0.253	0.040	0.70
Dmpk	25.76	0.003	0.17	Abcb6	25.769	0.007	0.31
Lrrc39	1.97	0.031	0.62	Slc16a11	3.399	0.005	0.25
Timm21	23.43	0.004	0.21	Gsn	0.422	0.049	0.76
Gal	16.79	0.037	0.68	Sod2	3.533	0.007	0.30
Etfa	23.49	0.007	0.29	Chp2	0.048	0.046	0.74
Spsb3	1.91	0.010	0.36	Pik3r2	18.945	0.016	0.46
Serpine2	0.18	0.006	0.29	Glb1l	28.060	0.012	0.40
Serinc4	1.35	0.007	0.30	Stx4	16.654	0.036	0.68
Otud7a	25.55	0.006	0.28	Fchsd2	4.060	0.041	0.70
Ptgds	0.31	0.002	0.14	Hipk1	10.676	0.001	0.10
Plpp5	5.97	0.046	0.74	Sult1a1	9.647	0.003	0.17
LOC100125364	13.93	0.000	0.03	Lrfn4	7.980	0.015	0.46
LOC690507	11.24	0.001	0.10	Egfl7	25.434	0.049	0.76
Parva	5.89	0.000	0.01	Mpv17l2	0.701	0.043	0.73
Ube3a	2.95	0.026	0.59	Rec8	30.117	0.006	0.27

Elmo3	10.84	0.000	0.00	Trpv3	31.107	0.000	0.00
Add2	7.04	0.024	0.56	Csrnp2	12.268	0.000	0.02
Rap1gds1	21.07	0.018	0.50	Rsbn1	16.720	0.033	0.63
Plekhg1	7.38	0.023	0.56	Ints11	1.663	0.014	0.45
Macf1	2.22	0.049	0.76	Exoc8	4.943	0.039	0.69
Lrrc14	3.78	0.001	0.06	Sipa1l2	5.466	0.022	0.54
Gpr162	2.75	0.010	0.36	Slc5a2	1.655	0.016	0.46
Strn4	2.60	0.032	0.62	Tmem198	3.401	0.045	0.74
Spata2L	6.36	0.005	0.23	Eef1g	0.227	0.015	0.46
Gtf3c1	3.40	0.026	0.58	Sirt2	4.026	0.019	0.52
Myo9b	6.04	0.005	0.23	Il4i1	3.247	0.027	0.59
Creb3	2.86	0.033	0.63	Tbc1d17	6.001	0.026	0.58
Tmem204	10.19	0.002	0.14	Scgb1a1	18.946	0.016	0.46
Pllp	23.43	0.004	0.22	Asrgl1	5.055	0.003	0.18
Dgat2	16.65	0.039	0.69	Atp1a3	2.805	0.012	0.41
Mlf2	0.20	0.004	0.22	Cntnap1	25.676	0.004	0.21
Dtna	25.69	0.008	0.31	Pdcd11	18.906	0.022	0.55
Angptl2	4.57	0.023	0.56	Ezh1	5.989	0.022	0.54
Tmc7	16.70	0.035	0.66	Best1	0.644	0.000	0.01
Angpt2	7.56	0.013	0.42	Apc	2.769	0.033	0.63
Prpf4b	30.14	0.001	0.11	Hcn3	0.201	0.022	0.54
Fanca	2.52	0.005	0.25	Cd81	4.032	0.003	0.18
Pcif1	8.15	0.000	0.00	Nsmce4a	0.057	0.047	0.75
Inpp5d	16.70	0.031	0.62	Ripk3	16.646	0.045	0.74
Kcne3	16.70	0.031	0.62	Bcl2l12	4.557	0.000	0.05
Tbc1d22a	25.78	0.008	0.32	Lipe	3.796	0.007	0.30
Slc25a46	0.29	0.040	0.70	Ceacam1	8.082	0.007	0.31
Cyp27a1	19.08	0.039	0.69	Dcst1	27.254	0.020	0.53
Tubb3	1.38	0.048	0.75	Celf3	36.891	0.000	0.02
Slc22a23	4.55	0.002	0.12	Gif	23.433	0.004	0.21
Igsf6	4.57	0.031	0.62	Ppp2r5b	6.512	0.012	0.40
Kcnt1	4.94	0.039	0.69	Sphk2	9.602	0.000	0.01
Cab39	2.74	0.012	0.41	Lsr	7.528	0.000	0.00
Atrnl1	0.19	0.006	0.27	Fxyd1	16.702	0.031	0.62
Nudt6	5.24	0.001	0.07	Fxyd3	3.451	0.000	0.00
Htr2b	9.65	0.002	0.16	Nrxn2	0.198	0.003	0.17
Fbxl22	2.42	0.028	0.61	Gramd1a	8.095	0.009	0.34
Rere	7.56	0.006	0.27	Fermt3	3.393	0.037	0.68

Table 18. CCI CXB-NE versus naïve differential expression data (non-coding genes). Includes differential expression data using one-way ANOVA analyses of pooled L4-L5 DRGs from RNA sequencing.

Gene	Gene Biotype	Fold Change	Raw P value	FDR
Mir3065	miRNA	30.161	0.001	0.091
Mir3588	miRNA	26.147	0.012	0.407
Mir3074	miRNA	12.945	0.000	0.000
AABR07031182.1	miRNA	16.702	0.031	0.622
AABR07073453.1	lincRNA	25.676	0.004	0.210
AC099089.1	miRNA	0.790	0.039	0.692
AABR07062800.1	lincRNA	7.281	0.004	0.222
AABR07033249.1	lincRNA	27.947	0.003	0.169
AABR07033570.1	lincRNA	12.285	0.000	0.026
AABR07051515.2	lincRNA	7.585	0.012	0.405
AABR07037523.2	miRNA	0.146	0.021	0.539
AABR07035926.2	lincRNA	30.197	0.003	0.169
AABR07006713.1	lincRNA	18.946	0.016	0.456
Rn60_1_2212.2	lincRNA	5.542	0.000	0.000
Rn60_1_2212.3	lincRNA	2.631	0.042	0.717
Rn60_1_2212.4	lincRNA	7.559	0.013	0.419

Table 19. CCI DF-NE vs CCI CXB-NE differential expression data (protein-coding genes). Includes differential expression data using one-way ANOVA analyses of pooled L4-L5 DRGs from RNA sequencing.

Gene	Fold Change	Raw P Value	FDR	Gene	Fold Change	Raw P Value	FDR
Slc26a1	2.656	0.000	0.005	Telo2	6.155	0.003	0.138
Tmem175	26.281	0.006	0.217	Cmtm5	6.164	0.004	0.169
Pdzk1	1.838	0.002	0.108	Wdr37	5.376	0.027	0.479
Zbtb24	3.231	0.014	0.327	Pcif1	6.240	0.000	0.000
Pln	5.957	0.000	0.026	Rnf25	27.582	0.006	0.203
Asf1a	33.638	0.000	0.007	Fancc	12.978	0.000	0.005
Scube3	6.934	0.000	0.000	Acly	1.565	0.031	0.498
Reep3	0.192	0.012	0.310	Clcn7	13.987	0.037	0.558
Jmjd1c	3.184	0.034	0.530	Lmntd2	14.034	0.031	0.498
Srrd	4.699	0.023	0.444	Kcne3	16.187	0.012	0.310
RT1-M3-1	14.017	0.029	0.487	Tbc1d22a	24.968	0.002	0.119
RT1-S3	2.972	0.013	0.317	Slc22a23	4.939	0.000	0.030
Ankrd61	6.497	0.002	0.115	Kcnt1	20.525	0.005	0.194
Fbxw8	3.756	0.003	0.146	Map3k4	5.976	0.045	0.620
Gatc	4.080	0.012	0.310	Spns1	7.387	0.019	0.391
Agpat3	3.828	0.032	0.512	Htr2b	4.857	0.003	0.142
Pcbp3	3.221	0.022	0.425	Mylpf	4.378	0.040	0.587
Gpr146	5.385	0.033	0.523	Ccdc172	14.017	0.029	0.487
P2rx4	13.958	0.039	0.577	Inpp4a	2.716	0.024	0.451
Por	14.022	0.030	0.496	LOC108348250	5.640	0.001	0.079
C2cd2	3.048	0.048	0.646	Optn	4.907	0.027	0.486
Slc51a	18.355	0.005	0.194	Mvb12a	22.724	0.003	0.132
Itpr2	20.693	0.017	0.364	F2rl2	10.425	0.000	0.000
Ube2l3	18.318	0.006	0.220	Slc22a8	16.145	0.023	0.446
Slc7a4	16.292	0.027	0.486	Acadvl	2.458	0.001	0.064
Ptpn13	18.306	0.007	0.225	Srrm1	5.003	0.007	0.235
RGD1311575	5.381	0.008	0.241	Syt5	3.570	0.009	0.259
Helq	14.058	0.033	0.523	Pde4dip	7.329	0.013	0.317
Adcy5	3.695	0.010	0.286	Ccar2	5.121	0.017	0.356
Mark1	13.954	0.040	0.583	Aak1	4.124	0.012	0.309
Trim41	5.411	0.038	0.571	Cul9	4.791	0.031	0.498
Fam129a	0.168	0.012	0.310	Prpf18	2.256	0.014	0.331
Galnt10	9.186	0.003	0.127	Per3	20.377	0.009	0.264
Cdkl2	6.009	0.032	0.512	Unc13a	6.652	0.017	0.357
Ero1b	6.651	0.000	0.034	Rabep2	10.955	0.014	0.330
Gemin5	8.484	0.005	0.194	Otud4	0.267	0.021	0.417
Zfp692	16.210	0.015	0.347	Plekhb1	2.694	0.004	0.153
Sstr2	15.908	0.033	0.522	Patz1	5.723	0.011	0.301
Myo19	5.623	0.001	0.045	Pold4	18.306	0.007	0.225

Myh10	2.297	0.049	0.658	Nisch	2.520	0.009	0.263
Arr3	17.860	0.000	0.004	RGD1308134	5.058	0.009	0.263
Srr	1.413	0.050	0.661	Pik3ip1	2.097	0.034	0.530
Gadd45gip1	3.171	0.033	0.520	Klhdc7a	14.019	0.029	0.490
Plcd3	20.525	0.005	0.194	Myh7b	6.502	0.001	0.063
Serpinf1	0.126	0.024	0.456	Ifit1	27.143	0.001	0.060
Hexim1	3.382	0.003	0.138	Rmi1	18.324	0.008	0.236
Nudt16l1	29.053	0.001	0.046	Scamp2	6.011	0.027	0.479
Col3a1	0.524	0.034	0.523	Emc9	0.631	0.000	0.017
Ogt	5.440	0.038	0.566	Acsl4	0.140	0.044	0.613
Slc6a4	14.017	0.029	0.487	Glb1l	8.111	0.016	0.350
Toml1l2	3.510	0.042	0.597	Ubqln1	3.540	0.040	0.589
Ubxn4	16.107	0.016	0.350	Fchsd2	5.196	0.009	0.254
Wdr26	7.150	0.044	0.618	Sult1a1	11.716	0.000	0.033
Clgn	4.650	0.043	0.607	Trpv1	20.687	0.012	0.309
Hmox2	2.934	0.012	0.310	Rec8	8.414	0.023	0.444
Pitpna	4.614	0.045	0.620	Ipo4	20.574	0.008	0.235
Cep350	4.261	0.023	0.446	Pld2	14.034	0.031	0.498
Tmem94	5.908	0.003	0.138	Trpv3	12.111	0.000	0.000
Tcaim	7.920	0.015	0.348	Csrnp2	6.174	0.000	0.009
Ptger1	2.071	0.015	0.339	Aspa	16.272	0.038	0.566
Vasn	4.135	0.016	0.350	Ubxn1	0.299	0.043	0.607
Abca8a	2.701	0.003	0.149	Jmjd8	0.774	0.018	0.378
Dnah9	9.187	0.001	0.061	Actn3	11.545	0.010	0.288
Eml5	2.312	0.043	0.607	Sipa1l2	6.646	0.013	0.314
Camta2	3.984	0.007	0.225	Scand1	5.973	0.048	0.644
Lrrc52	14.019	0.029	0.490	Tmem198	6.175	0.002	0.117
Elk3	6.210	0.035	0.535	Rab40c	16.186	0.012	0.310
Ddx39a	9.789	0.007	0.225	Eef1g	0.205	0.005	0.196
Brd1	16.233	0.016	0.351	Scgb1a1	18.356	0.005	0.194
Cox20	5.128	0.000	0.002	Asrgl1	9.165	0.000	0.004
Dcn	0.115	0.003	0.149	Gmpr2	3.269	0.002	0.094
Ofd1	3.804	0.020	0.404	Kif22	16.116	0.016	0.352
Fkbp3	10.411	0.003	0.133	Ezh1	24.864	0.001	0.065
Mta3	14.167	0.048	0.644	Best1	0.588	0.000	0.000
Muc15	1.690	0.030	0.495	Hdac4	7.961	0.015	0.347
Angptl1	7.194	0.000	0.030	Rhog	20.605	0.003	0.138
Arf6	0.126	0.004	0.174	Apc	2.536	0.025	0.462
Flrt3	6.871	0.000	0.030	Col5a3	2.162	0.014	0.338
Erbb3	2.365	0.002	0.118	Lipe	4.829	0.001	0.055
Agr3	20.648	0.005	0.183	Ceacam1	9.822	0.001	0.077
Agr2	33.680	0.000	0.031	Snrnp70	3.095	0.010	0.288
Arhgef25	7.294	0.007	0.225	Ltbp4	0.200	0.017	0.356
Sec16b	14.017	0.029	0.487	Celf3	6.126	0.004	0.169

Kif5a	1.760	0.007	0.231	Frmd8	18.379	0.008	0.251
Scn8a	2.509	0.046	0.626	Gif	6.645	0.040	0.583
Rassf5	3.082	0.025	0.464	Ppp2r5b	3.279	0.028	0.486
Gna11	5.375	0.027	0.479	Sphk2	3.894	0.002	0.098
Kcnmb1	20.466	0.007	0.225	Lsr	4.087	0.000	0.004
Pkp4	13.872	0.046	0.626	Fxyd3	1.710	0.012	0.310
LOC686013	6.125	0.004	0.169	Tnfaip8l2	22.858	0.007	0.235
Apob	9.657	0.008	0.244	Mark2	14.016	0.029	0.487
Zbtb44	14.155	0.041	0.592	Lix1l	7.871	0.019	0.389
Slc10a1	12.364	0.000	0.004	Celsr1	3.197	0.046	0.632
Dmtf1	5.138	0.014	0.331	Wfikkn1	6.155	0.012	0.309
Ezh2	3.371	0.006	0.220	Mpp6	14.034	0.031	0.498
LRRTM1	21.265	0.000	0.000	Atp8b5p	20.526	0.002	0.118
Stx18	4.412	0.001	0.065	Tnpo3	0.298	0.050	0.662
RGD1310352	0.466	0.030	0.490	RT1-M6-1	5.455	0.041	0.593
Dync1h1	1.753	0.001	0.056	Dhx37	0.061	0.047	0.642
Fkbp4	14.017	0.029	0.487	Lrrc19	22.627	0.005	0.194
Snf8	7.288	0.017	0.356	mrpl24	2.916	0.040	0.583
Crbn	2.830	0.009	0.265	Luzp1	12.355	0.001	0.049
Fndc9	5.681	0.002	0.112	LOC102546864	5.139	0.017	0.355
Neb	6.034	0.003	0.134	LOC100360821	18.470	0.026	0.470
Psapl1	42.204	0.000	0.001	AABR07052585.1	5.856	0.045	0.625
Casq1	4.820	0.047	0.641	Zdhhc2	8.552	0.009	0.254
Ano6	3.526	0.046	0.626	Ilf3	14.017	0.029	0.487
10-Mar	27.061	0.001	0.050	Tmem126a	10.127	0.000	0.005
Cacna1c	10.071	0.003	0.149	Evi2a	3.067	0.019	0.391
Il12rb2	4.023	0.004	0.172	Tmem184b	3.537	0.042	0.596
Mroh8	0.611	0.022	0.428	Hjurp	5.194	0.000	0.035
Pla2g4b	6.008	0.000	0.000	Ppp2r3a	5.218	0.000	0.020
Gdf11	7.294	0.007	0.225	Proca1	2.512	0.007	0.231
Kcnj9	11.274	0.000	0.001	LOC500300	7.679	0.003	0.127
C8a	14.017	0.029	0.487	Cldn20	6.651	0.017	0.355
Timp4	16.811	0.000	0.000	Ahctf1	7.258	0.025	0.456
Ncoa2	7.434	0.015	0.347	Ncbp1	7.222	0.029	0.487
Ssb	7.282	0.006	0.212	Tmem176a	0.449	0.027	0.484
Fos	0.233	0.012	0.310	Plec	1.684	0.005	0.190
Cinp	6.636	0.041	0.596	Cmya5	25.220	0.029	0.490
Atp8a2	2.371	0.034	0.530	Ggn	6.647	0.013	0.317
Ccne2	1.823	0.010	0.278	Aco2	4.873	0.000	0.002
Kcnh6	7.270	0.024	0.452	Klhl34	2.218	0.004	0.156
Lrrc4	8.379	0.000	0.000	Tnrc18	4.804	0.001	0.084
Plpp3	0.299	0.038	0.567	Nup50	27.398	0.003	0.132
Tagln2	0.690	0.009	0.261	Arhgap22	16.269	0.035	0.535
Orc3	6.668	0.017	0.363	Ppm1e	6.011	0.027	0.479

Slc9a8	3.751	0.010	0.287	Polr2b	0.357	0.000	0.000
Sbf1	3.801	0.021	0.412	Pcolce	3.036	0.031	0.510
Bsg	0.650	0.005	0.180	Gpr183	4.707	0.003	0.140
Gpr22	5.917	0.000	0.005	Nup188	4.494	0.009	0.258
Eid1	6.444	0.000	0.012	Tmem130	2.734	0.047	0.642
Rundc3b	25.205	0.005	0.194	Fer1l6	7.987	0.000	0.009
Nkiras1	16.186	0.012	0.310	Usp7	3.432	0.006	0.212
Invs	14.017	0.029	0.487	Zfhx2	7.106	0.000	0.000
Angptl3	5.381	0.008	0.241	Gpr17	7.141	0.000	0.000
Cops2	4.068	0.019	0.389	Myh6	22.701	0.000	0.000
Plekha5	16.087	0.032	0.512	Set	1.707	0.024	0.456
Pnisr	2.121	0.004	0.169	Krt80	18.749	0.029	0.488
Mpp5	20.516	0.007	0.231	Tspan32	25.170	0.011	0.290
Parp2	0.328	0.000	0.000	Gbf1	3.356	0.026	0.479
Sec24c	3.626	0.008	0.252	Adpgk	5.439	0.000	0.005
Thra	2.547	0.000	0.004	Rpl11	0.632	0.024	0.456
Immt	16.115	0.016	0.352	Lrrtm3	32.088	0.000	0.000
Otub2	4.658	0.043	0.607	LOC102555377	3.352	0.034	0.523
Nub1	0.251	0.030	0.494	Disp2	4.068	0.019	0.389
Fbxo2	16.071	0.044	0.613	LOC690784	4.986	0.020	0.404
Pgp	9.130	0.011	0.301	Snx17	4.632	0.004	0.172
Xpa	0.368	0.027	0.481	RGD1562319	9.186	0.003	0.127
LOC102552055	4.759	0.001	0.046	Sez6l2	9.745	0.006	0.215
Lrrn2	18.678	0.025	0.462	Fbxl2	6.011	0.027	0.479
Tstd2	1.441	0.012	0.310	Sgsm2	5.030	0.007	0.225
Dync1i2	3.142	0.047	0.641	Faxdc2	1.779	0.023	0.446
Camk2g	5.018	0.001	0.070	AABR07060293.1	6.831	0.003	0.138
Cdkn3	4.720	0.019	0.389	Ssx1	9.187	0.001	0.049
Frg1	14.017	0.029	0.487	Nbeal2	0.455	0.010	0.285
Slfnl1	16.082	0.035	0.535	Ankrd11	3.613	0.011	0.297
LOC100151767	0.672	0.002	0.091	Cdh15	5.775	0.016	0.350
Ctps1	3.136	0.016	0.353	Cryzl1	14.017	0.029	0.487
Stard9	3.831	0.001	0.065	Arhgef18	4.648	0.013	0.317
Dgkh	4.274	0.023	0.446	Cpa2	18.357	0.005	0.194
Smarcd3	4.173	0.002	0.108	Sh2b3	6.363	0.000	0.000
Eif4b	2.522	0.001	0.071	Tctn1	2.136	0.003	0.145
Prrc2b	2.216	0.043	0.607	Hmcn1	16.187	0.012	0.310
Dixdc1	7.883	0.015	0.347	Szt2	1.595	0.027	0.480
Trim32	7.309	0.007	0.231	Ctns	2.697	0.002	0.093
Dhx29	5.024	0.036	0.551	Dgat1	16.323	0.021	0.414
Ipo7	6.903	0.000	0.043	Eppin	4.418	0.010	0.283
Mycbp2	12.429	0.000	0.015	Acan	24.821	0.001	0.085
Sp2	6.465	0.009	0.265	Dhx30	12.377	0.010	0.286
Cryab	0.316	0.017	0.355	RGD1563145	20.527	0.002	0.118

Nr2c2	2.987	0.042	0.596	RT1-N2	23.195	0.011	0.301
Plekhh1	3.564	0.020	0.404	Rnf213	3.532	0.041	0.596
Cmtm3	16.220	0.014	0.332	Mt-nd5	1.265	0.024	0.451
Rpl32	0.261	0.004	0.170	Robo3	18.491	0.011	0.305
E2f5	6.662	0.015	0.347	Ormdl2	9.869	0.001	0.079
Kpna4	0.056	0.044	0.618	Dhx16	2.427	0.002	0.092
Arrdc4	20.525	0.005	0.194	Adck5	3.880	0.007	0.229
Ccdc22	6.058	0.040	0.587	Mroh1	3.341	0.032	0.512
Nfe2l3	5.382	0.003	0.127	Ankrd52	2.903	0.032	0.512
Bmp1	9.184	0.007	0.231	Lmf2	14.000	0.042	0.603
Pigh	2.385	0.022	0.431	AABR07000595.1	12.822	0.000	0.000
Ermp1	2.799	0.007	0.231	RGD1561034	2.101	0.018	0.378
Taf1d	14.016	0.029	0.487	RGD1561114	18.749	0.029	0.488
Has1	6.126	0.001	0.077	Mt-nd2	2.259	0.004	0.167
Cep295	14.560	0.000	0.000	Mt-nd4l	3.255	0.008	0.236
Copg2	2.184	0.032	0.513	Carm1	2.063	0.016	0.351
Htt	3.408	0.016	0.351	LOC100361645	4.159	0.006	0.218
Ank2	1.956	0.002	0.089	Mt-atp6	1.874	0.026	0.479
Lrp2bp	20.527	0.002	0.118	Uqcrc1	2.587	0.012	0.310
Masp2	3.047	0.001	0.064	Acsm3	3.124	0.018	0.367
Lama3	3.550	0.021	0.417	Scn11a	3.047	0.023	0.446
Rictor	14.000	0.042	0.603	Mab21l1	7.241	0.001	0.046
Rbsn	4.325	0.050	0.661	AC127605.1	33.346	0.000	0.036
Kif3c	2.604	0.048	0.642	Zrsr2	16.187	0.012	0.310
Adgrg6	14.017	0.029	0.487	AABR07072400.1	0.401	0.001	0.060
Pde3b	6.759	0.038	0.570	Mapk8ip3	1.907	0.018	0.368
Ccdc39	3.757	0.001	0.049	Mt-nd3	5.112	0.000	0.010
Tbck	16.273	0.017	0.355	Fam196a	4.454	0.000	0.003
Arfgef3	5.029	0.016	0.351	Atp8a1	18.356	0.005	0.194
Ap3m1	1.979	0.021	0.421	Fscn2	3.032	0.008	0.243
Psip1	2.806	0.000	0.036	Iqck	9.091	0.015	0.347
Il16	18.473	0.028	0.486	LOC100360933	16.186	0.012	0.310
Foxp3	2.350	0.001	0.065	Ulk1	18.356	0.005	0.194
Fbxo34	16.447	0.033	0.523	Hyi	3.965	0.008	0.243
Sat2	16.132	0.033	0.523	Kdm6b	14.016	0.029	0.487
Sgk1	3.343	0.032	0.512	Erich4	8.533	0.002	0.117
Galnt7	18.331	0.007	0.225	Spidr	3.591	0.004	0.169
Ifngr1	20.537	0.002	0.120	Eif2b5	2.378	0.045	0.626
Cstf3	3.045	0.005	0.184	Pram1	8.729	0.000	0.002
Xrcc3	3.538	0.043	0.607	Cfap157	1.915	0.013	0.317
Dst	1.729	0.000	0.035	Pate4	14.017	0.029	0.487
Med26	2.607	0.024	0.451	Ccdc152	0.588	0.000	0.010
Exosc4	14.017	0.029	0.487	AC126960.1	16.119	0.050	0.662
Glyatl2	9.171	0.006	0.208	Adgrg5	5.417	0.037	0.557

Zmym4	7.330	0.008	0.253	Rab26	2.361	0.001	0.055
Zfp598	14.016	0.029	0.487	Ccdc122	3.639	0.017	0.356
Isl1	13.859	0.048	0.645	Marveld1	0.195	0.029	0.487
Grin3b	2.038	0.004	0.160	Ccdc188	5.376	0.027	0.479
Tlcd1	0.703	0.000	0.000	AABR07006480.1	3.827	0.003	0.149
Gpr18	2.887	0.017	0.356	LOC687707	14.029	0.032	0.512
Cables1	3.522	0.032	0.512	Ncald	14.072	0.032	0.512
Tmem259	5.380	0.028	0.486	Fdps	0.640	0.037	0.558
Espl1	22.965	0.007	0.224	AABR07005040.1	24.865	0.001	0.065
Odf3	7.262	0.015	0.347	U2af1	0.074	0.000	0.022
Vps41	3.544	0.041	0.589	RT1-T24-3	6.064	0.045	0.620
Mov10	2.485	0.012	0.310	Irgq	3.852	0.032	0.513
Mettl3	2.506	0.008	0.248	Dbi	16.153	0.014	0.330
Cacna1d	3.352	0.037	0.558	Thyn1	1.920	0.025	0.463
Wnt4	7.895	0.022	0.435	Lrrtm2	4.381	0.000	0.000
Ccdc150	6.011	0.027	0.479	Bptf	5.403	0.032	0.512
Casz1	9.145	0.006	0.201	Card14	0.441	0.040	0.585
Appl1	16.088	0.032	0.512	Cdan1	16.177	0.000	0.001
Tex2	3.705	0.004	0.174	Cabyr	3.055	0.043	0.607
Elavl3	18.356	0.005	0.194	AC115420.2	2.415	0.003	0.129
Dcaf1	4.637	0.028	0.486	Klhdc8b	20.525	0.005	0.194
P2ry14	3.785	0.024	0.451	Olr338	18.331	0.007	0.225
Gpr87	20.616	0.012	0.310	LOC300308	18.468	0.026	0.479
Arhgap26	6.646	0.013	0.314	Apeg3	1.384	0.045	0.625
Itpkc	7.915	0.010	0.287	Myo18b	5.390	0.001	0.069
Ntrk1	0.232	0.033	0.513	Nynrin	14.017	0.029	0.487
Acat2l1	0.664	0.036	0.549	Pros1	0.065	0.040	0.584
Sbno2	0.701	0.000	0.000	AABR07000534.1	4.943	0.000	0.000
Gfod1	20.693	0.017	0.363	Pdss1	29.175	0.001	0.053
Jade1	18.614	0.016	0.350	Kdm4b	2.864	0.039	0.576
Pold2	0.496	0.013	0.317	Adamtsl4	6.945	0.000	0.021
Omg	6.372	0.002	0.092	Sh3gl1	10.434	0.000	0.000
Map1a	1.733	0.000	0.010	Myh2	9.015	0.023	0.442
Plce1	3.616	0.035	0.535	Pdia6	20.490	0.009	0.256
Josd1	16.323	0.021	0.414	Cstf2t	4.695	0.007	0.225
Zfhx3	2.132	0.047	0.642	Ttc16	2.154	0.043	0.607
S1pr3	3.150	0.047	0.639	Col10a1	3.759	0.009	0.261
Fxyd4	18.502	0.019	0.382	Ppp1r12b	2.072	0.030	0.498
Sigmar1	14.141	0.043	0.607	Nwd2	13.978	0.040	0.583
Atxn10	4.616	0.048	0.645	Usp34	3.412	0.045	0.626
Cbfb	3.805	0.034	0.532	Ahsa2	12.364	0.000	0.004
Chrnb1	20.525	0.005	0.194	Arhgef40	2.440	0.000	0.002
Tmbim1	21.271	0.000	0.000	AABR07034980.1	1.824	0.010	0.273
Mas1	9.813	0.001	0.055	Ak3	3.750	0.017	0.362

Arhgef11	6.502	0.004	0.157	AC130391.3	0.675	0.002	0.091
Myo7b	23.855	0.000	0.000	Ccpg1	3.703	0.010	0.272
Dmpk	7.331	0.008	0.249	Lama5	20.525	0.005	0.194
Prune2	2.096	0.015	0.347	B3gnt9	3.698	0.028	0.487
Lrrc39	2.009	0.016	0.350	Sim2	11.092	0.000	0.015
Timm21	22.696	0.002	0.118	Rps8	0.491	0.016	0.351
Fxn	0.049	0.013	0.317	Pex13	5.376	0.027	0.480
Coro2b	3.219	0.021	0.417	Setd1a	14.017	0.029	0.487
Spsb3	2.493	0.000	0.020	Ncor1	1.894	0.035	0.535
Rpl13	0.629	0.035	0.532	Vom2r80	16.513	0.038	0.565
Sfxn3	5.421	0.039	0.581	Mrfap1	0.474	0.035	0.535
Ubxn11	16.187	0.012	0.310	AABR07025316.1	5.967	0.000	0.000
Otud7a	24.744	0.002	0.094	Fam46b	18.356	0.005	0.194
Ticrr	14.023	0.030	0.492	LOC102552324	24.947	0.001	0.084
Ptgds	0.360	0.004	0.174	Kcnab1	2.638	0.024	0.450
Plpp5	7.358	0.015	0.347	Muc6	11.632	0.000	0.001
Suv39h2	16.187	0.012	0.310	Cav1	0.492	0.045	0.625
LOC100125364	3.727	0.007	0.228	Abr	4.066	0.020	0.396
Wdr34	1.633	0.032	0.513	Scn3b	3.915	0.003	0.133
LOC690507	13.594	0.000	0.023	Obscn	7.946	0.025	0.456
Taok1	15.924	0.041	0.592	AABR07013154.2	24.867	0.001	0.065
E2f4	10.427	0.005	0.190	Cfap99	2.656	0.008	0.253
Parva	4.266	0.000	0.010	RGD1562378	0.031	0.000	0.041
Myl12b	0.371	0.013	0.317	Col12a1	3.542	0.034	0.529
Ube3a	4.367	0.002	0.089	Col2a1	3.308	0.048	0.644
Elmo3	8.640	0.000	0.000	Nek9	18.399	0.013	0.317
Ctsa	0.392	0.012	0.310	Sptbn2	3.608	0.001	0.074
Ap2s1	14.039	0.032	0.512	Fbxl3	4.331	0.011	0.289
Plekhg1	5.384	0.027	0.481	Has3	8.530	0.000	0.001
Lrrc14	6.707	0.000	0.001	Itgb1bp1	6.685	0.017	0.355
Gpr162	2.424	0.015	0.347	Cc2d2a	18.451	0.009	0.253
Spata2L	5.717	0.001	0.064	Avpr2	11.379	0.001	0.074
Sema4c	3.146	0.040	0.583	Thbs3	6.659	0.016	0.350
Myo9b	4.170	0.007	0.225	AABR07059140.1	22.736	0.003	0.139
Cotl1	0.212	0.015	0.347	Ypel4	6.909	0.001	0.050
Plcd4	2.592	0.048	0.644	Kdm5d	4.814	0.001	0.046
Pcsk4	3.181	0.043	0.607	Wdfy3	1.754	0.045	0.625
Pltp	0.583	0.011	0.289	AABR07058091.2	6.349	0.000	0.025
Tmem204	7.258	0.001	0.061	LOC103694857	0.012	0.006	0.216
Dgat2	16.133	0.016	0.351	Phf10	3.046	0.024	0.451
RGD1561517	5.393	0.030	0.490	Kmt2d	3.105	0.001	0.079
Dtna	7.339	0.011	0.304	Scamp1	6.021	0.010	0.286
Angpt2	9.186	0.003	0.127	Rbm4b	4.082	0.000	0.032
Fanca	2.834	0.001	0.055	LOC679342	20.620	0.004	0.162

Epb41l3	2.003	0.004	0.174				

Table 20. CCI DF-NE vs CCI CXB-NE differential expression data (non-coding genes). Includes differential expression data using one-way ANOVA analyses of pooled L4-L5 DRGs from RNA sequencing.

Gene	Gene Biotype	Fold Change	Raw P value	FDR
Mir3065	miRNA	8.551	0.001	0.079
Mir3074	miRNA	16.267	0.000	0.000
Gm22953	miRNA	0.676	0.000	0.005
AABR07067736.1	miRNA	16.258	0.019	0.392
AABR07055846.1	miRNA	8.607	0.007	0.225
AABR07073453.1	lincRNA	24.865	0.001	0.065
AABR07027811.1	miRNA	0.392	0.001	0.045
AC130391.2	miRNA	0.280	0.000	0.007
AABR07058935.1	lincRNA	14.017	0.029	0.487
AC099089.1	miRNA	0.554	0.000	0.000
AABR07012583.1	miRNA	0.485	0.001	0.055
AABR07062800.1	lincRNA	15.776	0.000	0.005
AC114096.2	miRNA	0.256	0.000	0.000
AABR07033249.1	lincRNA	27.061	0.001	0.050
AABR07027752.1	miRNA	0.433	0.023	0.446
AABR07033570.1	lincRNA	50.960	0.000	0.000
AC105645.3	miRNA	0.486	0.003	0.129
AABR07027752.3	miRNA	0.360	0.000	0.015
AABR07021465.2	lincRNA	0.554	0.013	0.317
AABR07035926.2	lincRNA	5.094	0.013	0.313
AABR07006713.1	lincRNA	5.375	0.027	0.479
AABR07026509.1	lincRNA	15.885	0.038	0.571
AABR07027811.3	miRNA	0.302	0.000	0.002
Rn60_1_2212.2	lincRNA	4.974	0.000	0.000
Rn60_1_2212.3	lincRNA	4.166	0.005	0.194
Rn60_1_2212.4	lincRNA	3.805	0.019	0.389

Table 21. PANTHER Gene Ontology classifications of genes differentially expressed between CCI DF-NE and CCI CXB-NE animals. *Number of genes indicates the number of total genes annotated within the given class within the literature. One-way ANOVA analyses of pooled L4-L5 DRGs from RNA sequencing.

Biological Process	Number of Genes	P value	FDR
gene expression (GO:0010467)	727	6.65E-09	8.37E-05
response to drug (GO:0042493)	451	3.00E-08	1.89E-04
response to organic cyclic compound (GO:0014070)	426	3.48E-08	1.46E-04
response to toxic substance (GO:0009636)	239	6.52E-08	2.05E-04
cellular response to drug (GO:0035690)	178	4.25E-07	1.07E-03
protein stabilization (GO:0050821)	85	3.84E-06	8.06E-03
sensory perception of chemical stimulus (GO:0007606)	44	1.35E-05	2.42E-02
detection of chemical stimulus (GO:0009593)	39	1.86E-05	2.92E-02
sensory perception of smell (GO:0007608)	35	2.18E-05	3.05E-02
detection of chemical stimulus involved in sensory perception (GO:0050907)	30	2.38E-05	3.00E-02
detection of chemical stimulus involved in sensory perception of smell (GO:0050911)	24	3.25E-05	3.72E-02
Molecular Function	Number of Genes	P value	FDR
molecular transducer activity (GO:0060089)	268	5.66E-10	1.79E-06
signaling receptor activity (GO:0038023)	253	6.65E-09	1.05E-05
structural molecule activity (GO:0005198)	227	2.73E-07	2.88E-04
transmembrane signaling receptor activity (GO:0004888)	215	4.64E-07	3.67E-04
G protein-coupled receptor activity (GO:0004930)	106	2.92E-06	1.85E-03
structural constituent of ribosome (GO:0003735)	95	3.29E-05	1.74E-02
olfactory receptor activity (GO:0004984)	24	3.51E-05	1.59E-02
Cellular Component	Number of Genes	P value	FDR
membrane-bounded organelle (GO:0043227)	4105	1.94E-05	3.37E-02
intracellular membrane-bounded organelle (GO:0043231)	3864	2.55E-05	2.21E-02
cytoplasmic part (GO:0044444)	3391	5.22E-05	3.02E-02
organelle lumen (GO:0043233)	1739	5.96E-05	2.59E-02
membrane-enclosed lumen (GO:0031974)	1739	7.44E-05	2.58E-02
intracellular organelle lumen (GO:0070013)	1738	1.48E-04	4.29E-02
whole membrane (GO:0098805)	550	2.03E-04	5.03E-02
ribonucleoprotein complex (GO:1990904)	427	2.06E-04	4.48E-02

mitochondrial part (GO:0044429)	365	2.26E-04	4.36E-02
perinuclear region of cytoplasm (GO:0048471)	316	2.93E-04	5.08E-02
ribosome (GO:0005840)	138	3.07E-04	4.84E-02
mitochondrial protein complex (GO:0098798)	131	3.12E-04	4.52E-02
ribosomal subunit (GO:0044391)	116	3.21E-04	4.28E-02
oxidoreductase complex (GO:1990204)	56	3.52E-04	4.36E-02
respirasome (GO:0070469)	51	3.53E-04	4.09E-02
respiratory chain complex (GO:0098803)	49	3.85E-04	4.18E-02
mitochondrial respirasome (GO:0005746)	46	4.01E-04	4.09E-02
DNA packaging complex (GO:0044815)	31	4.01E-04	3.86E-02
nucleosome (GO:0000786)	26	5.55E-04	5.07E-02
cytoplasmic side of rough endoplasmic reticulum membrane (GO:0098556)	18	5.64E-04	4.89E-02
Reactome Pathway	Number of Genes	P value	FDR
Innate Immune System (R-RNO-168249)	340	2.01E-05	3.02E-02
Neutrophil degranulation (R-RNO-6798695)	199	2.73E-05	2.05E-02

References

1. International Association for the Study of Pain (IASP), IASP Taxonomy Working Group. Classification of Chronic Pain. Descriptions of Chronic Pain Syndromes and Definitions of Pain Terms 2011. Second, revised. Available from: http://www.iasp-pain.org/
2. Gaskin DJ, Richard P. The economic costs of pain in the United States. *Journal of Pain* 2012; 13(1): 715-724.
3. Nissen SE, Yeomans ND, Solomon DH, Luscher TF, Libby P, Husni ME, Graham DY, Borer JS, Wisniewski LM, Wolski KE, Wang Q, Menon V, Ruschitzka F, Gaffney M, Beckerman B, Berger MF, Bao W, Lincoff AM. Cardiovascular safety of celecoxib, naproxen, or ibuprofen for arthritis. *New England Journal of Medicine* 2016; 375: 2519-2529.
4. Finnerup NB, Attal N, Haroutounian S, McNicol E, Baron R, Dworkin RH, Kamerman PR. Pharmacotherapy for neuropathic pain in adults: a systematic review and meta-analysis. *The Lancet Neurology* 2015; 14(2): 162-173.
5. DeLeo J, Yezierski RP. The role of neuroinflammation and neuroimmune activation in persistent pain. *Pain* 2001; 90(1-2): 1-6.
6. Dworkin RH, Backonja M, Rowbotham MC, Allen RR, Argoff CR, Bennett GJ, Hewitt DJ. Advances in neuropathic pain: diagnosis, mechanisms, and treatment recommendations. *Archives of Neurology* 2003; 60(11): 1524-1534.
7. Deleo JA, Tanga FY, Tawfik VL. Neuroimmune activation and neuroinflammation in chronic pain and opioid tolerance/hyperalgesia. *The Neuroscientist* 2004; 10(1): 40-52.
8. Mika J, Zychowska M, Rojewska E, Przewlocka B. Importance of glial activation in neuropathic pain. *European Journal of Pain* 2013; 716 (1-3): 106-119.
9. Grace PM, Hutchinson MR, Maier SF, Watkins LR. Pathological pain and the neuroimmune interface. *Nature Reviews Immmunology* 2014; 14: 217-231.
10. Yoo S, van Niekerk EA, Merianda TT, Twiss JL. Dynamics of axonal mRNA transport and implications for peripheral nerve regeneration. *Experimental Neurology* 2010; 223: 19-27.
11. Huebner EA, Strittmatter SM. Axon regeneration in the peripheral and central nervous systems. *Results and Problems in Cell Differentiation* 2009; 48: 339-351.
12. Cattin A, Lloyd AC. The multicellular complexity of peripheral nerve regeneration. *Current Opinions in Neurobiology* 2016; 39: 38-46.
13. Bennett GJ, Xi J. A peripheral mononeuropathy in rat that produces disorders of pain sensation like those seen in man. *Pain* 1988; 33(1): 87-107.
14. Jaggi AS, Jain V, Singh N. Animal models of neuropathic pain. *Fundamental and Clinical Pharmacology* 2009; 25: 1-28.
15. Carlton SM, Dougherty PM, Pover CM, Coggeshall RE.. Neuroma formation and numbers of axons in a rat model of experimental peripheral neuropathy. *Neuroscience Letters* 1991; 131: 88-92.
16. Gabay E, Tal M. Pain behavior and nerve electrophysiology in the CCI model of neuropathic pain. *Pain* 2004; 110: 354-360.
17. Challa SR. Surgical animal models of neuropathic pain: pros and cons. International *Journal of Neuroscience* 2015; 125(3): 170-174.

18. Austin PJ, Wu A, Moalem-Taylor G. Chronic constriction of the sciatic nerve and pain hypersensitivity in rats. *Journal of Visual Experiments* 2012; 61: e3393. Doi:10.3791/3393.
19. Ji RR, Xu ZZ, Gao YJ.Emerging targets in neuroinflammation-driven chronic pain. *Nature Reviews Drug Discovery* 2014; 13(7): 533-548.
20. Vasudeva K, Vodovotz Y, Azhar N, Barclay D, Janjic JM, Pollock JA. In vivo and systems biology studies implicate IL-18 as a central mediator in chronic pain. *Journal of Neuroimmunology* 2015; 283: 43-49.
21. Ji RR, Chamessian A, Zhang Y. Pain regulation by non-neuronal cells and inflammation. *Science* 2016; 354(6312): 572-577.
22. Hucho T, Levine JD. Signaling pathways in sensitization: toward a nociceptor cell biology. *Neuron* 2007; 55: 365-376.
23. Fujioka Y, Stahlberg A, Ochi M, Olmarker K. Expression of inflammation/pain-related genes in the dorsal root ganglion following disc puncture in rats. *Journal of Orthopaedic Surgery* 2016; 24(1): 106-112.
24. Uttam S, Wong C, Amorin IS, Jafarnejad SM, Tansley SN, Yang J, Prager-Khoutorsky M, Mogil JS, Gkogkas CG, Khoutorsky A. Translational profiling of dorsal root ganglia and spinal cord in a mouse model of neuropathic pain. *Neurobiology of Pain* 2018; 4: 345-44.
25. Sherrington CS. The integrative action of the nervous system. 1906. Scribner, New York.
26. Pinho-Ribiero FA, Verri WA, Chiu IM. Nociceptor sensory neuron-immune interactions in pain and inflammation. *Trends in Immunology* 2017; 38(1): 5-19.
27. Grace PM, Hutchinson MR, Maier SF, Watkins LR. Pathological pain and the neuroimmune interface. *Nature Reviews Immunology* 2014; 14: 217-231.
28. Li M, Peake PW, Charlesworth JA, Tracey DJ, Moalem-Taylor, G. Complement activation contributes to leukocyte recruitment and neuropathic pain following peripheral nerve injury in rats. *European Journal of Neuroscience* 2007; 26(12): 3486-3500.
29. Zuo Y, Perkins NM, Tracey DJ, Geczy CL. Inflammation and hyperalgesia induced by nerve injury in the rat: a key role of mast cells. *Pain* 2003; 105(3): 467-479.
30. Austin PJ, Moalem-Taylor G. The neuro-immune balance in neuropathic pain: involvement of inflammatory immune cells, immune-like glial cells and cytokines. *Journal of Neuroimmunology* 2010; 229: 26-50.
31. Dubov P, Klusakova I, Svizenska IH. 2014. Inflammatory profiling of schwann cells in contact with growing axons distal to nerve injury. BioMed Research Int.
32. Michaelis M, Vogel C, Blenk KH, Arnarson A, Janig W. Inflammatory mediators sensitize acutely axotomized nerve fibers to mechanical stimulation in the rat. *Journal of Neuroscience* 1998; 18: 7581-7587.
33. Jessen KR, Mirsky R. Negative regulation of myelination: relevance for development, injury, and demyelinating disease. *Glia* 2008; 56(14): 1552-1565. Doi:10.1002/glia.20761.
34. Wang Y, Shan Q, Pan J, Yi S. Actin cytoskeleton affects Schwann cell migration and peripheral nerve regeneration. *Frontiers in Physiolology* 2018; 9(23).

35. Luchting B, Rachinger-Adam B, Heyn J, Hinske LC, Kreth S, Azad SC. Anti-inflammatory T-cell shift in neuropathic pain. *Journal of Neuroinflammation* 2015; 12: 1-10.
36. Stoll G, Griffin JW, Li CY, Trapp B.D. Wallerian degeneration in the peripheral nervous system: participation of both Schwann cells and macrophages in myelin degradation. *Journal of Neurocytology* 1989; 18: 671-683.
37. Mangodt TC, Van Herck MA, Nullens S, Ramet J, De Dooy JJ, Jorens PG, DeWinter BY. The role of Th17 and Treg responses in the pathogenesis of RSV infection. *Pediatric Research* 2015; 78(5): 483-491.
38. Kleinschnitz C, Hofstetter HH, Meuth SG, Braeuninger S, Sommer C, Stoll G. T cell infiltration after chronic constriction injury of mouse sciatic nerve is associated with interleukin-17 expression. *Experimental Neurology* 2006; 200: 480-485.
39. Happel KI, Zheng M, Young E, Quinton LJ, Lockhart E, Ramsay AJ ,Shellito JE, Schurr JR, Bagby GJ, Nelson S, Kolls JK. Cutting edge: roles of Toll-like receptor 4 and IL-23 in IL-17 expression inresponse to Klebsiella pneumoniae infection. *Journal of Immunology* 2003; 17:, 4432–4436.
40. Liu T, van Rooijen N, Tracey DJ. Depletion of macrophages reduces axonal degradation and hyperalgesia following nerve injury. *Pain* 2000; 86: 25-32.
41. Morin N, Owolabi SA, Harty MW, Papa EF, Tracey TF, Shaw SK, Kim M, Saab CY. Neutrophils invade lumbar dorsal root ganglia after chronic constriction injury of the rat sciatic nerve. *Journal of Neuroimmunology* 2007; 184(1-2): 164-171.
42. Wright HL, Moots RJ, Bucknall RC, Edwards SW. Neutrophil function in inflammation and inflammatory diseases. *Rheumatology* (Oxford) 2010; 49(9): 1618-1631. Doi:10.1093/rheumatology/keq045.
43. Skaper SD, Facci L, Giusti P. Mast cells, glia and neuroinflammation: partners in crime? *Immunology* 2014; 141: 314-327.
44. Leon A, Buriani A, Dal Toso R, Fabris M, Romanello S, Aloe, L, Levi-Montalcini R. Mast cell synthesize, store, and release nerve growth factor. *Proc National Academy of Sciences USA* 1994; 91(9): 3739-3743.
45. Noga O, Englmann C, Hanf G, Grutzkau A, Guhl S, Kunkel G. Activation of the specific neurotrophic receptors TrkA, TrkB and TrkC influence the function of eosinophils. *Clinical and Experimental Allergy* 2000; 32(9). Doi:10.1046/j.1365-2745.2002.01442.x.
46. Saleem M, Deal B, Nehl E, Janjic JM, Pollock JA. Nanomedicine-driven neuropathic pain relief in a rat model is associated with macrophage polarity and mast cell activation. *Acta Neuropathologica Communications* 2019; 7: 108.
47. Vasudeva K, Anderson K, Zeyzus-Johns B, Hitchens TK, Patel SK, Balducci A, Janjic JM, Pollock JA. Imaging neuroinflammation in vivo in a neuropathic pain rat model with near-infrared fluorescence and ^{19}F magnetic resonance. *PLoS ONE* 2014; 9(2): e90589.
48. Janjic JM, Vasudeva K, Saleem M, Stevens A, Liu L, Patel S, Pollock JA, Low-dose NSAIDs reduce pain via macrophage targeted nanoemulsion delivery to neuroinflammation of the sciatic nerve in rat. *Journal of Neuroimmunology* 2018; 318: 72-79.

49. Stevens AM, Liu L, Bertovich D, Janjic JM, Pollock JA. Differential expression of neuroinflammatory mRNAs in the rat sciatic nerve following chronic constriction injury and pain-relieving nanoemulsion NSAID delivery to infiltrating macrophages. *International Journal of Molecular Sciences* 2019; 20: 5269. Doi:10.3390/ijms20215269.
50. Liu T, van Rooijen N, Tracey DJ. Depletion of macrophages reduces axonal degradation and hyperalgesia following nerve injury. *Pain* 2000; 86: 25-32.
51. Ma W, Quirion R. Up-regulation of interleukin-6 induced by prostaglandin E_2 from invading macrophages following nerve injury: an in vivo and in vitro study. Journal of Neurochemistry 2005; 93: 664-673.
52. Ristoiu V. Contribution of macrophages to peripheral neuropathic pain pathogenesis. *Life Sciences* 2013; 93: 870-881.
53. Ginhoux F, Jung S. Monocytes and macrophages: developmental pathways and tissue homeostasis. *Nature Immunology Reviews* 2014; 14: 392-404.
54. Kanamori H, Matsubara T, Mima A, Sumi E, Nagai K, Takahashi T, Abe H, Iehara N, Fukatsu A, Okamoto H., Kita T, Doi T, Arai H. Inhibition of MCP-1/CCR2 pathway ameliorates the development of diabetic neuropathy. *Biomedical and Biophysical Research Communications* 2007; 360: 772-777.
55. Maiguel D, Farid MH, Wie C, Kuwano Y, Balla KM, Hernandez D, Barth CJ, Lugo G, Donnelly M, Nayer A, Moita LF, Schurer S, Traver D, Ruiz P, Vazquez-Padron RI, Ley K, Reiser J, Gupta V. Small molecule-mediated activation of the integrin CD11b/CD18 reduces inflammatory disease. *Science Signaling* 2001; 4(189).
56. Defrancesco-Lisowitz A, Lindborg JA, Niemi JP, Zigmond RE. The neuroimmunology of degeneration and regeneration in the peripheral nervous system. *Neuroscience* 2015; 302: 174-203.
57. Schafers M, Marziniak M, Sorkin LS, Yaksh TL, Sommer C. Cyclooxygenase inhibition in nerve injury- and TNF-induced hyperalgesia in the rat. *Experimental Neurology* 2004; 185: 160-168.
58. Lee S, Zhang J. Heterogeneity of macrophages in injured trigeminal nerves: cytokine/chemokine expressing vs. phagocytic macrophages. *Brain, Behavior, and Immunity* 2008; 26: 891-903.
59. Samad TA, Sapirstein A, Woolf CJ. Prostanoids and pain: unraveling mechanisms and revealing therapeutic targets. Na. New Biol., 240; 200-203.
60. Lai J, Porreca F, Hunter JC, Gold MS. 2004. Voltage-gated sodium channels and hyperalgesia. *Annual Reviews Pharmacological Toxicology* 2002; 44: 371-397.
61. England S, Bevan S, Docherty RJ. PGE2 modulates the tetrodotoxin-resistant sodium current in neuonatal dorsal root ganglion neurons via the cyclic AMP-protein kinase A cascade. *Journal of Physiology* 1996; 945: 429-440.
62. Fiebich BL, Schleicher S, Spleiss O, Czygan M, Hull M. Mechanisms of prostaglandin E2-induced interleukin-6 release in astrocytes: possible involvement of EP4-like receptors, p38 mitogen-activated protein kinase and protein kinase C. *Journal of Neurochem*istry 2001; 79: 950-959.
63. Franchi L, Eigenbrod T, Munoz-Planillo R, Nunez G. The inflammasome: a caspase-1 activation platform regulating immune responses and disease pathogenesis. *Nature Immunology* 2009; 10(3): 241. Doi:10.1038/ni.1703.

64. Ren K, Dubner R. Interactions between the immune and nervous systems in pain. *Nature Medicine* 2010;16(11): 1267-1276. Doi:10.1038/nm.2234.
65. McMahon S, Koltzenbeg M, Tracey I, Turk DC. Wall and Melzack's Textbook of Pain. 6th edition. 2013. Saunders, New York.
66. Ma W, Eisenbach JC. Morphological and pharmacological evidence for the role of peripheral prostaglandins in the pathogenesis of neuropathic pain. European *Journal of Neuroscience* 2002; 15: 1037-1047.
67. Coulombe F, Jaworska J, Verwa, M, Tzelepis F, Massoud A, Gillard J, Wong G, Kobinger G, Xing Z, Couture C, Joubert P, Fritz JH, Powell WS, Divangahi M. Targeted prostaglandin E2 inhibition enhances antiviral immunity through induction of type I interferon and apoptosis in macrophages. *Immunity* 2014; 40: 554-568. Doi:10.1016/j.immuni.2014.02.013.
68. Segond VB, Scholze A, Schaible HG. Prostaglandin E2 increases the expression of the neurokinin receptor in adult sensory neurons in culture: a novel role of prostaglandins. *British Journal of Pharmacology* 2003; 139: 672-680.
69. Ahdmadi S. PGE2 selectively blocks inhibitory glycinergic neurotransmission onto rat superficial dorsal horn neurons. *Nature Neuroscience* 2002; 5(1): 34-40.
70. Minami T, Nishihara I, Uda R, Ito S, Hyodo M, Hayaishi O. Characterization of EP-receptor subtypes involved in allodynia and hyperalgesia by intrathecal administration of prostaglandin E2 to mice. *British Journal of Pharmacology* 1994; 112(3): 735-740.
71. Patel SK, Zhang Y, Pollock JA, Janjic JM. Cycloxygenase-2 inhibiting perfluoropoly (ethylene glycol) ether theranostic nanoemulsions – in vitro study. *PloS ONE* 2013; 8, e55802.
72. Patel SK, Beaino W, Andersen CJ, Janjic JM. Theranostic nanoemulsions for macrophage COX-2 inhibition in a murine inflammation model. *Clinical Immunology* 2015; 160: 59-70.
73. Patel SK, Janjic JM. Macrophage targeted theranostics as personalized nanomedicine strategies for inflammatory disease. *Theranostics* 2015; 5(2): 150-172.
74. Saleem M, Stevens AM, Deal B, Liu L, Janjic JM, Pollock JA. A new best practice for validating tail vein injections in rat with near-infrared-labeled agents. *Journal of Visualized Experiments* 2019; 146: e59295.
75. Tracey DJ, Walker JS. Pain due to nerve damage: are inflammatory mediators involved. *Inflammation Research* 1995; 44: 407-411.
76. Staaf S, Oerther S, Lucas G, Mattsson JP, Ernfors P. Differential regulation of TRP channels in a rat model of neuropathic pain. *Pain* 2009; 114: 187-199.
77. Wu S, Lutz BM, Miao X, Liang L, Mo K, Chang Y, Du P, Soteropoulos P, Tian B, Kaufman AG, Bekker A, Hu Y, Tao Y. Dorsal root ganglion transcriptome analysis following peripheral nerve injury in mice. *Molecular Pain* 2016;12: 1-14.
78. Yin C, Hu Q, Liu B, Tai Y, Zheng X, Li Y, Xiang X, Wang P, Liu B. Transcriptome profiling of dorsal root ganglia in a rat model of complex regional pain syndrome type-I reveals potential mechanisms involved in pain. *Journal of Pain Research 2019;* 12: 1201-1216.

79. Stephens KE, Zhou W, Ji Z, Chen Z, He S, Ji H, Guan Y, Taverna S.D. Sex differences in gene regulation in the dorsal root ganglion after nerve injury. *BMC Genomics* 2019; 20: 147.
80. Ma, W, Quirion R. Does COX2-dependent PGE2 play a role in neuropathic pain? *Neuroscience Letters* 2008; 437: 165-169.
81. Kalinski P. Regulation of immune responses by prostaglandin E2. *Journal of Immunolology 2012;* 188: 21-28. Doi:10.4049/jimmunol.1101029.
82. Dixon WJ. The up-and-down method for small samples. Journal of American Statistical Assocation 1965; 60(312): 967-978.
83. Chaplan SR, Bach FW, Pogrel JW, Chung JM, Yaksh TL. Quantitative assessment of tactile allodynia in the rat paw. *Journal of Neuroscience Methods* 1994;53: 55-63.
84. Janjic JM, Patel SK, Patrick MJ, Pollock JA, DiVito E, Cascio M. Suppressing inflammation from inside out with novel NIR visible perfluorocarbon nanotheranostics. *Proc SPIE* 2013; 8596: 85960L-1.
85. Janjic JM, Shaw P, Zhang S, Yang X, Patel SK, Bai M. Perfluorocarbon nanoemulsions with fluorescent, colloidal and magnetic properties. *Biomaterials* 2014; 35: 4958-4968.
86. Livak KJ, Schmittgen TD. Analysis of relative gene expression data using real-time quantitative PCR and the $2^{-\Delta\Delta CT}$ method. *Methods* 2001; 25: 402-408.
87. Perry VH, Tsao JW, Fearn S, Brown MC. Radiation-induced reductions in macrophage recruitment have only slight effects on myelin degeneration in sectioned peripheral nerves of mice. *European Journal of Neuroscience* 1995: 7: 271-280.
88. Bruck W. The role of macrophages in Wallerian degeneration. *Brain Pathology* 1997; 7: 741-752.
89. Gaudet AD, Popovich PG, Ramer MS. Wallerian degeneration: gaining perspective on inflammatory events after peripheral nerve injury. *Journal of Neuroinfl*ammation 2001; 8: 110.
90. Peng J, Gu N, Zhou L, Evo UB, Murugan M, Gan W, Wu L. Microglia and monocytes synergistically promote the transition from acute to chronic pain after nerve injury. *Nature Comm*unications 2016; 7: e12029.
91. Costigan M, Scholz J, Woolf CJ. Neuropathic pain: a maladaptive response of the nervous system to damage. *Annual Reviews Neuroscience* 2009; 32: 1-32.
92. Cui JG, Holmin S, Mathiesen T, Meyerson BA, Linderoth B. Possible role of inflammatory mediators in tactile hypersensitivity in rat models of mononeuropathy. *Pain* 2000; 88: 239-248.
93. Heneka MT, Kummer MP, Latz E. Innate immune activation in neurodegenerative disease. *Nature Reviews Immunology* 2014; 14: 463-477.
94. Parkitna JR, Korostynski M, Kaminska-Chowaniec D, Obara I, Mika J, Przewlocka B, Przewlocki R. Comparison of gene expression profiles in neuropathic and inflammatory pain. *Journal of Physiology and Pharmacology* 2006; 57(3): 401-414.
95. Scholz J, Woolf CJ. The neuropathic pain triad: neurons, immune cells and glia. *Nature Neuroscience* 2007; 10(11): 1361-1368.

96. Zou Y, Zu F, Tang Z, Zhong T, Cao J, Guo Q, Huang C. Distinct calcitonin gene-related peptide expression in primary afferents contribute to different neuropathic symptoms following chronic constriction or crush injuries to the rat sciatic nerve. *Molecular Pain* 2016; 12: 1-17.
97. Cheever TR, Olson EA, Ervasti JM. Axonal regeneration and neuronal function are preserved in motor neurons lacking β-actin in vivo. *PLoS ONE* 2011; 6(3): e17768.
98. Hur E, Zhou F. 2012. Growing the growth cone: remodeling the cytoskeleton to promote axon regeneration. *Trends Neurosci*, 35(3), 164-174.
99. Saegusa H, Kurihara T, Zong S, Kazuno A, Matsuda Y, Nonaka T, Han W, Toriyama H, Tanabe T. Suppression of inflammatory and neuropathic pain symptoms in mice lacking the N-type Ca^{2+} channel. *EMBO* 2001; 20(10): 2349-2356.
100. Lee Y, Takami K, Kawai Y, Girgis S, Hillyard CJ, MacIntyre I, Emson PC. Distribution of calcitonin gene-related peptide in the rat peripheral nervous system with reference to its coexistence with substance P. *Neuroscience* 1985; 15(4): 1227-1237.
101. Vause CV, Durham PL. Calcitonin gene-related peptide differentially regulates gene and protein expression in trigeminal glia cells: findings from array analysis. *Neuroscience Letters 2010;* 473: 163-167.
102. Andersen S, Skorpen F. Variation in the COMT gene: implications for pain perception and pain treatment. *Pharmacogenomics* 2009; 10(4): 669-684.
103. Hartung JE, Ciszek BP, Nackley AG. Beta-2- and beta-3-adrenergic receptors drive COMT-dependent pain by increasing production of nitric oxide and cytokines. *Pain* 2014; 155(7): 1346-1355.
104. Pomonis JD, Rogers SD, Peteres CM, Ghilardi JR, Mantyh PW. Expression and localization of endothelin receptors: implications for the involvement of peripheral glial in nociception. *Journal of Neuroscience*, 2001; 21(3): 999-1006.
105. Ai N, Wood D, Yang E, Welsh WJ. Niclosamide is a negative allosteric modulator of group I metabotropic glutamate receptors: implications for neuropathic pain. *Pharmacological Research* 2016; 33(12): 3044-3056.
106. Ocana M, Cendan CM, Cobos EJ, Entrena JM, Baeyens JM. Potassium channels and pain: present realities and future opportunities. *European Journal of Pharmacology* 2004; 500(1-3): 203-219.
107. Tsantoulas C, McMahon SB. Opening paths to novel analgesics: the role of potassium channels in chronic pain. *Trends in Neuroscience* 2014; 37(3): 146-158.
108. Mannion RJ, Doubell TP, Coggeshall RE, Woolf C.J. Collateral sprouting of uninjured primary afferent A-fibers into the superficial dorsal horn of the adult rat spinal cord after topical capsaicin treatment to the sciatic nerve. J *Neuroscience* 1996; 16: 5189-5195.
109. Mantyh PW, Koltzenburg M, Mendell LM, Tive L, Shelton DL. Antagonism of nerve growth factor-TrkA signaling and the relief of pain. *Anesthesiology* 2011; 115(1): 189-204.
110. Nockemann D, Rouault M, Labuz D, Hublitz P, McKnelly K, Reis FC, Stein C, Heppenstall PA. The K^+ channel GIRK2 is both necessary and sufficient for

peripheral opioid-mediated analgesia. *EMBO Molecular Medicine* 2013; 5: 1263-1277.
111. Huang Y, Zang Y, Zhou L, Gui W, Liu X, Zhong Y. The role of TNF-alpha/NF-Kappa B pathweay on the up-regulation of voltage-gated sodium channel Nav1.7 in DRG neurons of rats with diabetic neuropathy. *Neurochemistry International* 2014; 75: 112-119.
112. Minett MS, Falk S, Santana-Varela S, Bogdanov YD, Nassar MA, Heegaard A, Wood J. Pain without nociceptors? Nav1.7-independent pain mechanisms. *Cell Reports* 2014; 6: 301-312.
113. Xu H, Ramsey IS, Kotecha SA, Moran MM, Chong JA, Lawson D, Ge P, Lilly J, Silos-Santiago I, Xie Y, DiStefano PS, Curtis R, Clapham DE. TRPV3 is a calcium-permeable temperature-sensitive cation channel. *Nature Letters* 2002; 418: 181-186.
114. Hu H, Xiao R, Wang C, Gao N, Colton CK, Wood JD, Zhu MX. Potentiation of TRPV3 channel function by unsaturated fatty acids. *Journal of Cell Physiology* 2006; 208: 201-212.
115. Moqric A, Hwang SW, Earley TJ, Petrus MJ, Murray AN, Spencer K, Andahazy M, Story GM, Patapoutian A. Impaired thermosensation in mice lacking TRPV3, a heat and camphor sensor in the skin. *Science* 2011; 307: 1468-1472.
116. Scanzano A, Cosentino M. Adrenergic regulation of innate immunity: a review. *Frontiers in Pharmacology* 2015; 6: 171.
117. Abbadle C, Lindia JA, Cumiskey AM, Peterson LB, Mudgett JS, Bayne EK, DeMartino JA, MacIntyre DE, Forrest MJ. Impaired neuropathic pain responses in mice lacking the chemokine receptor CCR2. *PNAS* 2003; 100 (13): 7947-7952.
118. Yang J, Zhang L, Yu C, Yang X, Wang H. Monocyte and macrophage differentiation: circulation inflammatory monocyte as biomarker for inflammatory disease. *Biomarker Research* 2014*;* 2:1.
119. Austin PJ, Kim CF, Perera CJ, Moalem-Taylor G.. Regulatory T cells attenuate neuropathic pain following peripheral nerve injury and experimental autoimmune neuritis. *Pain* 2012; 153(9): 1916-1931.
120. Galiegue S, Marchand MS, Dussossoy D, Carriere D, Carayon P, Bouaboula M, Shire D, Le Fur G, Casellas P. Expression of central and peripheral cannabinoid receptors in human immune tissues and leukocyte subpopulations. *Eur Journal of Biochem*istry 1995; 232: 54-61.
121. Desroches J, Bouchard JF, Gendron P, Beaulieu P. Involvement of cannabinoid receptors in peripheral and spinal morphine analgesia. *Neuroscience* 2014; 261: 23-42.
122. Rosetti F, Mayadas TN. The many face of Mac-1 in autoimmune disease. *Imunology Rev*iews 2015; 269: 175-193.
123. Sarafi MN, Garcia-Zepeda EA, MacLean JA, Charo IF, Luster AD. Murine monocyte chemoattractant protein (MCP)-5: a novel CC chemokine that is a structural and functional homologue of Human MCP-1. *Journal of Experimental Med*icine 1997; 185: 99-109.
124. Verge GM, Milligan ED, Maier SF, Watkins LR, Naeve GS. Fractalkine (CX3CL1) and fractalkine receptor distribution in spinal cord and dorsal root

ganglia under basal and neuropathic conditions. *European Journal of Neuroscience* 2004; 20: 1150-1160.
125. Hesslinger C, Kremmer E, Hultner L, Ueffing M, Irmgard Z. Phosphorylation of GTP cyclohydrolase I and modulation of its activity in rodent mast cells. *Journal of Biological Chemistry* 1998; 273(34): 21616-21622.
126. Bauer M, Meyer M, Brevig T, Gasser T, Widmer HR, Zimmer J, Ueffing M. Lipid-mediated glial cell derved neurotrophic factor gene transfer to cultured porcine ventral mesencephalic tissue. *Experimental Neurology* 2002; 177: 40-49.
127. Lorey SL, Huang YC, Sharma V. Constitutive expression of interleukin-18 and interleukin-18 receptor in tumour derived human B-cell lines. *Clinical Experimental Immunology* 2004; 136: 456-462.
128. Okamoto K, Martin DP, Schmelzer JD, Mitsui Y, Low PA. Pro- and Anti-inflammatory cytokine gene expression in rat sciatic nerve chronic constriction injury model of neuropathic pain. *Experimental Neurology* 2001; 169: 386-391.
129. Zhang Z, An J. Cytokines, inflammation and pain. *International Anesthes Clin* 2007; 45 (2):, 27-37.
130. Keyel PA. How is inflammation initiated? Individual influences of IL-1, IL-18 and HMGB1. *Cytokine* 2014; 69: 136-145.
131. Hinson RM, Williams JA, Shacter E. Elevated interleukin 6 is induced by prostaglandin E2 in a murine model of inflammation: possible role of cyclooxygenase-2. *Proc Natl Acad Sci USA* 1996; 93(10): 4885-4890.
132. Xu Y, Yoshitake AI, Arai R. Monoamine oxidase type B is localized to mitochondrial outer membranes in Mast cells, Schwann cells, endothelial cells and fibroblasts of the rat tongue. *Acta Histochem Cytochem* 2002; 35(5): 417-422.
133. Ma W, Eisenbach JC. Four PGE2 EP receptors are up-regulated in injured nerve following partial sciatic nerve ligation. *Experimental Neurology* 2003; 183: 581-592.
134. Echeverry S, Wu Y, Zhang J. Selectively reducing cytokine/chemokine expressing macrophages in injured nerves impairs the development of neuropathic pain. *Experimental Neurology* 2012; 240: 205-218.
135. Tomlinson JE, Zygelyte E, Grenier JK, Edwards MG, Cheetham J. Temporal changes in macrophage phenotype after peripheral nerve injury. *Journal of Neuroinflammation* 2018; 15: 185.
136. Calvo M, Dawes JM, Bennett DL. The role of the immune system in the generation of neuropathic pain. *Lancet Neurology* 2012; 11: 629-642.
137. Ellis A, Bennett DLH. Neuroinflammation and the generation of neuropathic pain. *British Journal of Anaesthesiology* 2013; 11(1): 26-37.
138. Hirata T, Narumiya S. Prostanoids as regulators of innate and adaptive immunity. *Advanced Immunol*ogy 2012; 116: 143-174.
139. Kalinski P. Regulation of immune responses by prostaglandin E2. *Journal of Immunology* 2012; 188(1): 21-28.
140. Zhou Y, Liu Z, Chen S, Li M, Shahveranov A, Ye D, Tian Y. Interleukin-6: an emerging regulator of pathological pain. *Journal of Neuroinflammation* 2016; 13: 141.

141. Hirota H, Kiyama H, Kishimoto T, Taga T. Accelerated nerve regeneration in mice by upregulated expression of interleukin 6 and IL-6 receptor after trauma. *Journal of Experimental Medicine* 1996; 183: 2627-2634.
142. Makwana M, Raivich G. Molecular mechanisms in successful peripheral regeneration. *FEBS* 2005; 272: 2628-2638.
143. Henken DB, Battisti WP, Chesselet MF, Murray M, Tessler A. Expression of β-preprotachykinin mRNA and tachykinins in rat dorsal root ganglion cells following peripheral or central axotomy. *Neuroscience* 1990; 39(3): 733-742.
144. Pinto FM, Almeida TA, Hernandez M, Devillier P, Advenier C, Candenas ML. mRNA expression of tachykinins and tachykinins receptors in different human tissues. *Experimental Journal of Pharmacology* 2004; 494: 233-239.
145. Chen W, Ennes HS, McRoberts JA, Marvizon JC. Mechanisms of μ-opioid receptor inhibition of NMDA receptor-induced substance P release in the rat spinal cord. *Neuropharmacology* 2018; 128: 255-268.
146. Kinkelin I, Brocker E, Koltzenburg M, Carlton SM. Localization of ionotropic glutamate receptors in peripheral axons of human skin. *Neuroscience Letters* 2000; 283: 149-152.
147. Sheu JY, Kulhanek DJ, Eckenstein FP. Differential patterns of ERK and STAT2 phosphorylation after sciatic nerve transection in the rat. *Experimental Neurology* 2000; 166: 392-402.
148. Nassar MA, Levato A, Stirling LC, Wood JN. Neuropathic pain develops normally in mice lacking both Nav1.7 and Nav1.8. *Molecular Pain* 2005; 1(24).
149. Villarinho JG, Oliveira SM, Silva CR, Cabreira TN, Ferreira J. Involvement of monoamine oxidase B on models of postoperative and neuropathic pain in mice. *European Journal of Pharmacology* 2012; 690: 107-114.
150. Murali SS, Napier IA, Moahhamdi SA, Alewood PF, Lewis RJ, Christie MJ. High-voltage-activated calcium current subtypes in mouse DRG neurons adapt in a subpopulation-specific manner after nerve injury. *Journal of Neurophysiology* 2015; 113: 1511-1519.
151. Boucher TJ, Okuse K, Bennett DLH, Munson, JB, Wood JN, McMahon SB. Potent analgesic effects of GDNF in neuropathic pain states. *Science* 2000; 290: 124-127.
152. Takasu K, Sakai A, Hanawa H, Shimada T, Suzuki H.Overexpression of GDNF in the uninjured DRG exerts effects on neuropathic pain following segmental spinal nerve ligation in mice. *Journal of Pain* 2011; 12(11): 1130-1139.
153. Yao J, Sasaki Y, Wen Z, Bassell GJ, Zheng JQ. An essential role for β-actin mRNA localization and translation in Ca^{2+} -dependent growth cone guidance. *Nature Neuroscience*, 2006; 9(10): 1265-1273.
154. Wang Y, Shan Q, Pan J, Yi S. Actin cytoskeleton affects Schwann cell migration and peripheral nerve regeneration. *Frontiers in Physiology*, 2018; 9(23).
155. Combadiere C, Murphy, PM, Wynick D. Intra-neural administration of fractalkine attenuates neuropathic pain-related behavior. *Journal of Neurochem*istry 2008; 106(2): 640-649.
156. Usoskin D, Furlan A, Islam S, Abdo H, Lonnerberg P, Lou D, Hjerling-Leffler J, Haeggstrom J, Kharchenko O, Kharchenko PV, Linnarsson S, Ernfors P.

Unbiases classification of sensory neuron types by large-scale single-cell RNA sequencing. *Nature Neuroscience* 2014; 18(1): 145-156. doi:10.1038/nn.3881.

157. Gong L, Wu J, Zhou S, Wang Y, Qin J, Yu B, Gu X, Yao C. Global analysis of transcriptome in dorsal root ganglia following peripheral nerve injury in rats. *Biochemical and Biophysical Research Communications 2016;* 478: 206-212.
158. Wu S, Lutz BM, Miao X, Liang L, Mo K, Chang Y, Du P, Soteropoulos P, Tian B, Kaufman AG, Bekker A, Hu Y, Tao Y. Dorsal root ganglion transcriptome analysis following peripheral nerve injury in mice. *Molecular Pain* 2016; 12: 1-14.
159. Gabay E, Tal M. Pain behavior and nerve electrophysiology in the CCI model of neuropathic pain. *Pain* 2004; 110(1-2): 354-360.
160. LaCroix-Fralish ML, Austin J, Zheng FY, Levitin DJ, Mogil JS. Patterns of pain: meta-analysis of microarray studies of pain. *Pain* 2011; 152: 1888-1898.
161. Dib-Hajj SD, Fjell J, Cummins TR, Zheng Z, Fried K, LaMotte R, Black JA, Waxman SG. Plasticity of sodium channel expression in DRG neurons in the chronic constriction injury of neuropathic pain. *Pain* 1999; 83(3): 591-600.
162. Obata K, Yamanaka H, Fukuoka T, Yi D, Tokunaga A, Hashimoto N, Yoshikawa H, Noguchi K. Contribution of injured and uninjured dorsal root ganglion neurons to pain behavior and the changes in gene expression following chronic constriction injury of the sciatic nerve in rats. *Pain* 2003; 101: 65-77.
163. Yin C, Hu Q, Liu B, Tai Y, Zheng X, Li Y, Xiang X, Wang P, Liu B. Transcriptome profiling of dorsal root ganglia in a rat model of complex regional pain syndrome type-I reveals potential mechanisms involved in pain. *Journal of Pain Research* 2019; 12: 1201-1216.
164. Stephens KE, Zhou W, Ji Z, Chen Z, He S, Ji H, Guan Y, Taverna SD. Sex differences in gene regulation in the dorsal root ganglion after nerve injury. *BMC Genomics* 2019; 20: 147.
165. Ray P, Torck A, Quigley L, Wangzhou A, Neiman M, Rao C, Lam T, Kim J, Kim TH, Zhang MQ, Dussor G, and Price TJ. Comparative transcriptome profiling of the human and mouse dorsal root ganglia: an RNA-seq-based resource for pain and sensory neuroscience research. *Pain* 2018; 159: 1325-1345.
166. Uttam S, Wong C, Amorim IS, Jafarnejad SM, Tansley SN, Yang J, Prager-Khoutorsky M, Mogil JS, Gkogkas CG, Khoutorsky A. Translational profiling of dorsal root ganglia and spinal cord in a mouse model of neuropathic pain. *Neurobiology of Pain* 2018; 4: 35-44.
167. Liu L, Karagoz H, Herneisey M, Zor F, Komatsu T, Loftus S, Janjic BM, Gorantla VS, Janjic JM. Sex differences revealed in a mouse CFA inflammation model with macrophage targeted nanotheranostics. *Theranostics* 2020; 10(4): 1694-1707. Doi:10.7150/thno.41309. eCollection 2020.
168. Mi H, Muruganujan A, Huang X, Ebert D, Mills C, Guo X, Thomas PD. Protocol update for large-scale genome and gene function analysis with the PANTHER classification system (v.14.0). *Nature Protocols* 2019; 14: 703-721.
169. Croft D, Mundo AF, Haw R, Milacic M, Weiser J, Wu G, Caudy M, Garapati P, Gillespie M, Kamdar MR, Jassal B, Jupe S, Matthews L, May B, Palatnik

S, Rothfels K, Shamovsky V, Song H, Williams M, Birney E, Hermjakob H, Stein L, D'Eustachio P. The Reactome pathway knowledgebase. *Nucleic Acid Research*. 2014; 42(D): D472-7. doi:10.1093/nar/gkt1102.
170. Sollner C, Wright GJ. A cell surface interaction network if neural leucine-rich repeat receptors. *Genome Biology* 2009; 10: R99. doi: 10.1186/gb-2009-10-9-r99.
171. Freichel M, Almering J, Tsvilovskyy V. The role of TRP proteins in mast cells. *Frontiers in Immunology* 2012; 3(150): 1-15. Doi:10.3389/fimmu.2012.00150.
172. Zhou J, Xiong Q, Chen H, Yang C, Fan Y. Identification of the spinal expression profile of non-coding RNAs involved in neuropathic pain following spared nerve injury by sequence analysis. *Frontiers in Molecular Science* 2017; 10(91): 1-22. Doi:10.3389/fnmol.2017.00091.
173. Wu S, Bono J, Tao Y. Long noncoding RNA: a potential target for neuropathic pain. *Expert Opinion Therapeutic Targets*, 2019; 23(1): 15-20. Doi:10.1080/14728222.2019.1550075.
174. Chandran V, Coppola G, Nawabi H, Omura T, Versano R, Huebner EA, Zhang A, Costigan M, Yekkirala A, Barrett L, Blesch A, Michaelevski I, Davis-Turak J, Gao F, Langfelder P, Horvath S, He Z, Benowitz L, Fainzilber M, Tuszynski M. A Systems-level analysis of the peripheral nerve intrinsic axonal growth program. *Neuron* 2016; 89: 956–970.
175. Hanz S, Perlson E, Willis D, Zheng J, Massarwa R, Huerta JJ, Fainzilber M. Axoplasmic importins enable retrograde injury signaling in lesioned nerve. *Neuron* 2003; 40(6): 1095-1104.
176. Liu P, Peng J, Han G, Ding X, Wei S, Gao G, Huang K, Chang F, Wang Y. Role of macrophages in peripheral nerve injury and repair. *Neural Regeneration Res*earch 2019; 14(8): 1335-1342.
177. Fantin A, Vieira JM, Gestri G, Denti L, Schwarz Q, Prykhozhij S, Peri F, Wilson SW, Ruhrberg C. Tissue macrophages act as cellular chaperones for vascular anastomosis downstream of VEGF-mediated endothelial tip cell induction. *Blood* 2010; 116: 829–840.
178. Turka LA, Goodman RE, Rutkowski. Interleukin 12: A Potential Link between Nerve Cells and the Immune Response in Inflammatory Disorders. *Molecular Medicine* 1995; (1): 690–699.
179. Huygen FJ, Ramdhani N, van Toorenenbergen A, Klein J, Zijlstra FJ. Mast cells are involved in inflammatory reactions during Complex Regional Pain Syndrome type 1. *Immunology letters* 2004; 91(2-3): 147-154.
180. Orekhov AN, Orekhova VA., Nikiforov NG, Myasoedova VA, Grechko AV, Romanenko EB, Chistiakov DA. Monocyte differentiation and macrophage polarization. *Vessel Plu*s 2019; 3(10).
181. Sjoberg J, Kanje M. The initial period of peripheral nerve regeneration and the importance of the local environment for the conditioning lesion effect. *Brain Research 1990;*. 529: 79–84.
182. Oudega M, Varon S, Hagg T. Regeneration of adult rat sensory axons into intraspinal nerve grafts: promoting effects of conditioning lesion and graft predegeneration. *Experimental Neurology* 1994; 129: 194–206.

183. Li S, Xue C, Yuan Y, Zhang R, Wang Y, Yongjun W, Yu B, Liu J, Ding F, Yuming Y, Gu X. The transcriptional landscape of dorsal root ganglia after sciatic nerve transection. *Scientific Reports* 2015; 5: 16888. Doi:10.1038/srep16888.
184. Scheib J, Höke A. Advances in peripheral nerve regeneration. *Nature Reviews Neuro*logy 2013; 9:668–676.
185. Abe N, Cavalli V. Nerve injury signaling. Current Opinions in Neurobiology 2008; 18:276–283.
186. Martin SL, Reid AJ, Verkhratsky A, Magnaghi V, Faroni A. Gene expression changes in dorsal root ganglia following peripheral nerve injury: roles in inflammation, cell death and nociception. *Neural regeneration research* 2019; 14(6): 939–947. https://doi.org/10.4103/1673-5374.250566
187. Chandran V, Coppola G, Nawabi H, Omura T, Versano R, Huebner EA, Zhang A, Costigan M, Yekkirala A, Barrett L, Blesch A, Michaelevski I, Davis-Turak J, Gao F, Langfelder P, Horvath S, He Z, Benowitz L, Fainzilber M, Tuszynski M. A Systems-level analysis of the peripheral nerve intrinsic axonal growth program. *Neuron* 2016; 89:956–970.
188. Gu Y, Qui Z, Liu D, Sun G, Guan Y, Hei Z, Li X. Differential gene expression profiling of the sciatic nerve in type 1 and type 2 diabetic mice. *Biomedical Reports 2018;* 9: 291-304.
189. Rathmann W, Ziegler D, Jahnke M, Haastert B, Gries FA. Mortality in diabetic patients with cardiovascular autonomic neuropathy. *Diabetic Medicine* 1993; 10: 820-824.
190. Clayton JA. Studying both sexes: a guiding principle for biomedicine. *FASEB Journal* 2016; 30(2): 519-524. Doi:10.1096/fj.15-279554.
191. Mapplebeck JC, Beggs S, Salter MW. Molecules in pain and sex: a developing story. *Molecular Brain 2017;* 10(1): 9. Doi:10.1186/s13041-017-0289-8.
192. Laumet G, Ma J, Kavelaars A. T Cells as an emerging target for chronic therpy. *Frontier Molecular Neuroscienc 2019; e* 12: 216. Doi:10.3389/fnmol.2019.00216
193. Sorge RE, Mapplebeck JC, Rosen S, Beggs S, Taves S, Alexander JK, Martin LJ, Austin JS, Sotocinal SG, Chen D, Yang M, Shi XQ, Huang H, Pillon NJ, Bilan PJ, Tu Y, Klip A, Ji RR, Zhang J, Salter MW, Mogil JS. Differential immune cells mediate mechanical hypersensitivity in male and female mice. *Nature Neuroscience* 2015; 18(8): 1081-183. Doi:10.1038/nn.4053.
194. Turner PV, Brabb T, Pekow C, Vasbinder MA. Administration of substances to laboratory animals: routes of administration and factors to consider. *Journal of the American Association for Laboratory Animal Science* 2011; 50 (5): 600–613.
195. Liu L, Bagia C, Janjic JM. The First Scale-Up Production of Theranostic Nanoemulsions. *BioResearch Open Access* 2015; 4 (1): 218–228. doi: 10.1089/biores.2014.0030.
196. Patel SK, Patrick MJ, Pollock JA, Janjic JM. Two-color fluorescent (near-infrared and visible) triphasic perfluorocarbon nanoemuslions. *Journal of Biomedical Optics* 2013; 18 (10): 101312. doi: 10.1117/1.JBO.18.10.101312.

197. O'Hanlon CE, Amede KG, O'Hear MR, Janjic JM. NIR-labeled perfluoropolyether nanoemulsions for drug delivery and imaging. *Journal of Fluorine Chemistry* 2012; 137: 27–33. doi: 10.1016/j.jfluchem.2012.02.004.
198. Cheng Y, Liu M, Hu H, Liu D, Zhou S. Development, Optimization, and Characterization of PEGylated Nanoemulsion of Prostaglandin E1 for Long Circulation. *AAPS PharmSciTech* 2016; 17 (2): 409–417. doi: 10.1208/s12249-015-0366-1.
199. Fofaria NM, Qhattal HS, Liu X, Srivastava SK. Nanoemulsion formulations for anti-cancer agent piplartine--Characterization, toxicological, pharmacokinetics and efficacy studies. *International Journal of Pharmaceutics* 2016; 498 (1–2): 12–22. doi: 10.1016/j.ijpharm.2015.11.045.
200. Ganta S. EGFR Targeted Theranostic Nanoemulsion for Image-Guided Ovarian Cancer Therapy. *Pharmaceutical Research* 2015; 32 (8): 2753–2763. doi: 10.1007/s11095-015-1660-z.
201. Shah L, Kulkarni P, Ferris C, Amiji MM. Analgesic efficacy and safety of DALDA peptide analog delivery to the brain using oil-in-water nanoemulsion formulation. *Pharmaceutical Research* 2014; 31 (10): 2724–2734. doi: 10.1007/s11095-014-1370-y.
202. Maruyama H. High-level expression of naked DNA delivered to rat liver via tail vein injection. *Journal of Gene Medicine* 2002. doi: 10.1002/jgm.28.
203. Hibbitt OC. Delivery and long-term expression of a 135 kb LDLR genomic DNA locus in vivo by hydrodynamic tail vein injection. *Journal of Gene Medicine* 2002. doi: 10.1002/jgm.1047.
204. Sebestyén MG. Mechanism of plasmid delivery by hydrodynamic tail vein injection. I. Hepatocyte uptake of various molecules. *Journal of Gene Medicine* 2006. doi: 10.1002/jgm.921.
205. Budker VG. Mechanism of plasmid delivery by hydrodynamic tain vein injection. II. Morphological studies. *Journal of Gene Medicine* 2006. doi: 10.1002/jgm.920.
206. Lecocq M. Uptake by mouse liver and intracellular fate of plasmid DNA after a rapid tail vein injection of a small or a large volume. *Journal of Gene Medicine* 2003. doi: 10.1002/jgm.328.
207. Park S, Park HM, Sun SH. Single-dose Intravenous Injection Toxicity of Water-soluble Danggui Pharmacopuncture (WDP) in Sprague-Dawley Rats. *Journal of Pharmacopuncture* 2018; 21 (2): 104–111. doi: 10.3831/KPI.2018.21.013.
208. Zhang X. Activatable fluorescence detection of epidermal growth factor receptor positive mediastinal lymph nodes in murine lung cancer model. *PLOS ONE* 2018; 13 (6): e0198224. doi: 10.1371/journal.pone.0198224.
209. Liu G. Tracking of transplanted human umbilical cord-derived mesenchymal stem cells labeled with fluorescent probe in a mouse model of acute lung injury. *International Journal of Molecular Medicine* 2018; 41 (5): 2527–2534. doi: 10.3892/ijmm.2018.3491.
210. Janjic JM, Srinivas M, Kadayakkara DK, Ahrens ET. Self-delivering nanoemulsions for dual fluorine-19 MRI and fluorescence detection. *Journal of the American Chemical Society* 2008; 130 (9): 2832–2841. doi: 10.1021/ja077388j.

211. Chang YC. An Automated Mouse Tail Vascular Access System by Vision and Pressure Feedback. *IEEE/ASME Transactions on Mechatronics* 2015; 20 (4): 1616–1623. doi: 10.1109/TMECH.2014.2360886.
212. Chen Q. Theranostic imaging of liver cancer using targeted optical/MRI dual-modal probes. *Oncotarget* 2017; 8 (20): 32741–32751. doi: 10.18632/oncotarget.15642.
213. Tansi FL. Activatable bispecific liposomes bearing fibroblast activation protein directed single chain fragment/Trastuzumab deliver encapsulated cargo into the nuclei of tumor cells and the tumor microenvironment simultaneously. *Acta Biomaterialia* 2017; 54: 281–293. doi: 10.1016/j.actbio.2017.03.033.
214. Li S, Johnson J, Peck A, Xie Q. Near infrared fluorescent imaging of brain tumor with IR780 dye incorporated phospholipid nanoparticles. *Journal of Translational Medicine* 2017. doi: 10.1186/s12967-016-1115-2.
215. Gao M, Yu F, Lv C, Choo J, Chen L. Fluorescent chemical probes for accurate tumor diagnosis and targeting therapy. *Chemical Society Reviews 2017*. doi: 10.1039/c6cs00908e.
216. Wang R, Han X, You J, Yu F, Chen L. Ratiometric Near-Infrared Fluorescent Probe for Synergistic Detection of Monoamine Oxidase B and Its Contribution to Oxidative Stress in Cell and Mice Aging Models. *Analytical Chemistry* 2018; 90 (6): 4054–4061. doi: 10.1021/acs.analchem.7b05297.
217. Han X, Song X, Yu F, Chen LA. Ratiometric Near-Infrared Fluorescent Probe for Quantification and Evaluation of Selenocysteine-Protective Effects in Acute Inflammation. *Advanced Functional Materials* 2017; 27 (28): 1700769. doi: 10.1002/adfm.201700769.
218. Garlanda C, Dinarello CA, Mantovani A. The interleukin-1 family: back to the future. *Immunit*y 2013; 11: 1003-1019.
219. Thornberry NA. A novel heterodimeric cysteine protease is required for interleukin-1 beta processing in monocytes. *Nature* 1992; 356: 768-774.
220. Landsman L, Bar-On L, Zernecke A, Kim K, Krauthgamer R, Lira SA, Weissman IL, Weber C, Jung S. CX3CR1 is required for monocyte homeostasis and atherogenesis by promoting cell survival. *Vascular Biology* 2017; 113(4): 963-974.
221. Zhang J, Jiang B, Gao Y. Chemokines in neuron-glial cell interaction and pathogenesis of neuropathic pain. *Cellular Molecular Life Sciebces* 2017; 74: 3275-3291.
222. Lin G, Zhang H, Sun F, Lu Z, Reed-Maldonado A, Lee Y, Wang G, Banie L, Lue TF. Brain-derived neurotrophic factor promotes nerve regeneration by activating the JAK/STAT pathway in Schwann cells. *Transl Androl Urol 2016;* 5(2): 167-175.
223. Jeon S, Lee K, Cho H. Expression of monocyte chemoattractant protein-1 in rat dorsal root ganglia and spinal cord in experimental models of neuropathic pain. *Brain Research* 2009; 1251, 103-111.
224. Bali KK. and Kuner R. Noncoding RNAs: key molecules in understanding and treating pain. *Trends in Molecular Medicine 2014;*. 20(8): 437-448.
225. Wu J, Wang C, Ding H. lncRNA MALAT1 promotes neuropathic pain progression through the miR-154-5p/AQP9 axis in CCI rat models. *Molecular*

Medicine Reports 2020; 21: 291-303.
226. Tang S, Zhou J, Jing H, Liao M, Lin S, Huang Z, Huang T, Zhong J, Wang H. Functional roles of lncRNAs and its potential mechanisms in neuropathic pain. *Clinical Epigenetics* 2019; 11(78).
227. Liu S. lncRNA nonratt0201972 siRNA regulates neuropathic pain behaviors in type 2 diabetes in rats through P2X7 in dorsal root ganglia. *Molecular Brain* 2016; 9(1).
228. Zhao X, Tang, Z, Zhang H, Atianjoh FE, Zhao J, Liang L, Wang W, Guan X, Kao S, Tiwari V, Gao Y, Hoffman PN, Cui H, Li M, Dong X, Tao Y. A long noncoding RNA contributes to neuropathic pain by silencing Kcna2 in primary afferent neurons. *Nature Neuroscience* 2013; 16(8): 1024-1032.
229. Lin S, Gregory RI. MicroRNA biogenesis pathways in cancer. *Nat Rev Cancer* 2015; 15(6): 321-333. Doi.10.1038/nrc3932.
230. Yang J, Xiong L, He X, Jiang L, Fu S, Han X, Liu J, Wang T. Oligodendrocyte precursor cell transplantation promotes functional recovery following contusive spinal cord injury in rats and is associated with altered microRNA expression. *Molecular Medicine Reports* 2018; 17: 771-782.
231. Bensen J, Graff M, Young KL, Sethupathy P, Parker J, Pecot CV., Currin, K., Haddad, S.A., Ruiz-Narvaez, E.A., Olshan, A.F. A survey of microRNA single nucleotide polymorphisms identifies novel breast cancer susceptibility loci in a case-control population-based study of African-American woman. *Breast Cancer Research* 2018; 20(45).
232. Koenig J, Werdehausen R, Linley JE, Habib AM, Vernon J, Lolignier S, Elijkelkamp N, Zhao J, Okorokov AL, Woods CG, Wood JN, Cox JJ. Regulation of Nav1.7: a conserved SCN9A natural antisense transcript expressed in dorsal root ganglia. *PLoS ONE* 2015; 10(6).
233. Calvo M, Davies AJ, Hebert HL, Weir GA, Chesler EJ, Finnerup NB, Levitt RC, Smith BH, Neely GG, Costigan M, Bennett DL. The genetics of neuropathic pain from model organisms to clinical application. *Neuron* 2019; 104: 637-653.
234. Dutartre P. Inflammasome and natural ingredients towards new anti-inflammatory agents. *Molecules* 2016; 21: 1492. Doi:10.3390/molecules21111492.
235. Mamik MK, Power C. Inflammasomes in neurological diseases: emerging pathogenic and therapeutic concepts. *Brain* 2017; 140: 2273-1185.
236. Sun S, Chen D, Lin F, Chen M, Yu H, Hou L, Li C. Role of interleukin-4, the chemokine CCL3 and its receptor CCR5 in neuropathic pain. *Molecular Immunology* 2016; 77: 184-292.
237. Tilley DM, Cedeno DL, Kelley CA, DeMaegd M, Benymain R, Vallejo R. Changes in dorsal root ganglion gene expression in response to spinal cord stimulation. *Chronic and Interventional* Pain 2017; 42(2), 246-251.
238. Brauckmann AL. Pilot study exploring the effect of targeted COX-2 inhibtion in macrophages responding to neuronal injury; promoting enhanced axonal regeneration. Duquesne University, Rangos School of Health Sciences Thesis. 2020.
239. Martinson F, Burns K, Tschopp J. The inflammasome: a molecular platform triggering activation of inflammatory caspases and processing of proIL-1beta.

M*olecular Cell* 2002; 10: 417-426.
240. Wang Y, Zhang X, Guo Q, Zou W, Huang C, Yan J. Cyclooxygenase inhibitors suppress the expression of P2X3 receptors in the DRG and attenuate hyperalgesia following chronic constriction injury. *Neurosciebce Letters* 2010; 478(2): 77-81.
241. Syriatowics JP, Hu D, Walker JS, Tracey DJ. Hyperalgesia due to nerve injury: role of prostaglandins. *Neuroscience* 1999; 94: 587-594.
242. Zhao Z, Chen SR, Eisenach JC, Busija DQ, Pan HL. Spinal cyclooxygenase-2 is involved in development of allodynia after nerve injury in rats. Neuroscience 2000; 97: 743-748.
243. Patel SK, Beaino W, Andersen CJ, Janjic JM. Theranostic nanoemulsions for macrophage COX-2 inhibition in a murine inflammation model. *Clinical Immunology* 2015; 160: 59-70.
244. Yu X, Liu H, Hamel KA, Morvan MG, Yu S, Leff J, Guan Z, Braz JM, Basbaum AI. Dorsal root ganglion macrophages contribute to both the initiation and persistence of neuropathic pain. *Nature Communications* 2020; 11 (264): doi:10.1038/s41467-019-13839-2.
245. de Rivero Vaccari J, Bastien D, Yurcisin G, Pineau I, Dietrich WD, de Konick Y, Keane RW, Lacroix S. P2X4 receptors influence inflammasome activation after spinal cord injury. *Journal of Neuroscience* 2012; 32(9): 3058-3066.
246. Schafers M, Marziniak M, Sorkin LS, Yaksh TL, Sommer C. Cyclooxygenase inhibition in nerve injury- and TNF-induced hyperalgesia in the rat. *Exp Neurol* 2004; 185: 160-168.
247. Uku R, Kolberg L, Kuzmin I, Arak T, Adler P, Peterson H, Vilo J. g:Profiler: a web server for functional enrichment analysis and conversion of gene lists (2019 update). *Nucleic Acids Research* 2019. doi:10.1093/nar/gkz369.
248. Mueller O, Lightfoot S, Schroeder A. RNA integrity number (RIN) – standardization of RNA quality control. *Agilent Technologies* 2016; publication PN 5989-1165EN.
249. Xu J, Pollock CH, Kajander KC. Chromic gut suture reduces calcitonin-gene-related peptide and substance P levels in the spinal cord following chronic constriction injury in the rat. *Pain* 1996; 64(3): 503-509.
250. Yu X, Liu H, Hamel KA, Morvin MG, Yu S, Leff J, Guan Z, Braz JM, Bausbaum AI. Dorsal root ganglion macrophages contribute to both the initiation and persistence of neuropathic pain. *Nature Communications* 2020; 11 (264): doi:.10.1038/s41467-019-13839-2.
251. Olingy CE, San Emeterio CL, Ogle ME, Krieger JR, Bruce AC, Pfau DD, Jordan BT, Peirce SM, Botchwey EA. Non-classical monocytes are biased progenitors of wound healing macrophages during soft tissue injury. *Scientific Reports* 2017; 7: 447. Doi.10.1038/s41598-017-00477-1.
252. Yu X, Leff J, Guan Z. Rapid isolation of dorsal root ganglion macrophages. *J of Visualized Experiments* 2019; 151 (e60023). Doi:10.3791/60023.
253. Cinar O, Olcmean E, Kalemci O, Bagriyanik A, Dogan A, Kucukebe B, Yilmaz O, Gokmen N. Ketorolac tromethamine promotes functional recovery and enhances nerve regeneration after sciatic nerve trauma in rats. *Journal of Neurological Sciences* 2012; 29, 1(3): 65-75.